,

Mechanical performance of polypropylene sandwich structures

Bc. Ladislav Uruba

Univerzita Tomáše Bati ve Zlíně
Fakulta technologická
Ústav výrobního inženýrství

Akademický rok: 2023/2024

ZADÁNÍ DIPLOMOVÉ PRÁCE
(projektu, uměleckého díla, uměleckého výkonu)

Jméno a příjmení: **Bc. Ladislav Uruba**
Osobní číslo: **T22654**
Studijní program: **N0788A270008 Konstrukce nástrojů**
Forma studia: **Prezenční**
Téma práce: **Mechanické vlastnosti lehčených polypropylénových sendvičů**

Zásady pro vypracování

Příprava a testování mechanických vlastností lehčených polypropylénových sendvičů:
- optimalizace skladby sendviče změnou hustoty a tloušťky (bi)axiálně orientované pěny
- návrh vrstvené výztuže
- mechanické testy - ohyb, tak, tlak

Forma zpracování diplomové práce: **tištěná/elektronická**
Jazyk zpracování: **Angličtina**

Seznam doporučené literatury:

Polymeric Foams: Innovations in Processes, Technologies, and Products, Shau-Tarng Lee (ed), ISBN 9780367782757, 2021, CRC Press
Foam Extrusion: Principles and Practice, Shau-Tarng Lee (ed), ISBN 1566768799, 2020, CRC Press
Polypropylene Handbook: Morphology, Blends and Composites, József Karger-Kocsis, Tamás Bárány (eds.), ISBN: 978-3--030-12903-3, 2020 Springer

Vedoucí diplomové práce: **prof. Ing. Berenika Hausnerová, Ph.D.**
Ústav výrobního inženýrství

Datum zadání diplomové práce: **2. ledna 2024**
Termín odevzdání diplomové práce: **10. května 2024**

L.S.

prof. Ing. Roman Čermák, Ph.D. v.r.
děkan

doc. Ing. Martin Bednařík, Ph.D. v.r.
ředitel ústavu

Ve Zlíně dne 27. února 2024

PROHLÁŠENÍ AUTORA
DIPLOMOVÉ PRÁCE

Beru na vědomí, že:

- diplomová práce bude uložena v elektronické podobě v univerzitním informačním systému a dostupná k nahlédnutí;
- na moji diplomovou práci se plně vztahuje zákon č. 121/2000 Sb. o právu autorském, o právech souvisejících s právem autorským a o změně některých zákonů (autorský zákon) ve znění pozdějších právních předpisů, zejm. § 35 odst. 3;
- podle § 60 odst. 1 autorského zákona má Univerzita Tomáše Bati ve Zlíně právo na uzavření licenční smlouvy o užití školního díla v rozsahu § 12 odst. 4 autorského zákona;
- podle § 60 odst. 2 a 3 autorského zákona mohu užít své dílo – diplomovou prací nebo poskytnout licenci k jejímu využití jen s předchozím písemným souhlasem Univerzity Tomáše Bati ve Zlíně, která je oprávněna v takovém případě ode mne požadovat přiměřený příspěvek na úhradu nákladů, které byly Univerzitou Tomáše Bati ve Zlíně na vytvoření díla vynaloženy (až do jejich skutečné výše);
- pokud bylo k vypracování diplomové práce využito softwaru poskytnutého Univerzitou Tomáše Bati ve Zlíně nebo jinými subjekty pouze ke studijním a výzkumným účelům (tj. k nekomerčnímu využití), nelze výsledky diplomové práce využít ke komerčním účelům;
- pokud je výstupem diplomové práce jakýkoliv softwarový produkt, považují se za součást práce rovněž i zdrojové kódy, popř. soubory, ze kterých se projekt skládá. Neodevzdání této součásti může být důvodem k neobhájení práce.

Prohlašuji,

- že jsem na diplomové práci pracoval samostatně a použitou literaturu jsem citoval. V případě publikace výsledků budu uveden jako spoluautor.
- že odevzdaná verze diplomové práce a verze elektronická nahraná do IS/STAG jsou obsahově totožné.

Ve Zlíně dne:

Jméno a příjmení studenta:

....
podpis studenta

ABSTRACT

This thesis delves into the mechanical optimization of sandwich structures made solely from polypropylene. These sandwich structures exclusively utilize thermoplastic material allowing for physical bonding through heat, thereby eliminating the need of adhesives. This approach not only simplifies manufacturing processes but also enhances recyclability and reduces the environmental footprint of the product. A special polypropylene foam manufactured by SPUR, a.s. is employed as a core material. The altered cell orientation, which significantly enhances its mechanical properties. As a skin material extruded polypropylene foil and polypropylene foil reinforced with long glass fibers were tested. Sandwich structure was optimized for maximum rigidity.

Keywords: polypropylene sandwich, mechanical performance, shear test, compression test

ABSTRAKT

Tato práce se zabývá optimalizací mechanických vlastností polypropylénových sendvičových struktur. Tyto sendvičové struktury tvoří výhradně termoplastické materiály (polypropylény), které umožňují fyzikální spojení pomocí tepla, čímž odpadá potřeba lepidel. Tento přístup nejen zjednodušuje výrobní procesy, ale také zvyšuje recyklovatelnost a snižuje ekologickou stopu výrobku. Materiál jádra sendviče tvoří unikátní polypropylenová pěna, kterou vyrábí společnost SPUR, a.s. Pěna má upravenu orientaci buněk, což výrazně zlepšuje její mechanické vlastnosti. Jako materiál výztuh slouží extrudovaný polypropylén, případně polypropylen vyztužený dlouhými skelnými vlákny. Sendvičová struktura byla optimalizována pro dosažení maximální tuhosti.

Klíčová slova: celopolypropylenový sendvič, mechanika sendvičových struktur, smyková zkouška, tlaková zkouška.

I hereby declare that the print version of my Bachelor's/Master's thesis and the electronic version of my thesis deposited in the IS/STAG system are identical.

CONTENTS

INTRODUCTION

This work focuses on optimizing the mechanical properties of sandwich structures that are made solely from polypropylenes – a core from polypropylene foam, and a skin from polypropylene foil and polypropylene foil reinforced with long glass fibers.

Theoretical part is focused on introduction of the characteristics of plastic cellular materials, including their microstructure and the role of density and gas content on their performance. The production process of polypropylene foams using various methods, including injection molding and extrusion with chemical or physical blowing agents, is then described. An analysis of the mechanical properties of polypropylene foams in relation to their microstructural features follows, covering behavior under compression, tension, and elastic deformation. Various types of sandwich structures are discussed and compared, including those based on thermoset resins, thermoplastics, and manufactured with the help of 3D printing methods. The mechanical performance of sandwich structures is examined in detail, with a focus on the analysis of behavior under pure bending and bending with shear forces.

Experimental part deals with an analysis of mechanical properties of a core and a skin of sandwiches. The core material – polypropylene foam, was tested in compression (according to ISO 844) and in shear (according to ISO 1922/ČSN 64 5436), skin material was tested in tensile (according to ISO 527) and compression (according to ASTM C 364) modes. Then, using analytical relations from the theoretical part, the structure was examined for maximum stiffness to weight ratio with the aim to optimize the mechanical properties of sandwich structures for their effective use in various applications.

I.   THEORY

1 CELLULLAR SOLIDS FROM POLYMERIC MATERIAL

Cellular plastics or plastic foams, also referred to as expanded or sponge plastics, generally consist of a minimum of two phases: a solid polymer matrix and gaseous phase derived from a blowing agent. There may be more than one solid phase present, as in the case of blends.

The production of polymeric cellular solid materials has increased in recent decades. The main reason for their popularity is their light weight, which fits the current trend of reducing the weight of products. They also exhibit good impact resistance properties, good thermal and acoustic insulation properties. This makes them suitable for many applications, both in the automotive industry and other sectors, such as construction and transport.

Their advantage is also the variability of properties, where foams made of many polymeric materials (PP, PUR, PVC) are available on the market in a range of densities ρ =1,6 kg·m^{-3} – 960 kg·m^{-3}. [1]

Cellular plastics can be made either by extrusion or injection molding. Injection molding is suitable for complex shapes of finished parts, such as cycling helmet inserts made from PS foams. Extrusion is more suitable for basic shapes, such as plates or profiles, but in an order of magnitude higher quantity.

An important problem in the application of cellular plastics is the complexity or impossibility of their reuse or recycling owing to the presence of nucleation agents, UV stabilizers, viscosity modifiers, flame retardants, etc.

1.1 Properties of plastic cellular solids

There are two main approaches to studying the cellular structure of foamed polymers. The first is called a graphical approach. As the name implies, it attempts to deduce material properties based on optical studies of cellular solid structures. The second approach may be referred to as physicochemical, which attempts to predict the material properties of cellular solids based on their polymer matrix composition and the mechanism of foaming. [1]

The mechanical properties of cellular plastic materials depend on several factors. The main factors affecting mechanical properties may include cellular solid density and shape of cells, and whether cells are interconnected (open) or closed.

1.1.1 Role of density and gas content

When describing cellular solids, we discuss their apparent density (or volumetric weight). The real density measures the weight of the material relative to its actual volume and remains constant. The apparent density includes the intercellular space and can vary depending on the structure of the material.

It is possible to state that with decreasing apparent density, the polymer fraction (solid) decreases, and the gas fraction (voids or cells) in the material increases. The gas content was determined by the nucleation and forming process.

In open-cell structures, the gas phase is air, whereas in foamed plastics with isolated cells (closed cells), it may be another gas depending on the blowing agent used. The diffusion process gradually replaced other gases with air. This may cause a change in the measurement of the weight over time owing to the difference between the blowing gas density and air density. [1]

1.1.2 Microstructure

Microstructure has a significant effect on the mechanical properties of cellular solids. The microstructure describes the shape and structure of cellular solids at a microscopic level. It describes the internal shape of a cellular solid, including its shape, packing, and porosity.

The cell size is determined by the type of polymer, its flow properties, and air content and is therefore also influenced by the type of blowing agent and the method of production. Some assumptions are that, typically, smaller cells will mean higher stiffness, while larger cells will mean higher pliability.

Cell orientation affect mechanical properties as seen in Figure 1. The orientation of cells is affected by many variables; however, the flow orientation during foaming and solidification is important in large cells with low density. In extruded cellular solids, cells are typically elongated from an ideal circular shape in the extrusion direction. In injection-molded products, elongation in the direction of flow is also evident; however, the problem is more complicated because the flow of polymer into the mould cavity is highly variable and changeable and can be predicted using simulation software such as Moldflow and Moldex. Typically, cells loaded in the direction of elongation (direction of flow) have better properties.
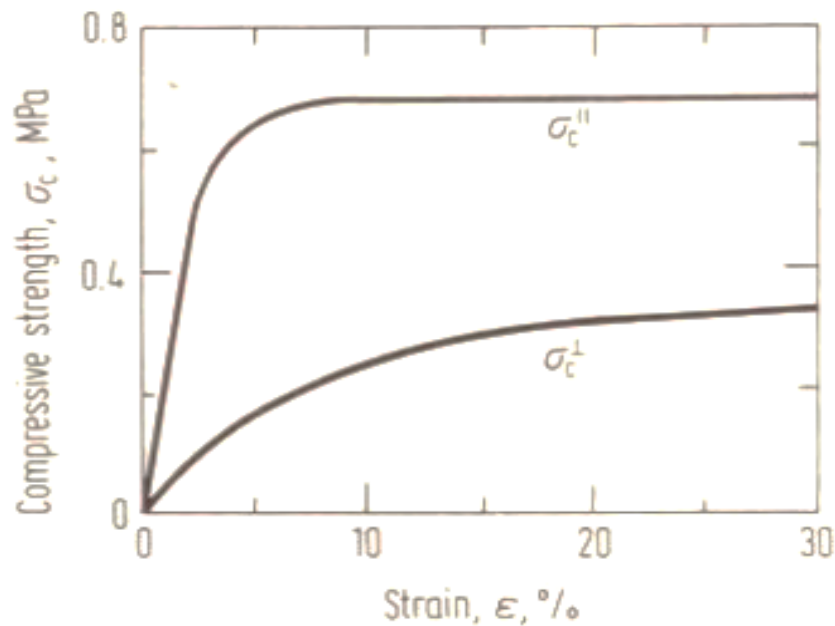
Figure 1 - Comparison of the compressive stress characteristics of PE cellular solid. ‖ – load in the direction of extrusion, ⊥ – load perpendicular to the direction of extrusion. [1]

In terms of microstructure, cells can be considered as separate shapes with thin walls connected by edges. The cell shapes were predicted using different models.

The available theories still fail to predict all the variations in the specific morphological structures that occur in real foams. However, the Harding model, based on the concept of a dodecahedral structure (twelve faces), covers a wide range of structures that occur in reality. In particular, the shapes of the closed cells examined under the microscope closely resembled a draining dodecahedron. The degree of runoff (the amount of polymer that drains from the cell walls into the fins) is higher for lower-molecular-weight polymers than for higher-molecular-weight polymers and lower for rigid foams than for flexible ones. The cell and edge shapes of the open-cell polymer foams resemble an open dodecahedron. Cracks and voids are more common in the cell walls of rigid foams than in those of flexible plastic foams. Most of the cell walls were pentagons, and the remainder were squares and hexagons in approximately equal amounts. The cells of rigid polyurethane foams can have up to 15 walls, and their shapes range from triangular to octagonal.[1][2]

The proportion of open and closed cells also significantly affects the mechanical properties of lightweight polymer materials. Open cells are typically made up of ribs only, as all of the

polymer is shed into these ribs/nodes during molding. In contrast, the closed cells had thin walls between the ribs. The thin walls trap gas in the cells, thereby improving their mechanical properties. The deformation mechanism of closed cells can be remotely compared to the deformation of thin-walled vessels with internal overpressure, where the internal overpressure helps prevent loss of stability. This logic explains why closed cells are preferable from a mechanical point of view.

Closed cells are less permeable to gases and air humidity, do not absorb other fluids or gases, and therefore have better thermal insulation properties. The acoustic insulating properties are better for open-cell materials. Shape of open and closed cell can be seen in Figure 2.
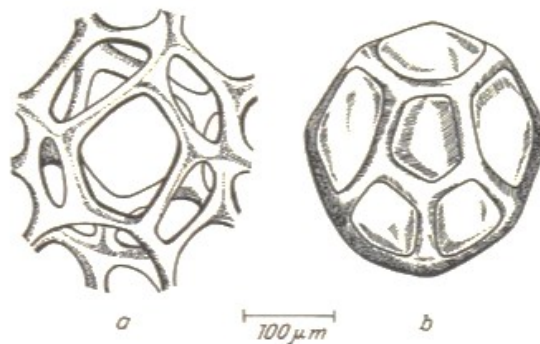
Figure 2 - Example of possible cell shape with a - open pores, b - closed pores.[1]

2 POLYOLEFIN FOAMS (WITH A SPECIAL FOCUS ON POLYPROPYLENE)

Polyolefin foams, such as those made from polypropylene or polyethylene, are characterized by good stiffness, flexibility, resistance to wear and tear, and resistance to various chemicals. Polypropylene foams, like most polyolefin foams, have mostly (90-98 % of closed cells) a closed cell microstructure.

This makes them suitable for applications where buoyancy is required, such as in marine applications. They are also widely used in the packaging industry because of their good shock-absorption capability owing to their closed cells.

Polypropylene foams are divided into two groups: low-density foams and high-density foams, and the limiting density is approximately $\rho = 240$ kg·m^{-3} (the data in the literature vary). Low-density foams are used in acoustic applications with limited use as structural components. High-density foams with good thermal and acoustic insulation properties are typically used as structural foams. In 2021, the global market for polypropylene foam was valued at approximately USD 1.02 billion. It is expected to grow at an estimated CAGR (compound annual growth rate) of approximately 5.9 % over the period 2024-2032, to a value of approximately USD 1.45 billion by 2027.[3]

In recent years, there has been a boom in the automotive industry, as the pressure to recycle cars and their components increases, helping to reduce weight and often the number of parts by starting to be used as structural members, such as in car seats.[4] Pressure on recyclability of car parts is created by European Union, which forces car manufacturers to use recyclable materials for at least 95 % of car weight. [5]

Polypropylene foams can be recycled relatively easily, unlike polyurethane foams (PUR) or polystyrene (PS). This is because polypropylene has a less complex chemical structure, monomer, and, in addition, it is not necessary to use such a high number of additives as stabilizing agents during production, which further complicates recycling.

Further, polypropylene foams are also used as concrete admixtures to reduce the weight and carbon dioxide emissions [6] employed in household applications such as seals, anti-vibration, and structural members.[4]

2.1 Production of polypropylene foams

There are three main methods to produce foam. They can be produced either by injection moulding or extrusion using physical or chemical blowing agents. Each method has its strengths and weaknesses.

2.1.1 Production of foams using injection moulding.

Foams made by injection moulding typically have an outer shell with small, even microscopic, cells, and their core contains larger cells. By using this technology, it is possible to create parts with complex geometries. If simulation software is used, geometry of part, injection mold and other process parameters can by alter in a way, that will utilize unique properties of this technology, such as cell orientation in direction of mold flow and different properties of skin and core. Foaming agents can be physical or chemical in nature. Physical foaming requires additional devices, whereas chemical foaming can produce hazardous gases. This problem is complex and is beyond the scope of this thesis. [7][8]

2.1.2 Production of foams using extrusion machines and chemical foaming agents

Polypropylene and other polyolefins are commonly modified for foaming to alter their rheological properties. Low melt viscosity is a common problem in foaming. Crosslinking slows down the decline in viscosity with increasing temperature. There are many ways to perform foam extrusion using chemical foaming agents, but they can be separated into three parts: sheet formation, crosslinking, and foaming. No commercially available process is continuous, and all require rest. Rests are used to facilitate control of the process, thereby increasing product quality, and allowing for balancing capacities among production steps. [1]

2.1.2.1 Crosslinking foams for extrusion using chemical blowing agent

Crosslinking not only stabilizes bubbles during expansion but also enhances the resistance of the cellular product to thermal collapse. Effect of crosslinking on mechanical properties of PP is shown in Figure 3. This enhanced resistance to collapse is necessary for some applications, such as cable insulation stabilized by radiation crosslinking, which improves the retention of antioxidants (additives against oxidation), as well as increasing the cut-through resistance during soldering. [9]Most commercial modification processes employ radiation (β-rays and X-rays) or peroxide cross-linking. Polyethylenes are suitable for radiation crosslinking; however, polypropylenes are prone to radical decomposition (β

cleavage), making it difficult to crosslink. Therefore, crosslinking of polypropylenes is supported with crosslinking aids.[1]

As crosslinking aid a citric acid (2,2,6,6-tetramethylpiperidin-1-oxyl) can be used[10]. Polypropylene can also be ionically grafted into PP-g-MAH by zinc. This modification is suitable for crosslinking and exhibits a higher melt strength, making it more suitable for foaming. [11]. There are many other crosslinking aids such as vinyl monomers, allyl alcohol derivatives, polybutadiene, and α-olefins. [1]
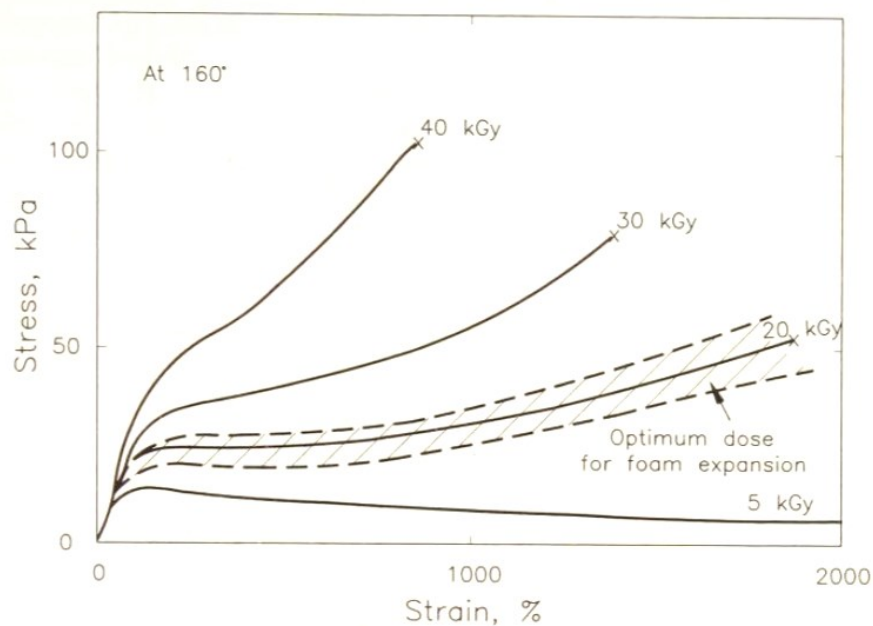

Figure 3 – Biaxial Stress-Strain responses of crosslinked polypropylene at varying radiation doses. [1]

There are three main groups of commercially available blowing agents: organic nitrogen compounds, sodium bicarbonate and its mixtures with citric acid, and sodium borohydride. Among these, only a few are suitable for foaming polyolefins - DNPA (N, N'-dinitro-sopenta-methylene-etramine) and OBSH (4,4'-oxybis (benzenesulfonyl hydrazide)).[1]Widely used is also AC (azodicar-bonamide)[10], which is probably most used chemical blowing agent, because its properties that meet most processing criteria, like decomposition temperature, rate of gas release, gaseous composition, ease of dispersion, storage stability, toxicity, and cost. It decomposes in the temperature range of $200 – 210$ °C but can be modified to start decomposing at approximately 130 °C. One gram of AC is able to decompose into 200-300 cm^3 of gas with composition: 65% - N_2, 32% - CO, 3% CO_2.

2.1.2.2 *Production processes*

There are numerous methods for producing foamed polymers using a chemical blowing agent. They are mainly distinguished by methods of crosslinking (chemical or radiation), oven-type (vertical or horizontal), and supporting methods (clips, PTFE belts, aircushions, etc.).

Production of radiation-crosslinked polypropylene foams can be divided into for steps:

1. Mixing polymer with a blowing agent and other additives (fire retardants and UV stabilizers)

2. Extruding mixture into a solid sheet

3. Crosslinking

4. Heating and foam expansion

The four main types of production are commercially used: Sekisui, Toray, Furukawa, and Hitachi, Table 1.

Table 1 - Commercial cross-linked polyolefin foam sheet processes according to [1]

Process identification	Cross-linking method	Oven type	Supporting method	References
Sekisui	Radiation	Vertical	Gravity, clips	[12]
Toray	Radiation	Horizontal	Molten salt	[13]
Furukawa	Chemical	Horizontal	Mesh wire belt, air cushion	[14]
Hitachi	Chemical	Horizontal	PTFE belt, bars/air cushion	[15]

2.1.3 Production of foams using extrusion machines and physical blowing agents

Compared with the process using chemical blowing agents, this process is simpler. A convectional extruder is modified to mix the blowing agent with the polymer melt. Then the mixture is cooled to the coldest temperature possible, that is, the foaming temperature (mixing temperature $T \approx 180$ °C, foaming temperature $T \approx 140$ °C). After cooling, the mixture is extruded using an extrusion die. The cells nucleate as the melt decompresses in the extrusion die and grow rapidly as the melt leaves the die. [1]

Viscosity is temperature dependent. The first polymer must be melted and supersaturated with a physical blowing agent; in this part, low viscosity is necessary, and high temperature is required to achieve low viscosity. In the expansion process (nucleation, bubble growth, and stabilization), the viscosity must be in the optimal range. A low viscosity results in excessive cell growth, thin cell walls. This led to cell collapse. If the viscosity is too high, the cells will be too small, and the product will not meet the required specifications as shown in Figure 4.

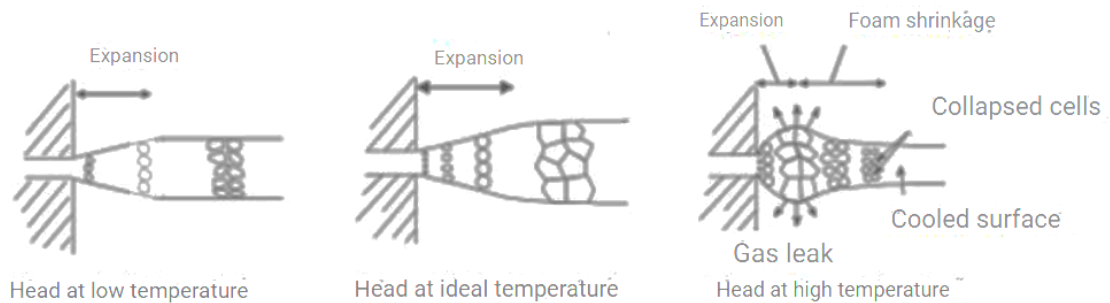For this reason, cooler is added after extruder.

Figure 4 – Effect of extrusion temperature on foaming [16]

The pressure plays a crucial role in foaming. A physical blowing agent is typically gas, cooled, and pressurized enough to become a liquid. In the liquid state, it is added and mixed into the polymer melt. The polymer melt typically occurs at a temperature of $T \approx 180$ °C. However, the blowing agent (gas) remains in its liquid state owing to the high pressure. The pressure must be greater than the critical pressure in all parts of the process; otherwise, nucleation will start too early. As the mixture exits, the die pressure began to decrease when the pressure is lower than the critical one, the blowing agent (gas) begins to expand and creates cells as illustrated in Figure 5.
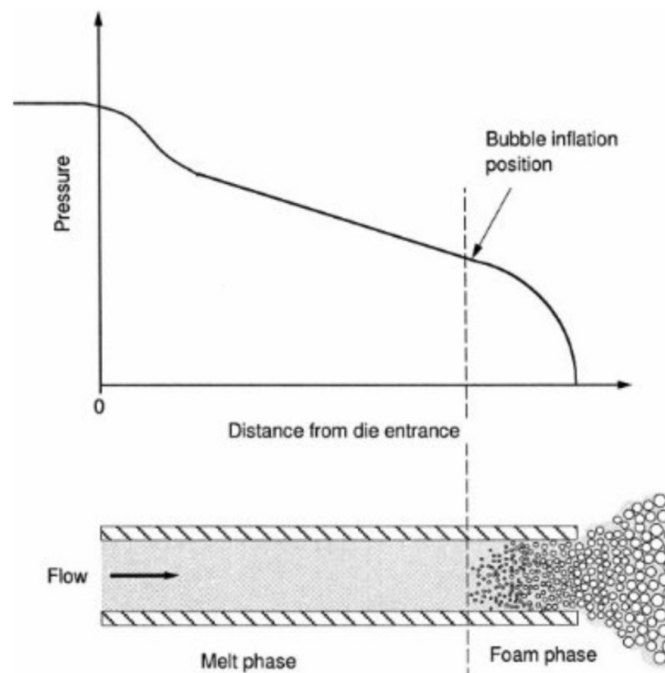
Figure 5 – Pressure profile along extrusion head. [16]

The selection of the blowing agent is challenging. The blowing agent must dissolve in a sufficient quantity of polymer melt under a moderately high pressure; however, at room temperature, it must not dissolve excessively into the cell walls of the expanded polymer. It must also permeate more slowly than air through the cell walls; otherwise, the cells would collapse or shrink. Apart from these physical properties, there are some technological requirements of working with these blowing agents, such as low toxicity, low flammability, low cost, and minimal environmental impact. Historically used blowing agents (hydrochlorofluorocarbons) met all the criteria, but they damaged the ozone layer; therefore, it is not possible to use them anymore. Commonly used blowing agents today are ethane, propane,

n–butane, i-butane, n-pentane, i-pentane, carbon dioxide, and nitrogen. Some are flammable and require special precautions in the working environment. [1]

2.2 Mechanical properties of polypropylene foams in relation to their microstructure

The literature describes the concepts of closed-cell deformation quite well, regardless of the material from which they are made, and there are also studies on the tensile and compressive behavior of polyolefinic and specifically polypropylene foams. However, the behavior of foams in shear, a shear test, is not often described in the literature. To date, no shear test data have been published for polypropylene foam.

A significant obstacle in the measurement of the mechanical properties of foam materials is the large inhomogeneity of the structure, which results in a relatively large dispersion of the measured values compared to the measurement for solid materials.

The properties of polypropylene foams depend on many factors; therefore, it is not possible to say, in general, whether polypropylene foams are more rigid or more elastic. It can be said that they are more elastic than typically rigid foams such as polystyrene foams of the same density. However, they are not as elastic as the latex-based foams. Typical stress-strain curves for different material are shown in Figure 6.[17]
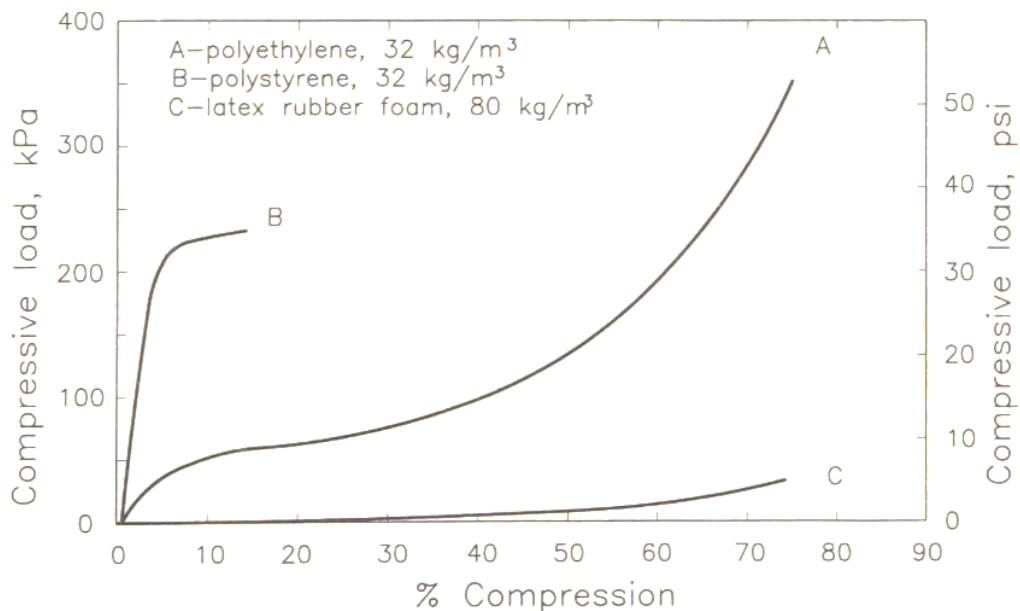
Figure 6 - Comparison of the compressive properties of foams made of different materials.

2.2.1 Mechanical properties of polypropylene foams in compression and tension

As shown in Figures 7 and 8, there are three distinct regions of the tensile curve for polyolefinic foams, including polypropylene foam. The first region is the region of elastic deformation, in which there is rotation around the edges and cell walls stretch/compress, and the stress gradually increases until it reaches its maximum. After the linear elastic region stress reached the critical limit, a loss of stability occurred. The edges and cell walls buckled, and the deformation continued to increase, whereas the applied force remained almost the same. In closed calls, the force slowly increases in this region because of the compression of gas inside the closed cells. This region is known as the plateau (plato). In this region, plastic deformation at the cell edges starts to occur, and then the stress starts to rise sharply. This is caused by the cell being so deformed that the opposite cell walls touch and thus can no longer rotate around the cell edges, but pure tension/compression occurs, similar to an unfoamed material. Damage occurred after the initiation of the first crack. In general, these regions can be described as the linear elasticity, collapse, and densification regions.

Young's modulus of elasticity E is equal to the slope of the line in the first region, that is, in the region of linear elasticity. If the foam is to be used as a structural foam, the limit of the maximum stress, which is bounded by the initial transition to the plastic region, is important.[17]
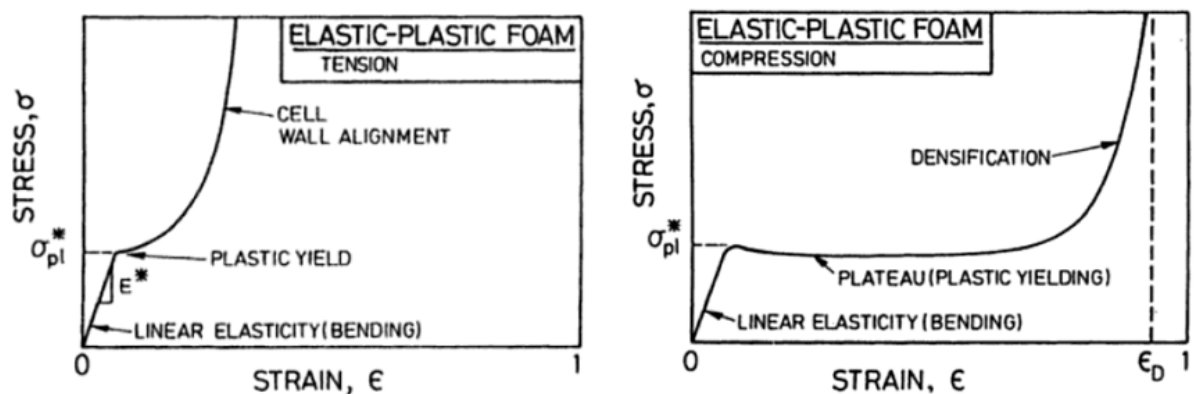

Figure 7 - Illustration of compressive and tensile deformation regions for a general elastic-plastic foam in tensile and compression tests.[17]
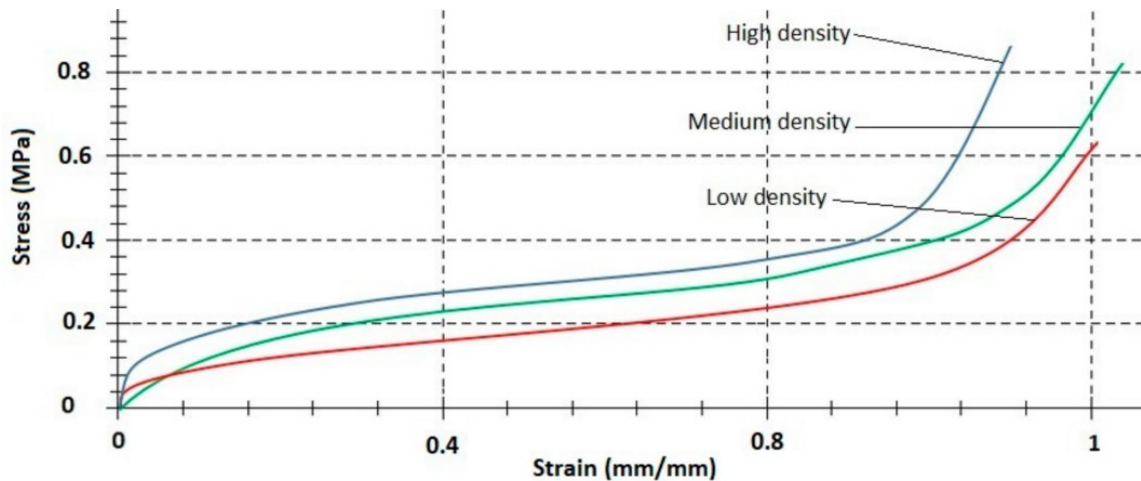
Figure 8 - Compression test curves for polypropylene foams of various densities: low $\rho =$ 20 kg·m^{-3}; medium $\rho =$ 80 kg·m^{-3}; high $\rho =$ 200 kg·m^{-3}.[18]

2.2.2 Mechanism of linear elastic deformation of general foam with closed cells

At least two constants are required to describe the isotropic behavior of foams: Young's modulus E, shear modulus G, bulk compressibility modulus K, and Poisson's number ν. At least five constants are required to describe an axisymmetric (orthotropic) structure, and nine constants are required for generally anisotropic foams: elasticity modulus in three directions, E_x; E_y; E_z, shear modulus G_{xy}; G_{xz}; G_{yz}, Poisson's ratios ν_{xy}; ν_{yz}; ν_{xz}.

The deformation mechanism for closed cells starts with small deformations by the rotation and bending of walls and nodes; gradually, there is a simple tension/pressure in the cell walls.

The deformation mechanism is shown schematically in Figure 9. In real cells, the shape is far more complicated, but for understanding the basics of foam mechanics, this model is perfect and there is no need to use complicated cell models, such as dodecahedrons.
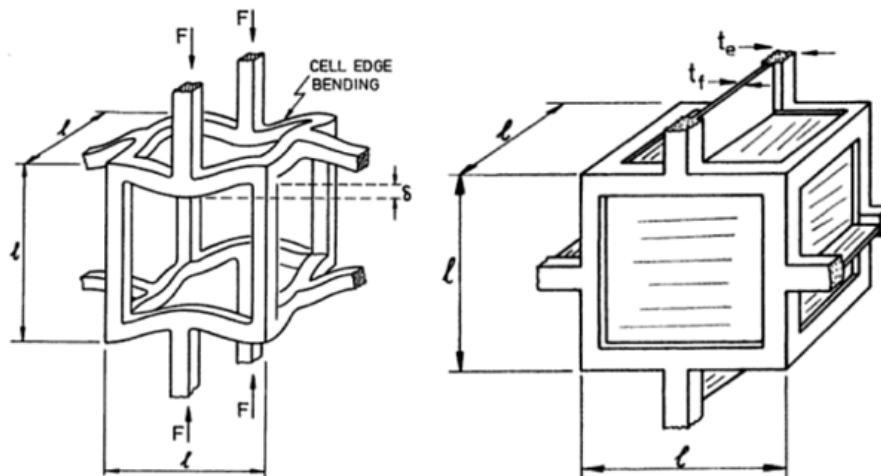

Figure 9 - Idealized cell shape sketch. Open cell on the left, closed cell on the right.[17]

Equations 1 and 2 provide a basic understanding of the mechanical properties and their relation to cell shape and size. However, they do not cover the membrane stresses in the cell walls. The bending stiffness of the cell walls and the effect of the enclosed gas pressure change, if the pressure inside the cell is atmospheric before deformation, are negligible in linear elastic deformation [17]:

$$E^* = \frac{\sigma}{\varepsilon} = \frac{C_1 E_s I}{l^4} \tag{1}$$

where:

E^* - foam modulus of elasticity

E_s – unfoamed polymer modulus of elasticity

ε – strain δ/l

δ – displacement

l – beam length (edge length)

F – loading force

I – second moment of area

C_1 – geometrical constant of proportionality (data shows that $C_1 \approx 1$) [17]

Then one can write:

$$\frac{E^*}{E_s} = C_1 \left(\frac{\rho^*}{\rho_s} \right) \tag{2}$$

where:

E^* - foam modulus of elasticity

E_s – unfoamed polymer modulus of elasticity

C_1 – geometrical constant of proportionality

ρ^* - foam density

ρ_s – unfoamed polymer density[17]

The membrane stresses induced by the stretching or compression of the walls caused by the rotation of the nodes and the deformation of the cells can be described by Equations 3 and 4. The deformation mechanism is illustrated in Figure 10. When force F is applied, deformation δ occurs; thus, the work done by this force in the linear elasticity regime is 1/2 $F\delta$. The bending stress in the cell walls is given by 1/2 $S\delta^2$, where S ($S \approx E_s I/l^3$) is the wall bending stiffness. The wall stretching stress can be determined as $1/2 E_s \varepsilon^2 V_f$, where ε ($\varepsilon \approx \delta/l$) is the wall stretching strain, V_f ($l^2 t$) is the wall volume:

$$\frac{1}{2}F\delta = \alpha\frac{E_S I \delta^2}{l^3} + \beta E_S\left(\frac{\delta}{l}\right)^2 l^2 t_f \tag{3}$$

where:

E_s – unfoamed polymer modulus of elasticity

δ – displacement

l – edge length

t_f – cell wall thickness (see fig. 6)

F – loading force

I – second moment of inertia

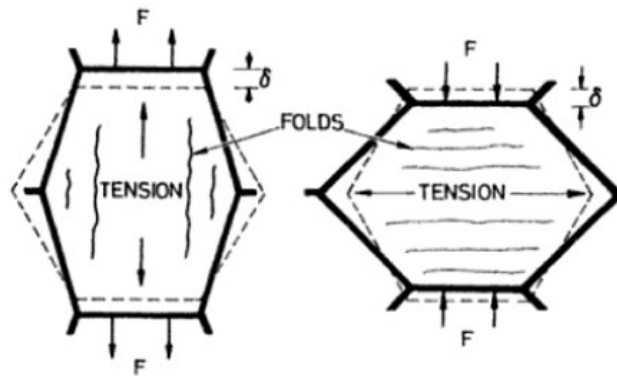α and β are proportionality constants. [17]

Figure 10 - Idealized deformation of closed cells in tension and compression.[17]

If we plug $I \approx t_e{}^4$ and $E^* \approx (F/l^2)/(\delta/l)$ in Equation 3, we obtain an equation of the form:

$$\frac{E^*}{E_S} = \alpha'\frac{t_e^4}{l^4} + \beta'\frac{t_f}{l} \tag{4}$$

where:

E^* - foamed modulus of elasticity

E_s – unfoamed polymer modulus of elasticity

t_f – cell wall thickness

t_e – cell edge thickness

l – beam length (edge length)

α', β' – constants of proportionality [17]

2.2.3 Mechanism of non-linear elastic deformation of general foam with closed cells

Linear elasticity typically describes a small area of foam deformation, up to about 2 %. However, polypropylene foams and other elastic foams are reversibly deformable - elastic beyond this area, but the stress versus elongation curve is no longer elastic. Therefore, the term nonlinear elasticity is used. This is the so-called plateau region. There is little or no increase in stress despite increasing elongation. This is sometimes incorrectly referred to as the plasticity region. Schematic sketch of buckled cell is shown in Figure 11.
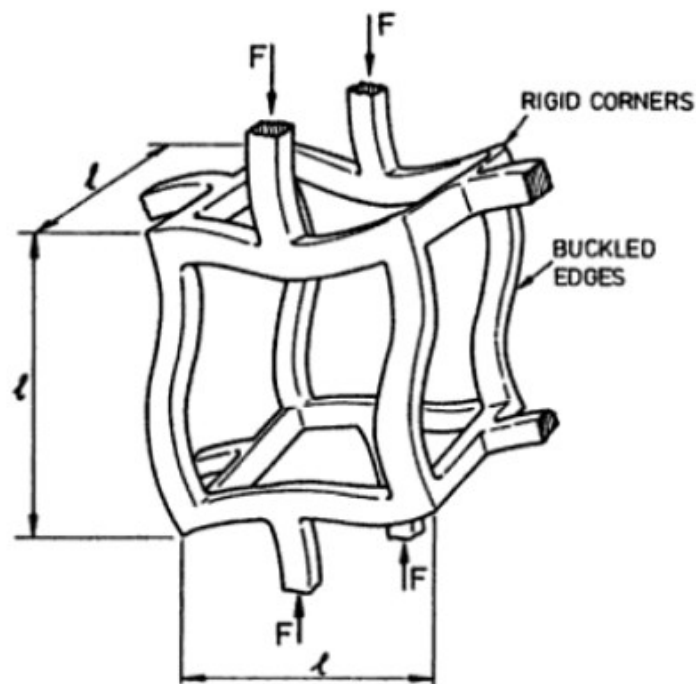

Figure 11 – Idealized mechanism of cell loss of stability in elastic region. [17]

The critical load, when cell collapse occurs, can be calculated for foams by neglecting the influence of cell walls using Euler's relations

$$F_{crit} = \frac{n^2 \pi^2 E_s I}{l^2} \tag{5}$$

where:

F_{crit} – critical strength

n - the degree of constraint at the end of the elements (based on Euler's relations for the buckling of thin members)

E_s – unfoamed polymer modulus of elasticity

l – edge length

I – second moment of inertia [17]

If the load reaches a critical level, the cells collapse, which initiates the collapse of surrounding cells. The stress at which this occurs is referred to as critical and can be written as:

$$\sigma_{crit} \approx \frac{F_{crit}}{l^2} \approx \frac{E_S I}{l^4} \tag{6}$$

where:

σ_{crit} – critical stress

F_{crit} – critical strength

E_s – unfoamed polymer modulus of elasticity

l – edge length

I – second moment of inertia [17]

When $I \approx t^4$ and $\rho^*/\rho_s = (t/l)^2$ is plugged, the resulting equation is

$$\frac{\sigma_{crit}}{E_S} = C_4 \left(\frac{\rho^*}{\rho_S}\right)^2 \tag{7}$$

where:

σ_{crit} – critical stress

E_s – unfoamed polymer modulus of elasticity

C_4 – geometrical constant of proportionality

ρ^* - foam density

ρ_s – unfoamed polymer density[17]

When stability is lost, the contribution from wall deformation is not significant, as they put almost no resistance to deformation after they lost of stability. However, the effect of the confined gas in the cell is more dominant in this regime, resulting in a slight increase in stress in the plateau region. In open cells, this increase was not observed. The pressure in the cell during deformation can be expressed as:

$$p \approx \frac{p_0\,\varepsilon}{1-\varepsilon-\left(\rho^*/\rho_S\right)} \tag{8}$$

where:

p – gas pressure in cell after deformation

p_0 – gas pressure in cell before deformation, typically $p_0 = p_{atm}$

ρ^* - foam density

ρ_s – unfoamed polymer density

ε – strain [17]

We can add this to Equation 7 and obtain the relationship for the critical stress as follows:

$$\frac{\sigma_{crit}}{E_S} = C_4 \left(\frac{\rho^*}{\rho_S}\right)^2 + \frac{p_0\, \varepsilon}{1 - \varepsilon - \left(\rho^*/\rho_S\right)} \qquad (9)$$

where:

σ_{crit} – critical stress

E_s – unfoamed polymer modulus of elasticity

C_4 – geometrical constant of proportionality

p_0 – gas pressure in cell before deformation, typically $p_0 = p_{atm}$

ρ^* - foam density

ρ_s – unfoamed polymer density

ε – strain [17]

For polyolefin foams, the coefficient C_4 typically reaches the value ranging from 0.03 to 0.05. This correlated well with the measured data as illustrated in Figure 12. [17]
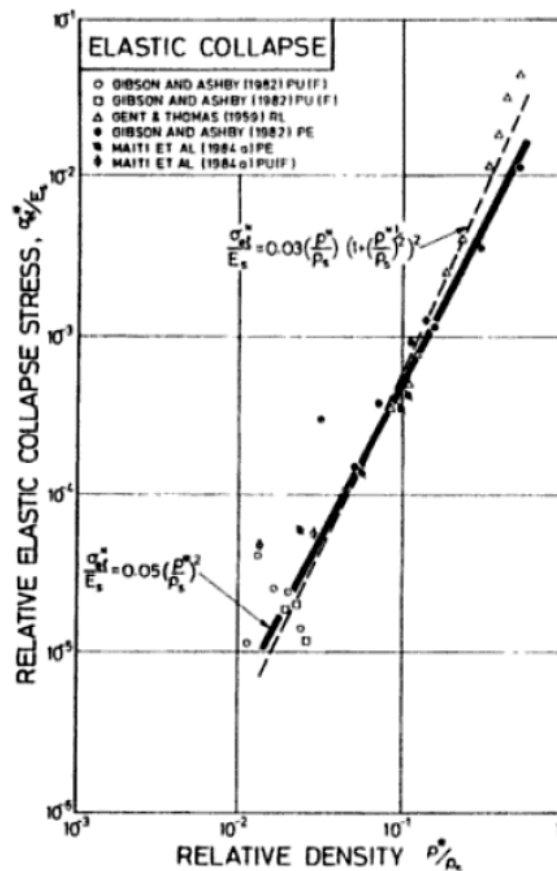

Figure 12 - Dependence of relative critical stress on relative density. The data points represent measured values from pressure tests on polyethylene (PE) and polyurethane (PUR) foams with open cells (unfilled symbols) and closed cells (filled symbols). The curves are fitted with Equations 7 (solid line) and Equation 9 (dashed line) [17]

2.2.4 Mechanism of plastic deformation of a closed-cell general foam cell

Foams made from materials with plastic yield points (rigid polymers, metals, etc.) collapse plastically when loaded beyond the linear elastic regime. Plastic collapse, such as elastic buckling, provides a long horizontal plateau to the stress–strain curve, but the strain is no longer recoverable, as in the nonlinear elastic regime. [17]

When force F is applied in the middle of the beam element bending moment, equivalent to $M = F(l/2)$, it causes stress at the cell edges. The resulting bending stress in linear elasticity has a typical linear distribution – maximum stress at the ends and zero stress at neutral axes. When the force is increased, the maximum stress remains the same, but the regions where the stress is maximum continue to deform plastically. The stress was not distributed linearly, but as shown in Figure 13. After the stress in almost the entire cross section reaches the maximum edge, it becomes plastic. An idealized model of cell edges becoming plastic is shown in Figure 14.
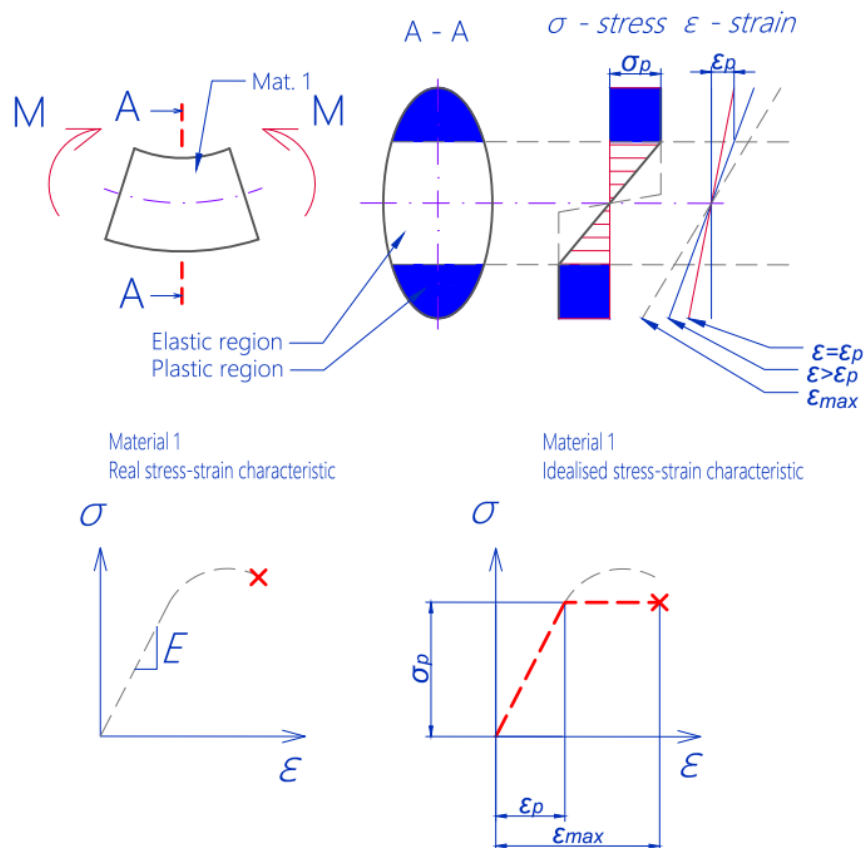

Figure 13 – Elastic and plastic regions in cross section of a polymer. As in ref. [19]
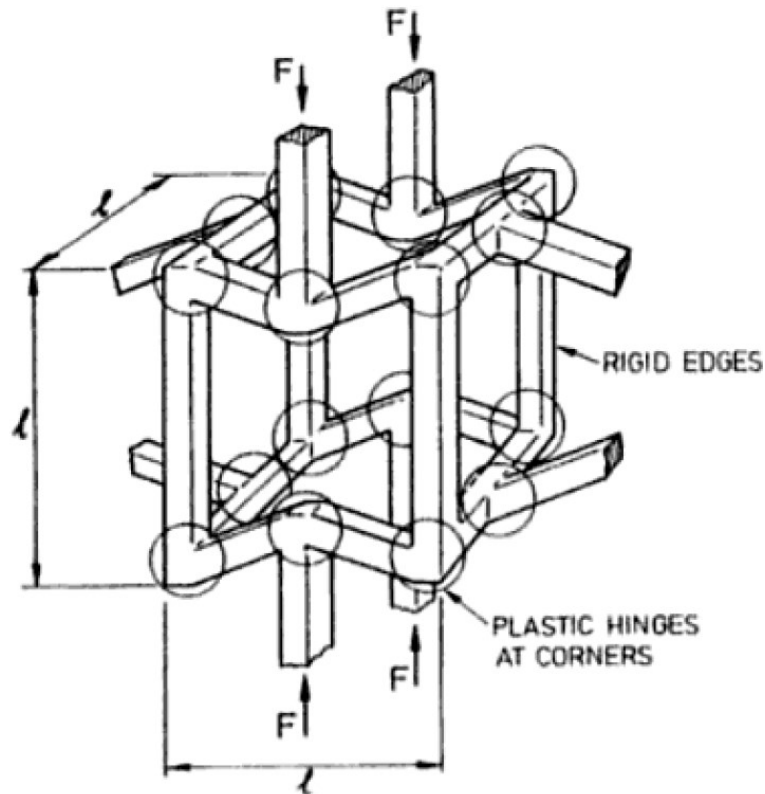
Figure 14 - Idealized mechanism of cell plastic deformation. [17]

Plastic moment for beam with square cross section can be written as:

$$M_p = \frac{\sigma_{ys} t^3}{4}$$ (10)

where:

Mp – plastic bending moment

σ_{ys} – yield strength of cell wall material

t – beam thickness [17]

Maximum plastic stress can be written:

$$\sigma_{pl} = \frac{M_p}{l^3}$$ (11)

where:

Mp – plastic bending moment

σ_{pl} – stress when plastic deformation occurs

l – beam length [17]

If $\rho^*/\rho_s = (t/l)^2$ is substituted into Equation 11, the following equation is obtained [17]:

$$\frac{\sigma_{pl}}{\sigma_{ys}} = C_5 \left(\frac{\rho^*}{\rho_s}\right)^{3/2} \tag{12}$$

where:

σ_{ys} – yield strength of cell wall material

σ_{pl} – stress when plastic deformation occurs

C_5 – geometrical constant of proportionality

ρ^* - foam density

ρ_s – unfoamed polymer density [17]

Foams with closed cells have membranes that span their face. The plastic collapse causes the membrane to be in the compression direction. Because they are thin, the force required to crumple them is small. However, at some angles, the membranes are stretched, and the work of plastic deformation contributes significantly to the yield strength of the foam.

The plastic displacement δ of one cell allows the applied force F to work $W=F\delta$ angle of rotation of the plastic hinges is proportional to δ/l and the plastic work performed by rotating these hinges is proportional to $M_p \, \delta/l$. The cell face is stretched by distance, which is proportional to the deformation δ, deformation does work, which scales as $\sigma_{ys}\delta t_f l$. Equating these gives:

$$F\delta = \alpha M_p \frac{\delta}{l} + \beta \sigma_{ys} t_f l \delta \tag{13}$$

where:

σ_{ys} – yield strength of cell wall material

t – beam thickness

l – beam length

δ – displacement

F – loading force

α, β – constants [17]

2.2.5 Relation between shear modulus and modulus in compression/tension

The shear modulus was calculated using a formula similar to that of the Young's modulus. If shear stress is applied, the walls respond again by bending. The bending deflection is defined as Fl^3/E_sI -, and the modulus G is given by the ratio τ/γ, which corresponds to F/l^2 and δ/l, respectively:

$$G^* = \frac{\tau}{\gamma} = \frac{C_2 E_s I}{l^4} \tag{14}$$

where:

G^* - foam shear modulus

E_s – unfoamed polymer modulus of elasticity

γ – strain, given by the relation δ/l

δ – deflection

l – edge length

F – loading force

I – second moment of inertia

C_2 – geometrical constant of proportionality [17]

This equation provides approximation of shear modulus, but shear modulus can be affected by many variations such as cell orientation etc., therefor it is always better to measure the actual shear modulus using standardized test.

3 SANDWICH STRUCTURES

Sandwich structures are composite structures composed of two or more materials (Figure 15). Typically, a thick lightweight core material creates a distance between the skin materials and the thin skin material, which provides stiffness and strength. This combination resulted in a light but stiff structure.

Figure 15 – Sandwich structure.

They are typically used in specialized high-end applications, and their design is tailored for applications such as structural parts of aircrafts, race cars, spaceships, and satellites.[20] However, with increasing pressure to reduce weight and emissions, they are also beginning to emerge in everyday applications such as buses and other forms of public transport. Furthermore, sandwich structures are utilized as panels for halls and roofs, where although they do not serve as structural members, they provide sound and thermal insulation and are rigid and highly resistant to weather conditions if designed and installed correctly. [21]

There is wide range of materials for sandwich structures, Figure 16. Cores are typically made of light materials such as foams (polymeric, metallic [22]), honeycombs (polymeric, metallic, paper, balsa wood etc.), corrugated solids (metallic, polymeric) or solids (balsa wood, cork etc.) Although core mechanical properties are important, the primary factor resisting deformation in a sandwich structure is the skin material. Nevertheless, the core material must have good mechanical properties, mainly in terms of shear and good resistance to compression. The core is firmly bonded to the skin material; thus, good adhesion is a desirable property, based on factors such as the polar surface properties of polymers, specific roughness of foams, and addition of mineral additives. Adhesion of core and skin is directly linked to mechanical properties of sandwich structure.[23]
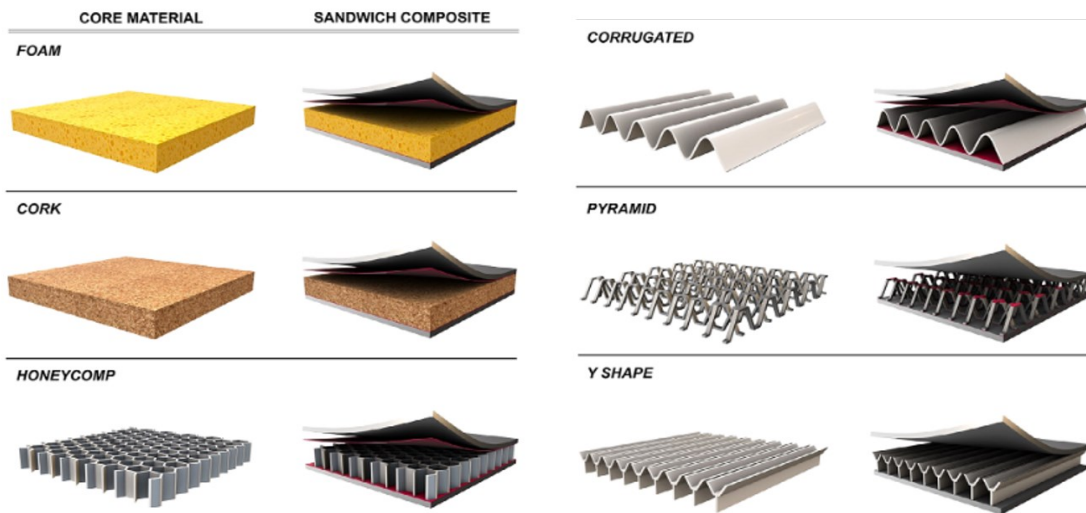
Figure 16 – Different types of sandwich structures.[24]

Other desirable properties of core materials include material are good elasticity, and thus, brittle materials are generally not used for these applications. Flame retardancy is also required for certain applications such as construction materials and automotive components, to ensure safety and compliance with regulatory standards. Good recyclability and environmental impact are the criteria that are increasingly significant in the process of choosing materials, although foams and sandwich structures still pose great challenge for recyclability.

The skin material is typically thin but stiff and strong, as it is a primary load-bearing element. Typical materials include thin sheets of metals (aluminum or steel) and thin sheets of composites reinforced with long fibers (glass or carbon fibers). However, the range is much wider. The main requirements for these materials are good compressive/tensile load characteristics, which are their main loading modes. During compression, the skin is often subjected to buckling. They should also have good environmental resistance to moisture, temperature changes, UV radiation, and ozone. They are often exposed to these influences, unlike core materials, which are protected from them.

Some sandwich structures utilize additional adhesive layers for better bonding of the core and skin materials. It is used mainly for materials with bad or very bad adhesion, such as a combination of aluminum skin and balsa core, or thermosetting polymers and honeycomb structures. The adhesion layer needs to be relatively cheap, able to maintain its properties in the desired temperature range, and safe. An adhesive can be applied in the form of a liquid or film. The working time of the chosen adhesive is crucial; a longer working time implies a longer production time.

3.1 Types of sandwich structures

Sandwich structures can be made in many ways. Here are some common examples.

3.1.1 Thermoset resin-based methods

There are multiple methods that use thermosetting resins. They are characterized by good temperature- and chemical-stability. The bond between the skin and core material is typically very strong. Hazardous chemicals are often used, and the process takes hours to produce one part because of the long curing time used in resins. Curing is often performed at elevated temperatures, which further increases the price of the final part.

Hand layup is one of the oldest, easiest, and most commonly used methods for fabricating composite laminate structures.[25]

This method involves using continuous fibers in various forms, such as unidirectional, woven, knitted, or stitched fabrics, along with different fiber orientations and laminar layers as needed. The matrix was applied over the fiber layers using a roller, and excess resin was removed. A releasing agent was applied to the mold surface to prevent it from sticking. Despite being cost-effective and suitable for large structures, skilled labor is necessary to ensure quality. This method is typically limited to structural applications such as boat hulls and vessels owing to defects that can be induced and are extremely difficult to identify. [26]

Vacuum infusion process utilizes uniform atmospheric pressure to consolidate the resin and fibers in the laminate. The laminate was sealed in an airtight bag and air was evacuated using a vacuum pump to ensure uniform pressure. Components, such as peel ply and releasing agents, aid in perfect bonding between the layers of the laminate and prevent the resin from sticking to the mold or other surfaces. Sealant tapes ensure a tight seal, whereas the bleeder layer removes the excess resin. Curing at a defined temperature completes the process, resulting in high-quality parts with good layer adhesion and minimal emission. However, they are not suitable for high-volume production and require expensive curing ovens. Various fiber reinforcements have been tested to enhance their properties.[27]

Autoclave molding, an extension of the vacuum infusion process, produces precise high-quality parts that are unattainable through standard methods. This advanced process applies high pressure and temperature to compact the composite, ensuring void-free results. Utilizing composite prepregs lined with fibers for the desired thickness, the material was pressurized onto a molding plate and hardened to shape. Peel plies and breather cloth aid in the process and are later vacuum bagged to remove air. The parts were cured in an autoclave.

Although effective, this method is costly, time-consuming, and mainly used in aerospace and military applications. Part quality depends on the applied pressure, curing conditions, and materials used.[28]

The *pultrusion* process is a high-volume method for fabricating composites, involving continuous fiber lamination to achieve uniform cross-section parts, Figure 17. The process is similar to extrusion; however, it differs in that the parts are pulled rather than pushed. It begins with fiber impregnation, followed by resin removal for proper bonding. The preform die shaped the composites, which were then cured in heating dies and cut to the desired dimensions. This automated process enables quick production of laminates with a high fiber volume fraction, minimal labor, and improved properties. Part quality depends on the resin viscosity, fiber volume fraction, temperature profiles, and pultrusion speed. However, only constant cross-sections can be produced.[29]
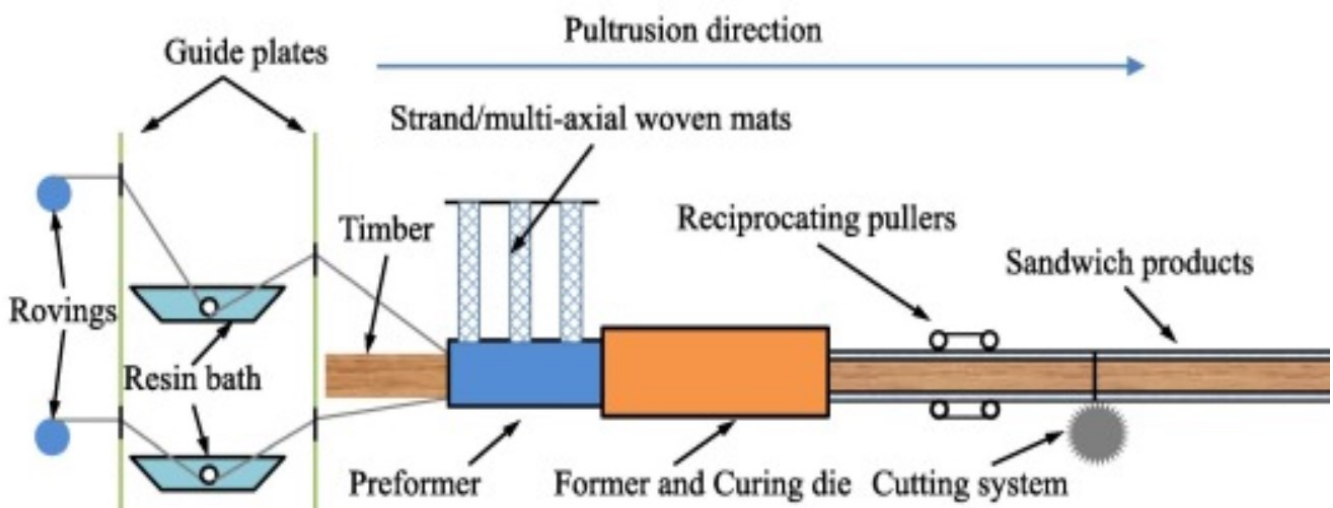

Figure 17 – Schematic example of pultrusion sandwich line. [30]

3.1.2   Thermoplastic based methods

Thermoplastic sandwich structures can be joined using thermosetting adhesives, such as dual-component glues. However, this process is time consuming. To save time, the core and skin can be bonded using heat, which is faster. Bonding using heat takes: minutes, while joining with the help of thermosetting adhesives reaches: low tens of hours, thus dramatically increasing production.

Thermoplastic-based sandwich structures can be fabricated from variety of materials, the most common of which are PEEK, PP, HDPE, PEI, and PA. Different core and skin materials can be combined. [31]

Because thermoplastic sandwich structures are typically produced in high volumes, their components are typically made using extrusion. Injection moulding is applicable for complex geometries and lower volume productions.

3.1.2.1   Simple shapes

Extruded foams or honeycombs are typically used as core materials. Skin materials are typically thermoplastic polymers such as PP and PEEK reinforced with continuous fibers.

Skin and core materials can be bonded using heat and pressure. The heat softens the thermoplastic materials, allowing them to flow and intermingle at the interface, while the pressure ensures intimate contact between the skin and core, promoting the adhesion and structural integrity of the sandwich composite.

For polymers with poor adhesion (polyolefins) or structures with small contact areas (honeycomb core), an adhesive layer is typically used, which requires a lower melting temperature than other materials of the structure.

It is also possible to insert reinforcing fibers into skin materials using the thermoforming – dual-step method. [32] Although this process is simple, many variables need to be considered to create a high volume of products with consistent quality. In a thermoforming press, UV heaters preheat the core and skin materials separately. They are then brought together and bonded using pressure and heat. Pressure and heat are provided by the heated mold plates of the thermoforming press. However, tight processing windows exist. Specific amounts of heat must be applied to skin and core materials. This depends on the power of preheating, preheating time, temperature of the mold plates, and contact time between the heated mold plates and material. If there is too much heat, the materials can start to flow, and the core

material collapses during pressure bonding. If there is insufficient heat, the bond may fail prematurely or may not be created at all. The heat and pressure must be evenly distributed; otherwise, the final structure is not homogeneous and may include defects. Heat distribution can be negatively affected by workshop conditions such as, air movement and room temperature changes. The pressure distribution may be negatively affected by local inhomogeneity in the core material.

The influence of pressure and temperature on the mechanical properties of the resulting product was investigated; however, no relevant data were found. [32]Each combination of materials behaves differently, and the optimal processing conditions must be found for each separately. Every type of material has its own challenges.

3.1.2.2 *Complex shapes*

For special applications, injection molded skins are made and between them is injected foam.

With in-mold foaming, foam cores of complex shapes can be fabricated without significant material waste. Moreover, inserts, such as connecting elements and ribbings, can be integrated into foam cores during foaming. Furthermore, foam cores with predefined density distributions, such as high and low densities in potentially highly and lowly stressed areas, respectively, can be produced with in-mold foaming. Finally, when foaming occurs between two skins, a fusion bond between the skins and foam core can be generated (especially when the skins and foam core are based on the same matrix), leading to high bonding strengths.[33]

3.1.3 3D printing -based methods

Additive manufacturing offers an innovative approach for producing sandwich structures. This technology enables the creation of complex composite structures by gradually depositing material layer-by-layer according to computed models (FFF method). The advantages of 3D printing are the efficient use of materials and the ability to create intricate geometries with minimal waste. Thermoplastic polymers, such as ABS or PLA, are predominantly used. Thus, it is possible to print foamed polymers that can be used as light-core structures. For printing foamed polymers HDPE, PEI and PA are typically used.[34]

Polymers reinforced with fibers can be also printed using the FFF method. Typically, these are short fibbers with a length of approximately 10 mm. However, it is possible to incorporate long fiber reinforcements for superior mechanical properties achievable using the FFF method. [35]

3.2 Mechanics of sandwich structures

Sandwich structures typically have rather good mechanical properties with respect to their weight. This is mainly due to pure bending and resistance to buckling. Sandwich structures are inhomogeneous, and their mechanics differ vastly from those of homogenous structures.

Analysis of beam sandwich structure

The theory is similar to the ordinary engineering beam theory, with the addition of shear stresses and transverse shear deformations. This theory is often referred to as Timoshenko beam theory. For simplicity, all beams are assumed to have a unit width, and thus, all loads, bending moments, stiffnesses, etc., are also given per unit width.[36]Mechanics of beam structures is best understood on example of pure bending.

3.2.1 Mechanics of pure bending – four-point bend test

Assuming perfect joining of the individual components of the composite rod during pure bending, the imaginary fibers experience elongation or compression. Fibers that are neither stretched nor compressed are referred to as the neutral planes. The neutral plane coincides with the neutral axis and serves as the origin of the *y*-axis in the coordinate system. Bernoulli's hypothesis, asserting that the cross section remains planar during bending, allows for the formulation of an equation describing the strain of an imaginary fiber positioned at a distance y from the neutral axis [36]:

$$\varepsilon\,(y,z) = \frac{1}{r}y \tag{15}$$

where:

ε – deformation

r – radius of curvature of the neutral plane

y – distance of hypothetical fiber from neutral axis.

Mechanics of general inhomogeneous structure in pure bending can be seen in Figure 18.
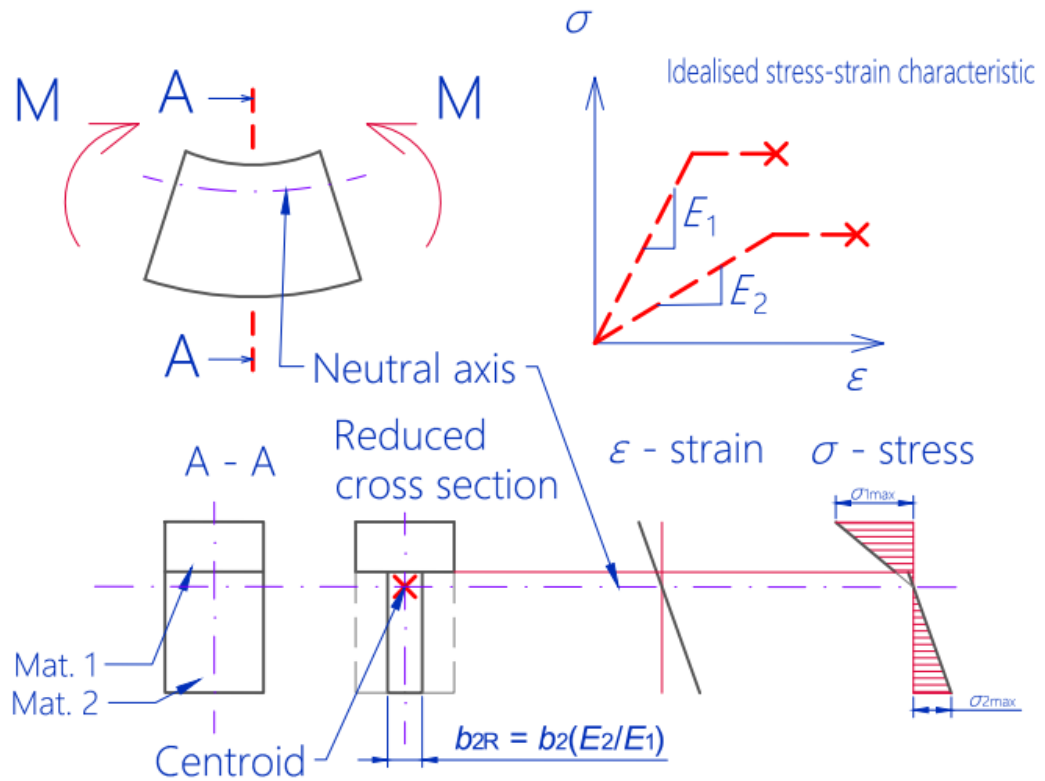
Figure 18 -Behavior of general inhomogeneous composite structure in pure bending. As in ref. [19]

For this theory to hold, there must be symmetry in the geometrical shape and structural properties about the y axis.

Bending moment is in cross-section balanced by normal stresses [36]:

$$M = \int_{(S)} dN \cdot y = \int_{(S)} \sigma(y) \cdot y \cdot dS \qquad (16)$$

where:

M – bending moment

N – normal force

y – distance of hypothetical fiber from neutral axis

S – cross-section area

$\sigma(y)$ – stress based on position in y

In linear elasticity region Hook´s law holds:

$$\sigma(y) = E(y) \cdot \varepsilon(y) \tag{17}$$

where:

$\sigma(y)$ – stress based on position in y

$E(y)$ – elasticity modulus based on position in y

$\varepsilon(y)$ – strain based on the position in y

Substituting the deformation equation (Equation 15) and physical equation (Equation 17) to the equilibrium equation (Equation 16), the equation for the general bending of a non-homogenous structure is derived as follows [36]:

$$\frac{1}{r} = \frac{M}{\int_{(S)} E(y) y^2 dS} = \frac{M}{K} \tag{18}$$

where:

M – bending moment

y – distance of hypothetical fiber from neutral axis

S – cross-section area

r – radius of curvature of the neutral plane

$E(y)$ – elasticity modulus based on position in y

K – flexural rigidity

From this equation, it is evident that the flexural rigidity is a key factor in the design of sandwich structures. To calculate the flexural rigidity, we need to understand the theory of reduced cross-sections (sometimes referred to as equivalent cross-sections [37]). The structure is split into individual elements based on their mechanical properties (Young modulus E). Sandwich structures are typically split into two or three different elements: the core, skin, and sometimes adhesion layers. However, the adhesion layers are often neglected. Reduced cross section general nonhomogeneous structure can be seen in Figure 18, reduced cross section of general sandwich structure is illustrated in Figure 19.
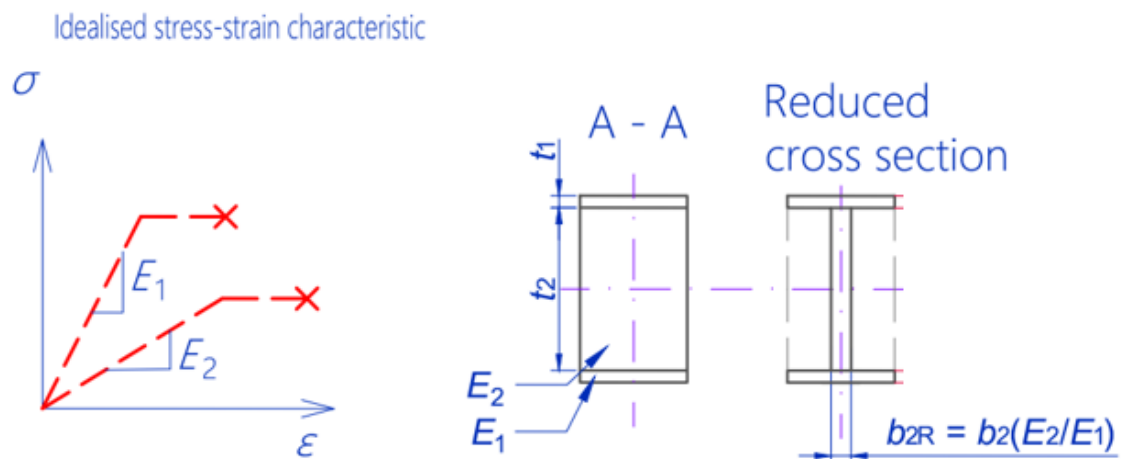
Figure 19 – Reduced cross section of general sandwich structure. As in ref. [19]

After splitting, reduced cross-sections can be calculated using following equation:

$$b_{iR} = \frac{E_i}{E_1} b_i \tag{19}$$

where:

b_R – reduced width

b – original width

E_i – flexural modulus of element

E_1 – flexural modulus of stiffest element (typically skin) [38]

After the reduced cross sections are calculated, the centroid and second moment of inertia can be evaluated. The neutral axis is located at the centroid.

Flexural rigidity for general bending of non-homogenous structure can be written as:

$$K = \sum_{i=1}^{n} E_i J_i \tag{20}$$

where:

K – flexural rigidity

E – elasticity modulus

J – second moment of area [38]

Second moment of area is apparently given by:

$$J_i = \int_{(Si)} y^2 dS_i \tag{21}$$

where:

J – second moment of area

y – distance of the centroid from the neutral axis

S_i – area

The second moment of area for the entire reduced cross-section (J_R is the sum of all the individual moments of area J_i.

Flexural rigidity for sandwich structure with two symmetric skins and core – as seen in Figure 20, can be written as:
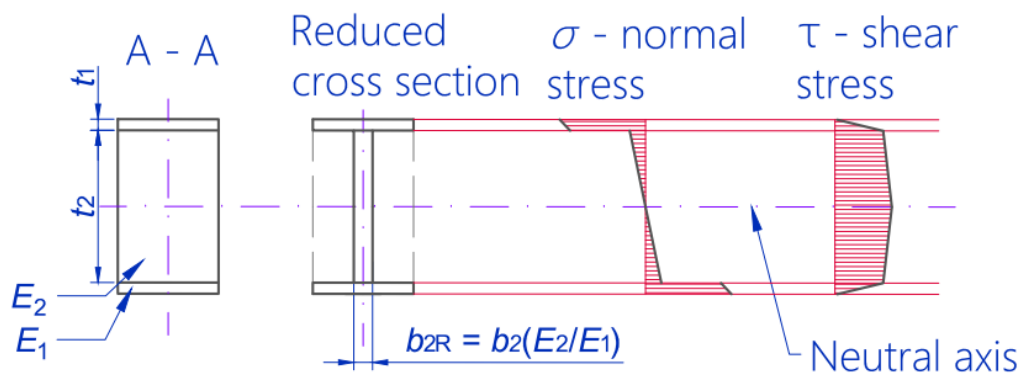
Figure 20 – Symmetrical sandwich cross-section with key annotations illustrating stress distribution for pure bending. As in ref. [19]

$$K = \int E y^2 dy = \sum_{i=1}^{n} E_i J_i = \frac{E_1 t_1^3}{6} + 2E_1 t_1 \left[\frac{d}{2}\right]^2 + \frac{E_2 t_2^3}{12} = \frac{E_1 t_1^3}{6} + \frac{E_1 t_1 d^2}{6} + \frac{E_2 t_2^3}{12} \tag{22}$$

$$= 2 \cdot K_1 + K_0 + K_2$$

where:

K_0 – bending stiffness of the skins about the neutral axis

K_1 – bending stiffness of the skins about their individual neutral axes.

K_2 – bending stiffness of the core

d – distance of centroids of the skins ($d=t_1+t_2$) [36]

This expression can be further simplified for sandwich structures with thin skins or weak core.

Criteria for thin skin approximation:

$$\frac{d}{t_1} > 5.77 \text{ alternatively } 3 \cdot \left(\frac{d}{t_1}\right)^2 > 100 \tag{23}$$

where:

t_1 – skin thickness

d – distance of centroids of the skins ($d=t_1+t_2$) [36]

Criteria for weak core approximation:

$$\frac{6E_1 t_1 d^2}{E_2 t_2^3} > 100 \tag{24}$$

where:

E_1 – skin elasticity modulus

t_1 – skin thickness

E_2 – core elasticity modulus

t_2 – core thickness

d – distance of centroids of the skins ($d=t_1+t_2$) [36]

Effect of approximations can be seen in Figure 21.
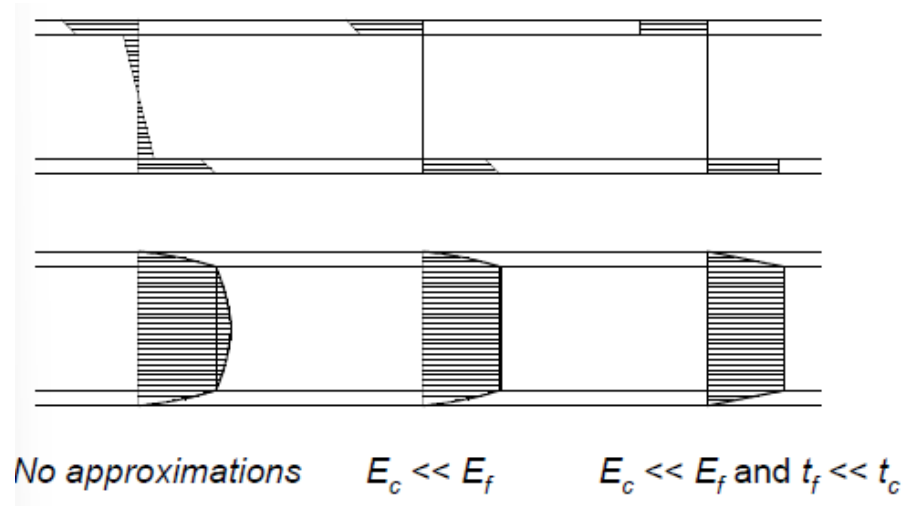
Figure 21 – Effect of approximations on stress distribution.

If both criteria are satisfied it is possible to approximately write:

$$K = K_0 = \frac{E_1 t_1 d^2}{2} \tag{25}$$

where:

K – flexural rigidity/bending stiffness of whole sandwich structure

K_0 – bending stiffness of the skins about the neutral axis

E_1 – skin elasticity modulus

t_1 – skin thickness

d – distance of centroids of the skins ($d=t_1+t_2$) [36]

All materials have different mechanical properties in compression and tension. This difference in mechanical properties is significant in composite materials reinforced with long fibers, which are commonly used as skin materials. However, this difference in mechanical properties can be significant even in extruded thermoplastics, whether reinforced or not.

This effect is called bimodularity of skin layers. Asymmetrical sandwich structure is illustrated in Figure 22.

To calculate flexural rigidity for the sandwich structure with the asymmetrical skins neutral axis needs to be defined first. It can be determined using first moment of inertia integrated over entire reduced cross section.
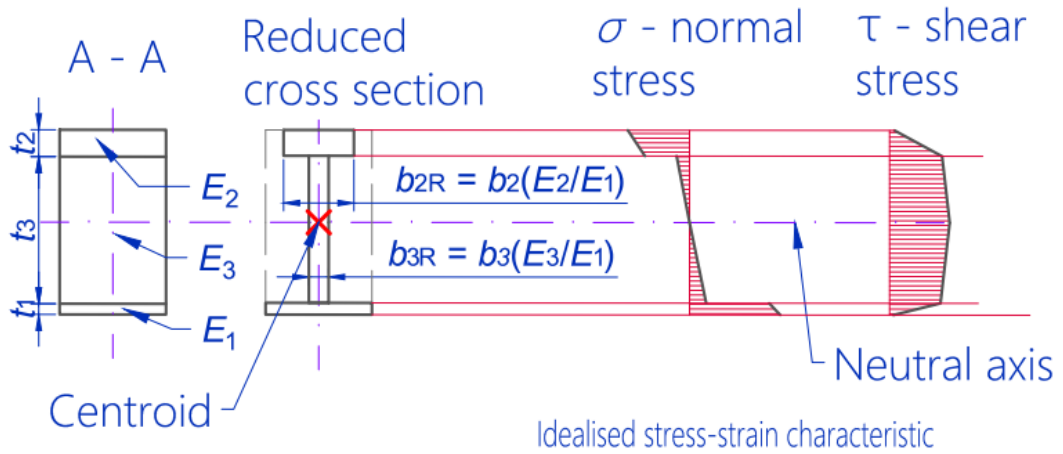
Figure 22 - Asymmetrical sandwich cross-section with key annotations illustrating stress distribution for pure bending. As in ref. [19]

$$E_1 t_1 \left(\frac{t_1}{2} + t_3 + \frac{t_2}{2}\right) + E_3 t_3 \left(\frac{t_3}{2} + \frac{t_2}{2}\right) = e[E_1 t_1 + E_3 t_3 + E_2 t_2] \qquad (26)$$

where:

$E_{1,2,3}$ – layer elasticity modulus (numbering by stiffness – stiffest = 1)

$t_{1,2,3}$ – layer thickness

e – centroid location (distance from the middle axis of the lower skin to

the neutral axis)[36]

Flexural rigidity is then:

$$K = \frac{E_1 t_1^3}{12} + \frac{E_2 t_2^3}{12} + \frac{E_3 t_3^3}{12} + E_1 t_1 (d - e)^2 + E_2 t_2 e^2 + E_3 t_3 \left(\frac{t_3 + t_2}{2} - e\right)^2 \qquad (27)$$

where:

$E_{1,2,3}$ – layer elasticity modulus (numbering by stiffness – stiffest = 1)

$t_{1,2,3}$ – layer thickness

d – distance of centroids of the skins ($d = t_1/2 + t_2/2 + t_3$) [36]

e – centroid location (distance from the middle axis of the lower skin to

the neutral axis)[36]

For weak core $E_{core} \ll E_{skin}$ *(weak core approximation)*, and thin skins t_1, $t_2 \ll t_3$ *(thin skin approximation)* is possible to write:

$$K = K_0 = E_1 J_r \approx \frac{E_1 t_1 E_2 t_2 e^2}{E_1 t_1 + E_2 t_2}$$ (28)

where:

K_0 – bending stiffness of the skins about the neutral axis

$E_{1,2,3}$ – layer elasticity modulus (numbering by stiffness – stiffest = 1)

$t_{1,2,3}$ – layer thickness

e – centroid location (distance from the middle axis of the lower skin to

the neutral axis)

J_r – second moment of area of reduced cross section.

Normal stress caused by bending moment in analyzed layer – i is then calculated using:

$$\sigma_i(y) = \frac{E_i}{E_1} \frac{M}{J_r} y$$ (29)

where:

$\sigma_i(y)$ – stress in the analyzed layer as a function of the distance from the neutral axis

E_i – flexural modulus of element

E_1 – flexural modulus of stiffest element (typically skin)

M – bending moment

J_R – second moment of area for whole reduced cross-section

y – distance from the neutral axis

Stress must be calculated for each layer individually, and individually compared to the maximum stress value for each material.

3.2.2 Mechanics of bending with shear forces - three-point bend test

During applications, the sandwich structures are often subjected not only to bending but bending with shear forces. Shear stress is transmitted through core. This means that in most applications core shear modulus is important.

Shear stress emerges in even basic three-point bend test. Therefore, this test in not suitable to assess bending properties of sandwich structures. But it can be crucial for assessing mechanical properties in real world application.

Shear stress is typically maximum in neutral axis ($y = 0$). Equation for asymmetrical sandwich structure:

$$\tau(y) = \frac{T}{S}\left[E_1 t_1 (d-e) + \frac{E_3}{2}\left(d - e - \frac{t_1}{2}\right)^2 - y^2\right] \tag{30}$$

where:

τ – shear stress

T – force

$E_{1,2}$ – layer elasticity modulus (numbering by stiffness – stiffest = 1)

$t_{1,2}$ – layer thickness

e – centroid location (distance from the middle axis of the lower skin to

the neutral axis)

S – shear stiffness of sandwich structure

d – distance of centroids of the skins ($d=t_1+t_2$) [36]

When assuming weak core (*weak core assumption* Equation 24) simplified equation can be used:

$$\tau_{max} = \frac{T}{S}\frac{E_1 t_t E_2 t_2 d^2}{E_1 t_t + E_2 t_2} \tag{31}$$

where:

τ – shear stress

T – force

$E_{1,2}$ – layer elasticity modulus (numbering by stiffness – stiffest = 1)

$t_{1,2}$ – layer thickness

e – centroid location (distance from the middle axis of the lower skin to the neutral axis)

S – shear stiffness of sandwich structure

d – distance of centroids of the skins ($d=t_1+t_2$) [36]

When assuming thin skins (*thin skin assumption* Equation 23) simplified equation can be used:

$$\tau_{max} = \frac{T}{d} \tag{32}$$

where:

τ – shear stress

T – force

S – shear stiffness of sandwich structure

d – distance of centroids of the skins ($d=t_1+t_2$) [36]

Equations 30,31 and 32 are for unit length. Exact value of shear stiffness is derived through an energy balance equation. The process involves calculating the average shear angle of the cross-section and integrating it over the cross-sectional area, considering shear stress and strain values. This approach provides an exact determination of the shear stiffness, however using the approximations for a sandwich with *thin skins*, $t_{skin} \ll t_{core}$, *weak core*, $E_{core} \ll E_{skin}$, and assuming the shear modulus of the skins to be large it is possible to write [36]:

$$S = \frac{G_3 d^2}{t_3} \tag{33}$$

where:

S – shear stiffness of sandwich structure

G_3 – shear modulus of core

t_3 – thickness of core

d – distance of centroids of the skins ($d=t_1+t_2$) [36]

Total displacement is given by combining deformation caused by the bending moment with deformation caused by the shear forces:

$$\delta = \delta_M + \delta_T \tag{34}$$

where:

δ – total displacement

δ_M – displacement by bending moment

δ_T – displacement by shear forces

This can be seen in Figure 23, where cantilever sandwich beam with a known length l and rectangular shape is fully fixed in on one side and loaded by force F opposite side.
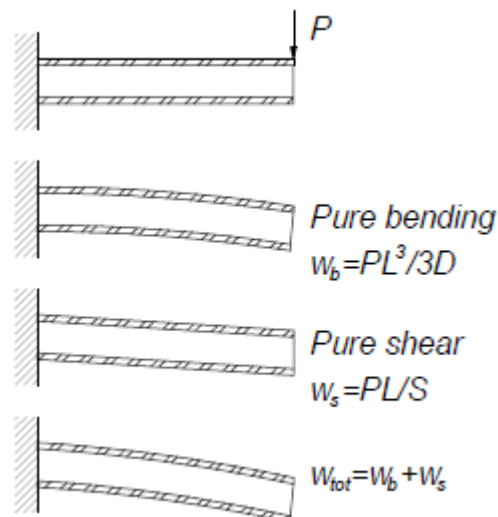

Figure 23 - A cantilever sandwich beam illustrating bending, shear, and total superimposed deformation.

Total displacement is then:

$$\delta = \delta_M + \delta_T = \frac{Fl^3}{3K_0} + \frac{Fl}{S} \tag{35}$$

where:

δ – total displacement

δ_M – displacement by bending moment

δ_T – displacement by shear forces

F – force

K_0 – flexural stiffness (assumed only as bending stiffness of the skins about the neutral axis)

S – shear stiffness

l – beam length[36]

In the three-point bend test, a sandwich beam with a known length l and rectangular shape is supported at two points and loaded by a force F at the midpoint of the beam (assuming thin skins, a weak core, and a large shear modulus of the skins). Mechanics of this are illustrated in Figure 24. The maximum displacement is then determined by:

$$\delta = \delta_M + \delta_T = \frac{Fl^3}{48K_0} + \frac{Fl}{G_3 bt_3} \qquad (36)$$

where:

δ – total displacement

δ_M – displacement by bending moment

δ_T – displacement by shear forces

F – force

K_0 – flexural stiffness (assumed only as bending stiffness of the skins about the neutral axis)

G_3 – shear modulus of core

l – beam length

b – beam width

t_3 – thickness of core
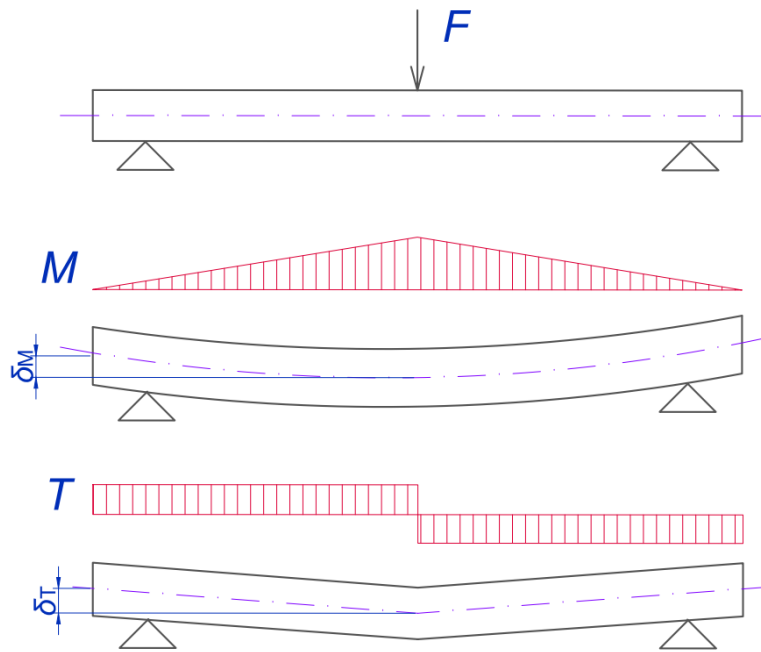
Figure 24 – Superposition of deformations due to shear and bending stress in three point bend test of sandwich structure. [39]

3.2.3 Failure mods

Sandwich panels can fail in several ways, each mode giving one constraint on the load bearing capacity of the sandwich. Depending on the geometry of the sandwich and the loading, different failure modes become critical and set the limits for the performance of the structure. Most common failure mods are shown in Figure 25. [36]
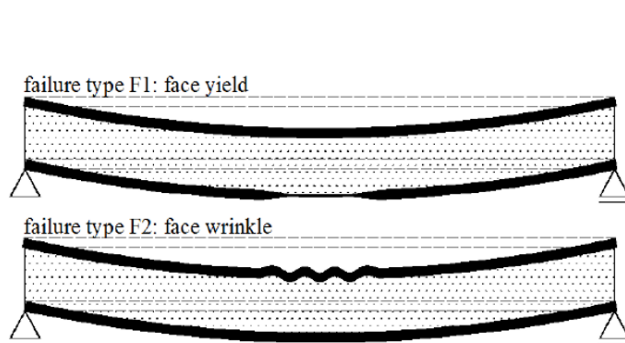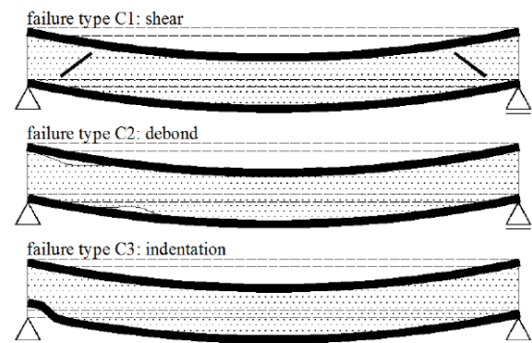

Figure 25 – Failure mods in skins and core.[36]

Skin yield occurs in skin in tension when normal stress exceeds maximum allowed stress. In relatively elastic skins this results in plastic deformation of skin and consequential plastic deformation of core until cracks start to propagate and structure fails. If skin is relatively brittle, especially in materials reinforced with long fibers, failure may occur abruptly without significant plastic deformation.

Skin wrinkle occurs on the skin subjected to compression when it loses stability. The skin is partially supported by the core, but this support is relatively weak. When stability is lost, wrinkles occur, followed shortly thereafter, within tenths of milliseconds, by debonding and skin fracture. This can be seen in Figure 26.
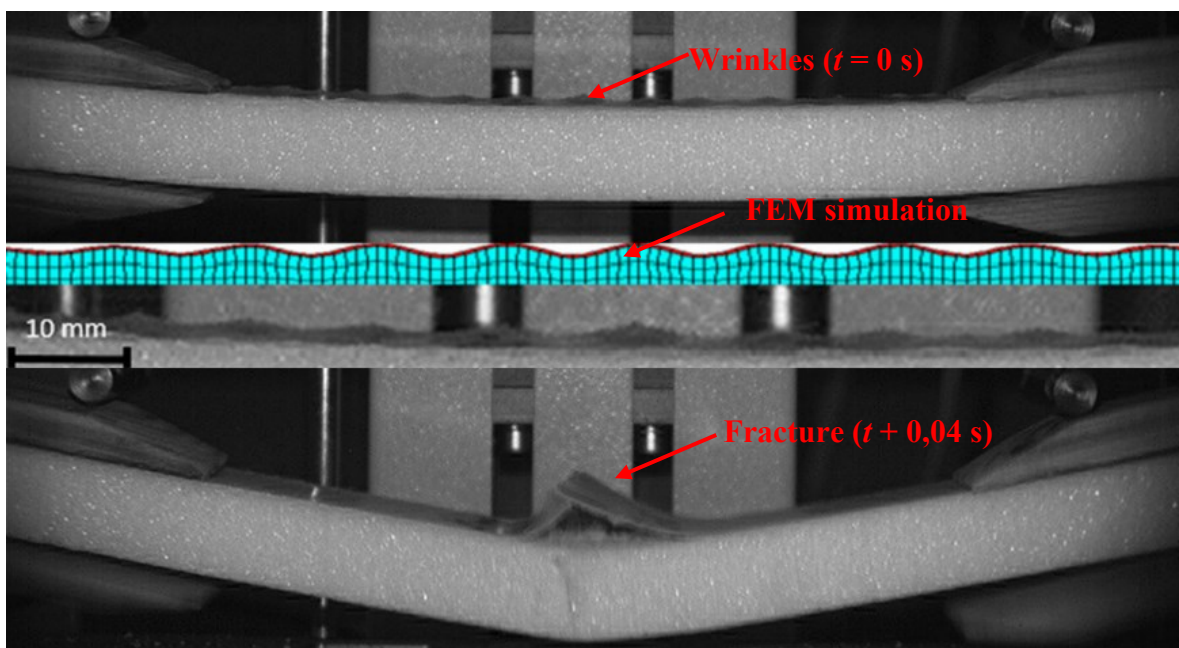
Figure 26 – Skin wrinkle and fracture, with FEM simulation.[38]

Core shear failure occurs when shear stress in core is larger than shear strength of the core. Shear failure is not always visible and can be challenging to identify. Determining of shear strength of core can be challenging especially for foam cores made from PP. Typically cracks are inclined 45° from skins, this is typical for pure shear cracks. Criteria for sheal failure can be written as [36]:

$$\tau_c = \left[\left(\frac{\sigma_3}{2}\right)^2 + \tau_3^2\right] < \tau_A \tag{37}$$

where:

τ_c – combined shear stress

τ_3 – shear stress in core

τ_a – maximum allowed shear stress

σ_3 – normal stress

Debonding means that the adhesive joint bonding of the skin to the core fails. This can occur due to overloading. The shear stress in the bond line is almost as high as in the middle of the core, and if the adhesive joint has less strength than the core it will fail prior to the core. This, however, should be avoided by choosing an adhesive and a manufacturing method the prevents the above from happening. The bond line will also be subjected to high stresses if there is a thermal field with high gradient acting on the skin. Since the core usually is a very good thermal insulator, whereas the skin usually is not, especially if a metal skin is used, then if the skin is subjected to a temperature change, sunshine for example, the thermal gradient will be very high in the interface causing high thermal stresses in the bond line. The adhesive joint may also fail due to fatigue, impact, ageing or numerous other causes. The main problem with debonding failures are that they are sub-surface, making them difficult to detect and can therefore grow into critical size before detected.[36]

Indentation of the core occurs at concentrated loads, such as fitting, corners, or joints. Practically they can be avoided by applying the load over a sufficiently large area. What actually happens when point loads are applied is that the skin will act as a plate on an elastic support. The skin will bend independently of the opposite skin and if the deformation and thus the elastic stress supplied by the core exceed the compressive strength of the core, the core will fail. In practice, there are many ways to enhance the local strength of a sandwich to avoid indentation.[36]

II. EXPERIMENTAL

4 CORE TESTING

As core material innovative polypropylene foam structure is used. First polypropylene and additives are melted in extruder, then physical blowing agent is mixed in. Then is this melt extruded through circular extrusion head and cut to form plan. Planks are joined together using heat and then cut, to alter cell orientation. This process is described in more detail in next chapter. Effect of cell orientation was described in detail in Chapter 1.1.2 and effect of cell orientation on mechanical properties in compression can be seen in Figure 1.

Foam was manufactured by company SPUR under trade names – HARDEX XPP OPTIMA and HARDEX XPP PERFORMANCE. Spur produced this product using patented technology (Figure 27). [40]
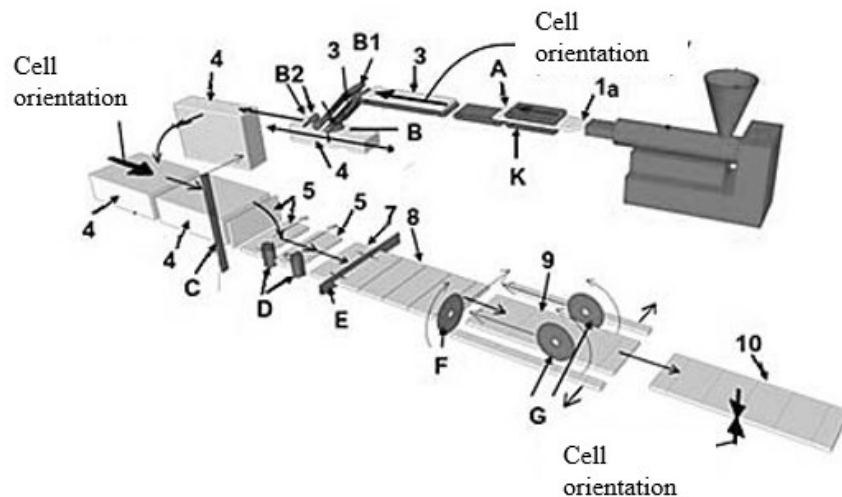
Figure 27 – Schematic of altering cell orientation for HARDEX XPP production. [40]

4.1 Compression test preparation

Compression test was conducted according to ISO 844. Core isn't typically loaded with normal stress. But if local load is placed on sandwich structure good compression properties of core material are desirable as they play crucial role in resisting skin indentation as discussed in Chapter 3.2.3 – Failure Mods. Furthermore, literature describes mechanical properties in compression in detail. Therefor mechanical properties of core were investigated with special focus on cell orientation and density. Specimen sizes were 100 x 100 mm with varying thickness between $t = 16 – 24$ mm due to production.

Tests were conducted at certified testing machine Zwick/Roell 1456 set according to ISO 844.

4.2   Shear test preparation

Shear test was conducted according to ISO 1922.

Shear testing was far more complicated than compression testing. Firs support plates were modeled in CATIA V5 according to standard ISO 1922, Testing apparatus was made by company SPUR. SPUR also provided specimens for testing, different densities (ρ = 60,80,120 kg·m^{-3}) each with two different orientation of ribs – ribs are from heat bonding of foam planks as seen in Figure 28. Samples are bonded to support plates using adhesive, first cyanoacrylate glue was used, but it did not create bond strong enough. All test was than conducted using 3D 8010 DP adhesive. This adhesive is specially designed to joint nonpolar polymers, such as polypropylene. For one sample more than 20 g of adhesive was used.

Preparing test specimens was time consuming. Adhesive had to cure for at least 24 h. After test cleaning of support bars took several hours. Best method of cleaning support bars was to mechanically remove adhesive using abrasive method (surface grinder or angle grinder with abrasive disc). It is also possible to chemically clean support bars using solvent (C6000). This process takes at least 24h and can lead to bad adhesion of following specimens.

Figure 28 – From left: 3D model of testing apparatus, pattern for application of adhesive, shear test with visible inhomogeneities in samples, end of shear test with visible deformations.

5 SKIN TESTING

As skin materials extruded polypropylene and pultruded glass fibers with polypropylene was considered and tested. Both are well-known materials that have been used for long time.

Polypropylene was manufactured by company SPUR. Polypropylene is made out of approx. 58 w% of polypropylene (50 % homopolymer, 50 % copolymer), 40 w% talc, 0.6 w% processing additives, 0.4 w% antioxidants and UV stabilizers, 1.5 w% pigments. Composition can be slightly modified.

Pultruded polypropylene reinforced with long glass fibers was manufactured by company Profol Composites under tradename proUD 0°. It composes of 72 w% of glass fibers, and rest is polypropylene, pigment and processing additives. According to manufacturer is weight per unit area m = 320 g/m2 (ISO 10352) and Young modulus in tension E = 37 000 MPa, and maximum stress in tension is σ = 1000 MPa (ISO 527–4).
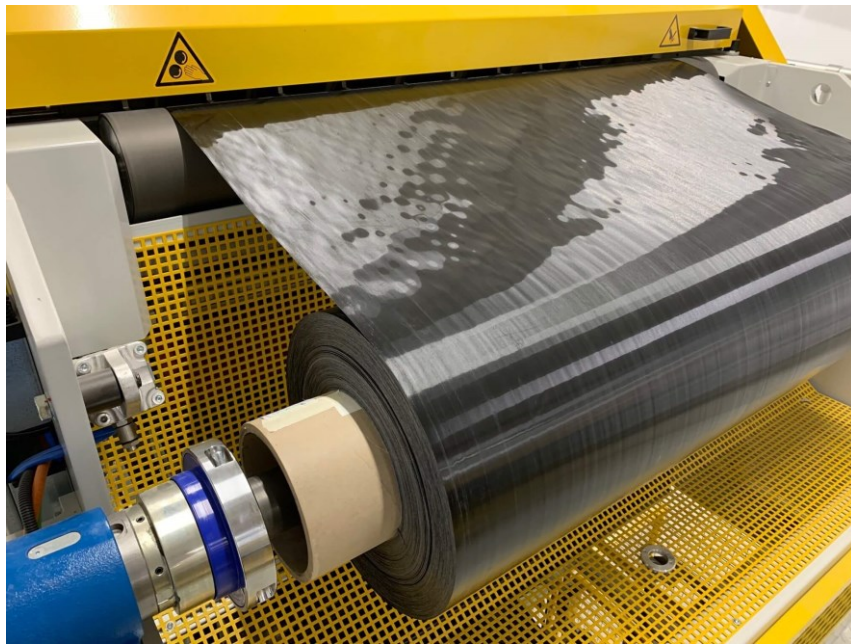
Figure 29 – Production of proUD 0°. [41]

Since skin materials are often subjected to stress in either a tension or a compression, their properties were investigated.

5.1 Tension test preparation

Tensile test of faces was conducted according to ISO 527:2023 (ISO 527-1; ISO 527-3;ISO 527-4). Specimens were cut out of thin sheet on 100W laser - LTT | ILS 3N-T100-NCC-B2-12. Sample cutting out is shown at Figure 30
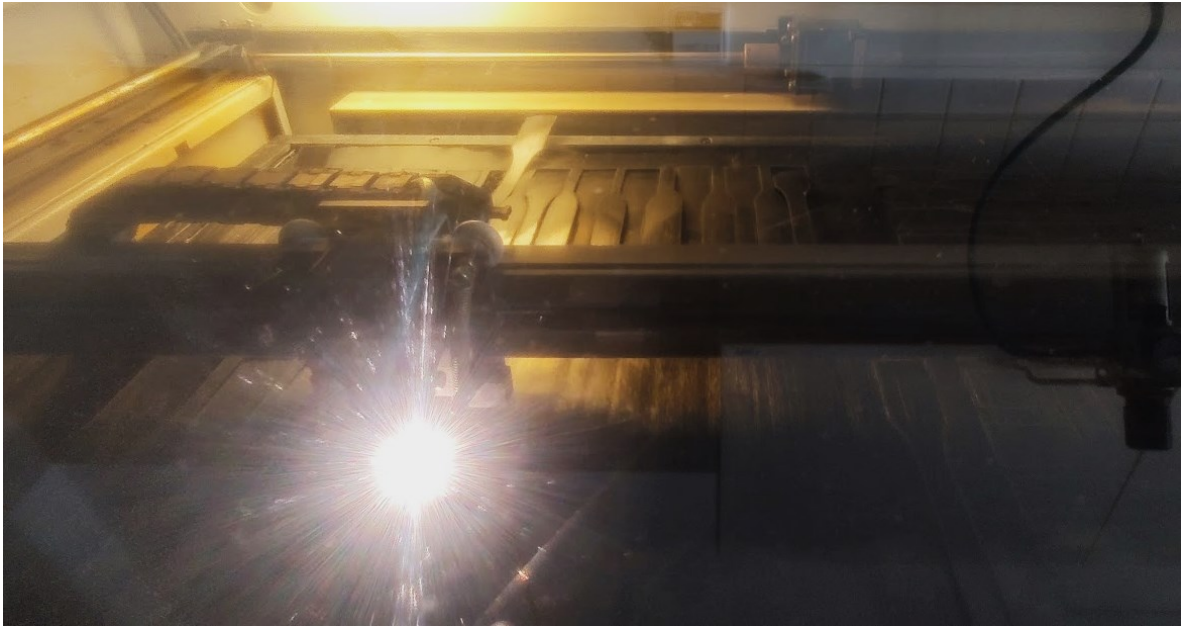
Figure 30 – Specimen cut out on 100W laser.

Polypropylene was tested according to ISO 527-3 on Zwick/Roell 1456, test setup can be seen at Figure 30. Specimens dimension were 160 mm, 25 mm, specimens' thickness were 0.8 mm and distance between jaws was 100 mm. For this test mechanical spring-operated jaws were strong enough to hold specimens in place for testing.
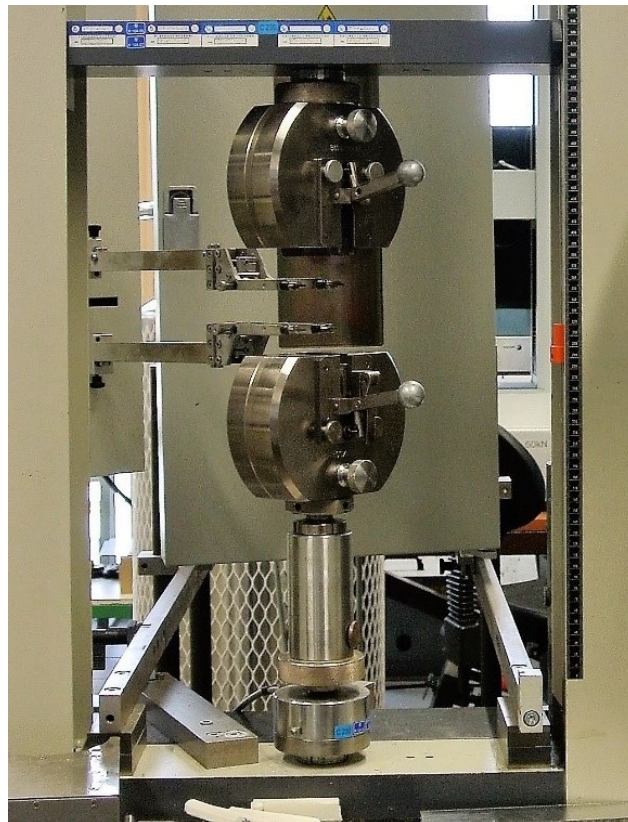

Figure 31 – Testing machine with spring operated jaws and extensometers. [42]

Polypropylene reinforced with long glass fibers was tested according to ISO 527-4. Specimen was cut out according to shape of Specimen 1B as required in standard, specimen shape can be seen in Figure 32. Then polypropylene patches were heat bonded at ends of specimens, so that they would not slip out of jaws while testing. For this laboratory hot press was used, temperature of press faces was set to $T = 145\ °C$, specimens were hot pressed for approx. 45 s. Press used was EMG SAREL (manufactured by EMG Zlín). Right after hot pressing were specimens put between two cold steel plates (plate weight approx. 2 kg) for at least one minute. This can be seen at Figure 33. Specimen thickness was 0.2 mm and jaws gripped specimen as required by standard. Test was conducted on certified machine Zwick/Roell 1456, with pneumatic jaws. Tests were also carried out without polypropylene patches, but the method of breakage of the samples and the values obtained were not satisfactory - on Zwick/Roell 1456 with spring jaws or pneumatic jaws, nor on Testomatric 350M with pneumatic jaws (the jaws with knurled and abrasive were tested).
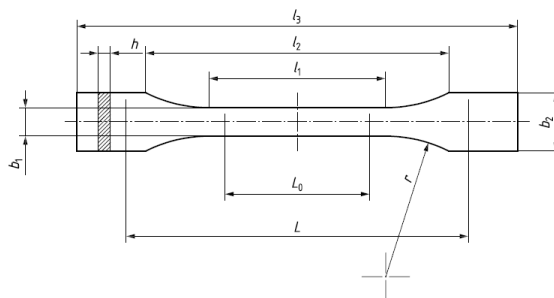
Symbol	Name	Dimensions in millimetres
l_3	Overall length [a]	≥150
l_1	Length of narrow parallel-sided portion	60,0 ± 0,5
r	Radius [b]	≥60
b_2	Width at ends	20,0 ± 0,2
b_1	Width of narrow portion	10,0 ± 0,2
h	Thickness	2 to 10
L_0	Gauge length (recommended for extensometers)	50,0 ± 0,5
L	Initial distance between grips	115 ± 1

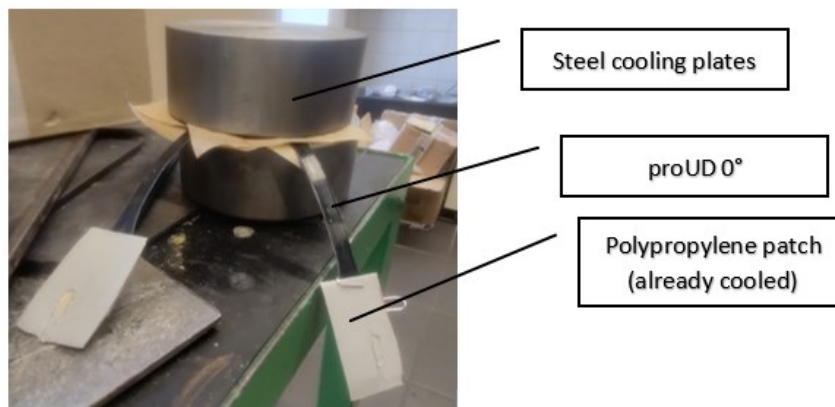Figure 32 – Specimen 1B as required in standard. [43]

Figure 33 – Cooling after heat bonding, to avoid warping.

5.2 Compression test preparation

Compression test was conducted according to ASTM C 364 – standard test method for edgewise compressive strength of sandwich construction. In this test sandwich structure is tested in compression, and then are compression properties of skins are extrapolated (mechanical properties of core are known and was measured in different test). Test set up can be seen at Figure 34. Specimens were cut out of sandwich panel on 100W laser - LTT | ILS 3N-T100-NCC-B2-12. Firstly, was material cut from one side, then flipped and cut from other side, so that core material is thermally affected as little as possible.

Specimen dimensions was as standard requires – 100 x 50 mm, thickness is given by manufacturing limitations $t \approx 20$ mm.
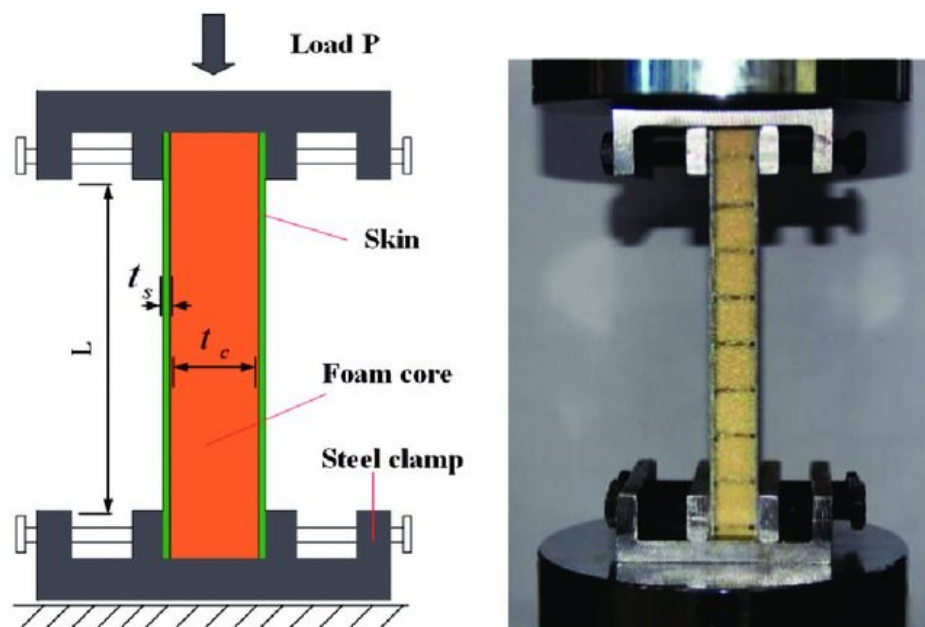
Figure 34 – Schematic of apparatus for testing according to ASTM C 364.[44]

6   SANDWICH TESTING

For verification of optimized structure and it´s flexural rigidity sandwich structure has to be tested in bending. Three-point bend test is not suitable as there are significant shear forces in the entire length of sample. Four-point bending is more suitable as there are shear force only in small part of specimen length (between support and loading rod). In middle of sample is uniformly distributed bending moment. Stress distribution for both test is shown in Figure 35.
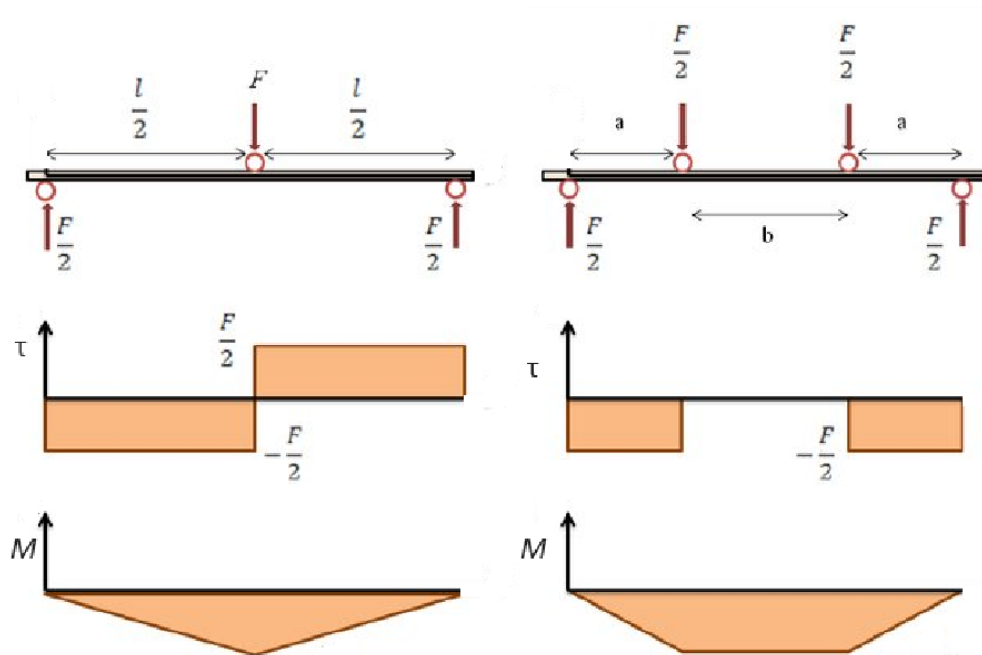

Figure 35 – Three- and four-point bend test normal and bending stress distribution.[45]
Samples were manufactured in SPUR laboratory, using three step method.

1. Skins layers were joined together with adhesion layer using hot press ($T \approx 170\ °C$; $t \approx 20 - 50\ s$)

2. Core layer was joined with adhesion layers using hot press ($T \approx 155°C$; $t \approx 5 - 10\ s$)

3. Prepared skin and core structures were joined together using hot press ($T \approx 150\ °C$; $t \approx 50 - 90\ s$) and then clamped in tempered press to prevent warpage. ($T \approx 25\ °C$; $t \approx 80\ s$)

Using this method plates 250 x 250 mm were prepared. Than using table saw samples were cut out to final dimensions.

Samples structure:

1. Series – 5x proUD0° (~ 1 mm) – Foam 80 kgm^{-3} (∥)- 5x proUD0° (~ 1 mm)

2. Series – 2x proUD0° (~ 0.4 mm) – Foam 80 kgm^{-3} (∥)– 3x proUD0° (~ 0.6 mm)

3. Series – 4x proUD0° (~ 0.8 mm) – Foam 80 kgm^{-3} (∥) - 6x proUD0° (~ 1.2 mm)

4. Series – 6x proUD0° (~ 1.2 mm) – Foam 80 kgm^{-3} (∥)- 9x proUD0° (~ 1.8 mm)

5. Series – extruded polypropylene (~ 0.4 mm) – Foam 80 kgm^{-3} (⊥)- extruded polypropylene (~ 0.4 mm)

6. Series – extruded polypropylene (~ 0.4 mm) – Foam 80 kgm^{-3} (∥)- extruded polypropylene (~ 0.4 mm)

6.1 Bend test preparation

Four-point bend test was set up according to ASTM D393. Sample dimensions differ from specimen dimension required by standard due to manufacturing limitations (maximum specimen thickness according to standard is 9 mm, and minimum core thickness possible is ≈ 20 mm). Sample dimensions are similar to ref. [46], there for width 50 mm and length over 220 mm. The distance between test supports was 200 mm, while the minor support distance was 100 mm. Test set up can be seen in Figure 36. Three-point test was conducted similarly, distance between test support was 200 mm. Tests was conducted on Testomatric M350 – 5CT.

To prevent indentation test supports were supported by steel plates similar to reference [38]. Using support helped, but skins still indented at ends of support.
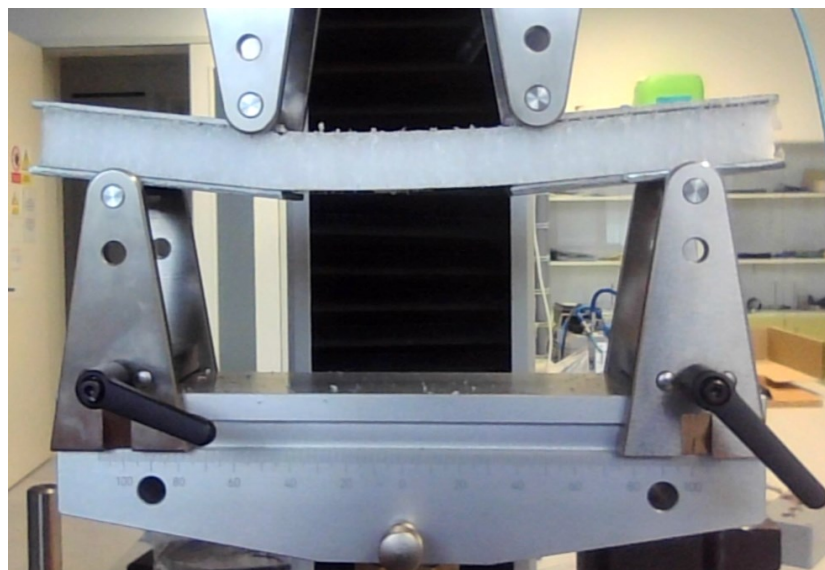

Figure 36 – Four-point test set up.

III. RESULTS AND DISCUSSION

7   CORE TESTING

As core material polypropylene foam structure is used. The foam is extruded from a circular head, then cut with a knife and straightened into a flat strip. This strip is than cut to specified length. Foam panels are later joined to form big blocks together using hot air. These big blocks are then cut using saw. This joining into big blocks and later cutting allows control over cell orientation and foam thickness. This process results in foam with "ribs" after joining with hot air. Process is schematically illustrated in Figure 37, resulting structure can be seen in Figure 38. Foam´s mechanical properties are strongly dependent on foam density, rib orientation and cell orientation.
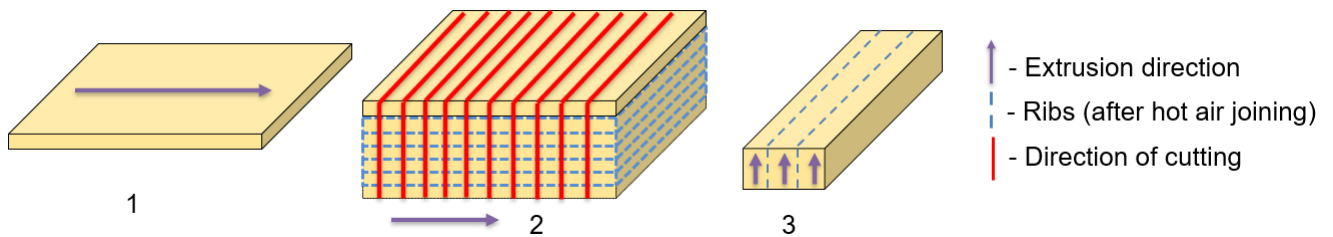
Figure 37 – Schematic illustration of foam production.
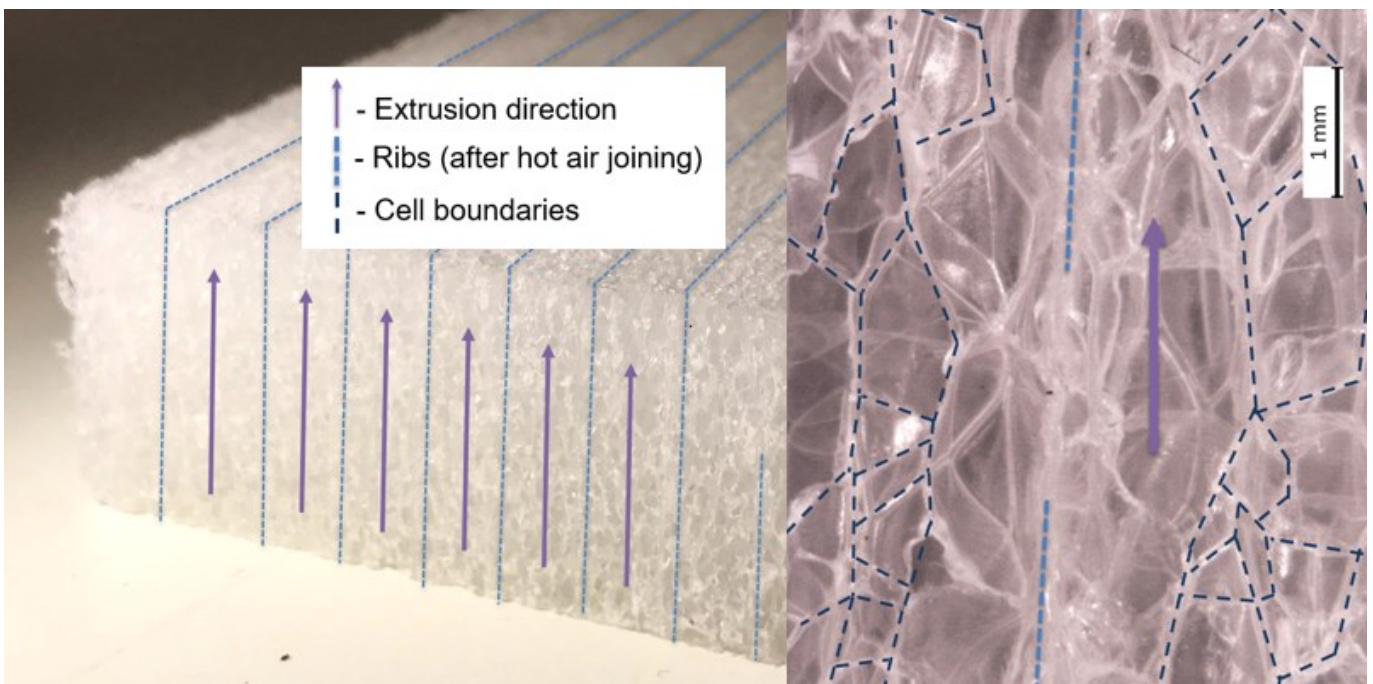
Figure 38 – Foam macrostructure (left) and microstructure (right).

7.1 Compression test

Compression test was conducted according to ISO 844. Core is not typically loaded with normal stress. But if local load is placed on sandwich structure good compression properties of core material are desirable as they play crucial role in resisting skin indentation as discussed in Chapter 3.2.3 – Failure Mods. Furthermore, literature describes mechanical properties in compression in detail. Therefor mechanical properties of core were investigated with special focus on cell orientation and density. Samples were provided by SPUR company. Sample sizes were 100 x 100 mm with varying thickness between t = 16 – 24 mm.

Test were conducted at certified testing machine Zwick/Roell 1456 set according to ISO 844.

ISO 844 is used to test mechanical properties in compression in linear elastic region (strain – $\varepsilon \leq 10$ %). Results can be seen in Tables 1,2 and Figures 39,40.

Table 2– Stress and elastic modulus of different foam densities in compression test parallel (∥) to extrusion direction.

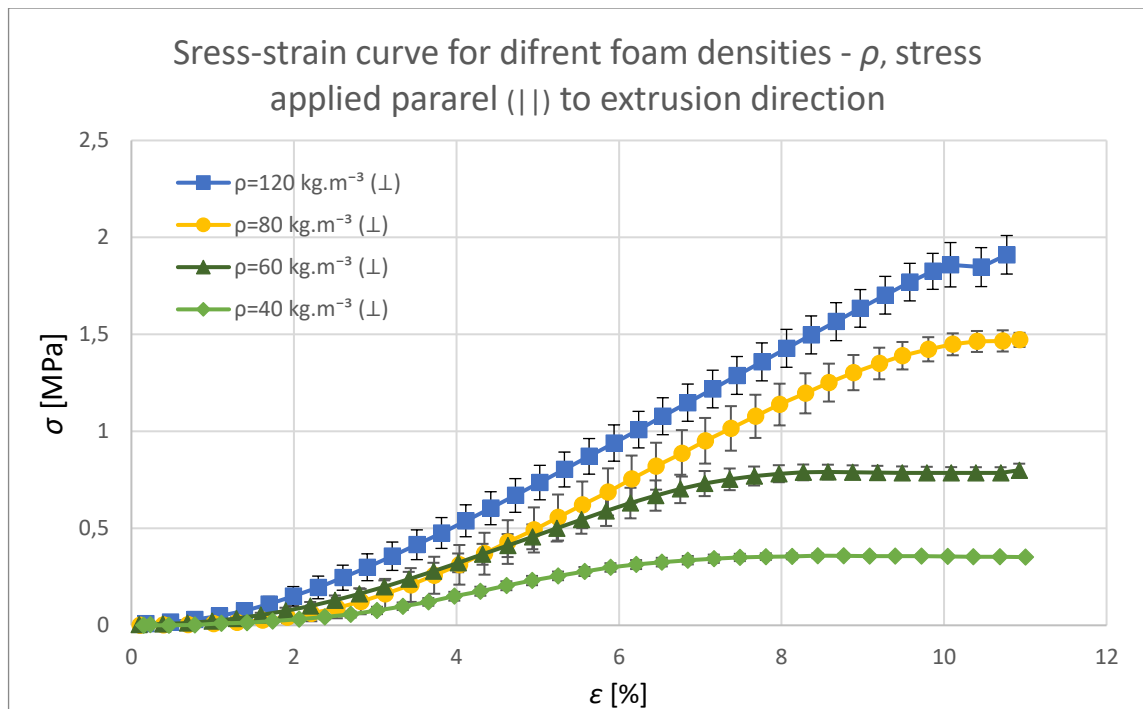| ρ [kg·m^{-3}]	40	60	80	120
E [MPa]	9.4 ± 0.88	15.2 ± 2.12	22.2 ± 0.16	22.3± 0.64
σ at 10% [MPa]	0.353 ± 0.0064	0.785 ± 0.0315	1.443 ± 0.0620	1.899 ± 0.0454

Figure 39 – Stress-strain curve for different foam densities - ρ, stress applied parallel (∥) to extrusion direction, with error bars.

Table 3 – Stress and elastic modulus of different foam densities in compression test perpendicular (⊥) to extrusion direction.

ρ [kg·m^{-3}]	40	60	80	120
E [MPa]	0.4 ± 0.04	1.0 ± 0.21	2.3 ± 0.23	2.4± 0.18
σ at 10% [MPa]	0.029 ± 0.0012	0.062 ± 0.0046	0.137 ± 0.0039	0.158 ± 0.0031
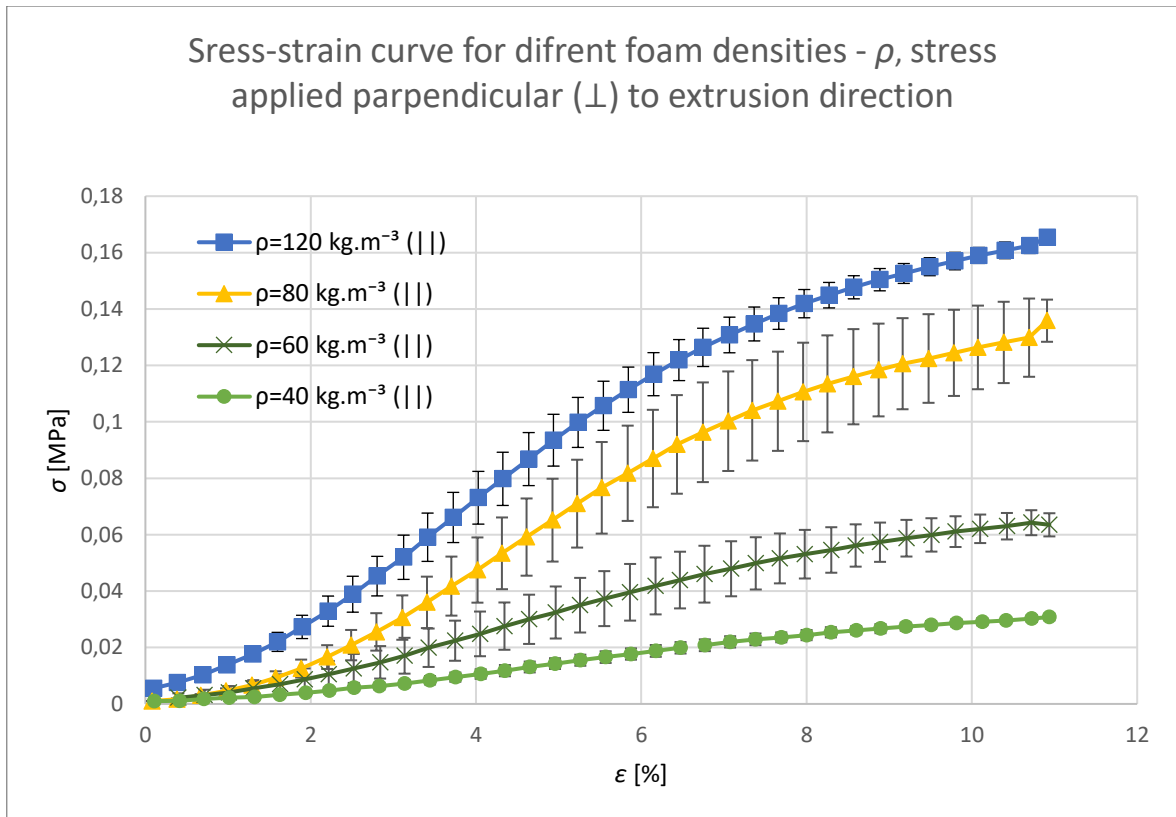
Figure 40 – Stress-strain curve for different foam densities - ρ, stress applied perpendicular (⊥) to extrusion direction, with error bars.

Obtained data are consistent with literature findings. Region of linear elasticity is clearly visible. Density affects mechanical properties in compression as predicted by Ashley and Gibson equations (see Chapter 2.2). With increasing density mechanical properties improve. Modulus of elasticity – E is dependent on density (see Equation 2). With increasing density modulus of elasticity – E increases. Cell orientation has crucial effect on mechanical properties, as illustrated in Figure 1. Cells are elongated in extrusion direction, as seen in Figure 28. Loading perpendicular to extrusion direction (⊥) results in worse mechanical properties, than for cells loaded parallel to extrusion direction (∥). Effect of strain rate and temperature was not tested, but literature suggest it also has crucial effect. [46]

To illustrate full range of mechanical properties (strain – $\varepsilon \sim 85$ %) other tests were conducted. However, the data from these tests are only used for comparison with literature and not for determining statistically significant values to be used for calculations. Results can be seen in Figure 41.
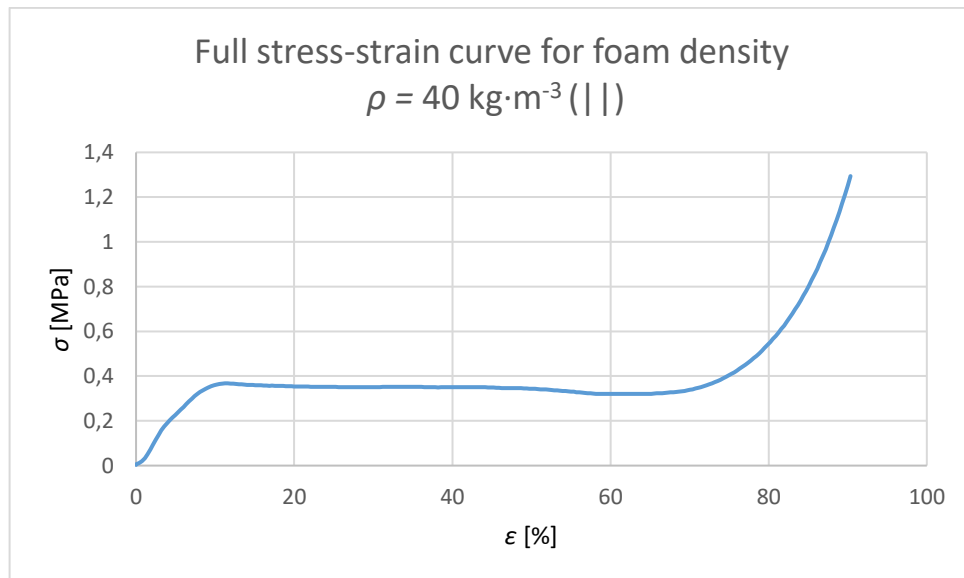

Figure 41 – Full stress-strain curve for foam density – $\rho = 40$ kg·m⁻³, stress applied parallel (‖) to extrusion direction.

All 3 regions of deformation are clearly visible – elastic region, plato and densification.

7.2 Shear test

Shear test was conducted according to ČSN 64 5436, which is similar to ISO 1922. Core typically transmits all shear forces, therefor it is important to investigate its mechanical properties as it can limit ultimate strength of sandwich structure due to core shear failure (see Chapter 3.2.3 – Failure Mods). No data for polyolefinic foam shear test was found.

Effect of density and effect of rib orientation on mechanical properties were investigated. Density plays role, but due to testing being both time consuming and costly not enough consistent data were conducted. Role of rib orientation was significant, and for density $\rho = 80$ kg·m⁻³ were consistent data conducted as seen in Figure 42.
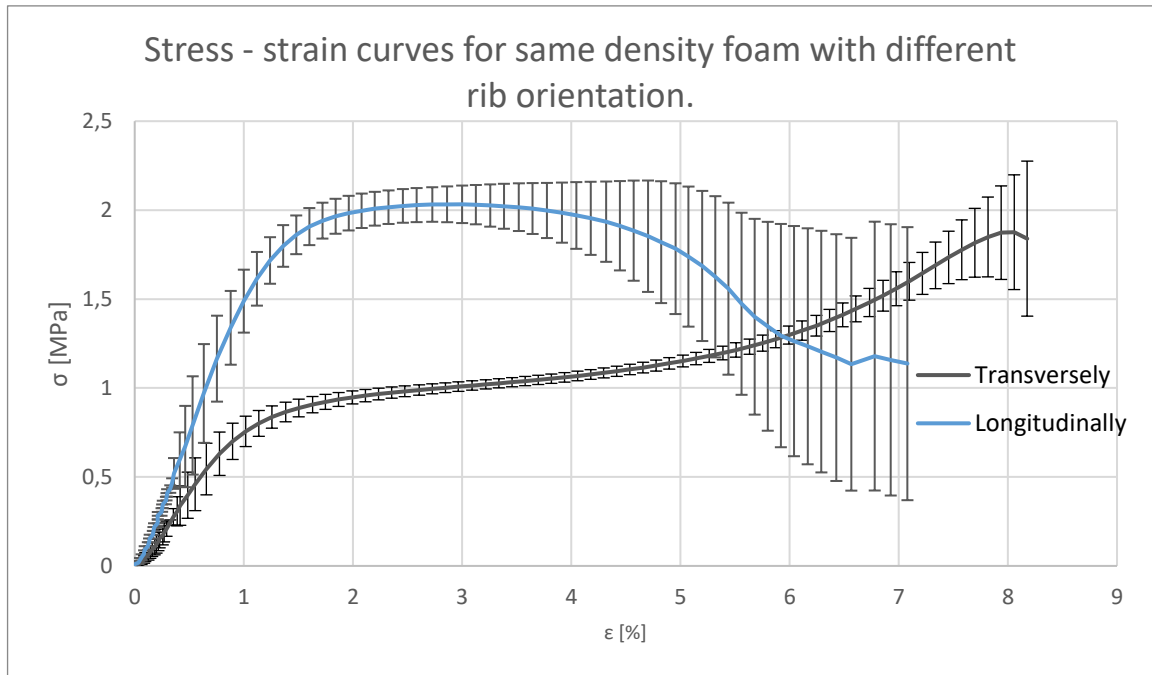
Figure 42 – Stress - strain curves for same density foam with different rib orientation.

In specimens with ribs transversely stress strain curve has typical S shape. In starts with linear region, then rib and cell collapse occur after this densification and tearing occurs. Rib and cell collapse is not homogenous, this causes data to be inconsistent, and causes local debonding and adhesive failure, this failure spreads rapidly and sample (foam) debonds fully from support plate. In specimens with ribs longitudinally cells start to deform, but ribs did not collapse.

For design process linear elasticity region is crucial, form stress-strain plots maximum stress in linear elasticity region was estimated, estimated data can be seen in Table 3 and 4.

Table 4 – Values from shear test ISO 1922.

ρ (rib orientation)	60 - longitudinally			60 - transversely			80 - longitudinally		
N (significant)	4			3			9		
	σ_{max} [MPa]	σ_{el}[MPa]	E[MPa]	σ_{max}[MPa]	σ_{el}[MPa]	E[MPa]	σ_{max}[MPa]	σ_{el}[MPa]	E[MPa]
x	0.6	0.45	56.2	0.2	0.35	24.3	0.8	0.85	76.7
s	0.1	*	3.1	0.1	*	3.9	0.1	*	9.4

Table 5 – Values from shear test ISO 1922.

ρ (rib orientation)	80 - transversely			120 - longitudinally			120 - transversely		
N (significant)	7			5			2		
	σ_{max}[MPa]	σ_{el}[MPa]	E[MPa]	σ_{max}[MPa]	σ_{el}[MPa]	E[MPa]	σ_{max}[MPa]	σ_{el}[MPa]	E[MPa]
x	1	0.4	52.6	0.9	1	74.1	0.7	0.8	111.5
s	0.1	*	13.5	0.1	*	15.5	0	*	2.4

8   SKIN TESTING

Skins are predominantly loaded in tension or compression, therefor they mechanical properties in these loading conditions were investigated.

8.1   Tensile test

Tensile test of skins was conducted according to ISO 527 (ISO 527-1;ISO 527-3;ISO 527-4). As skin material extruded polypropylene, pultruded glass fibers with polypropylene, Table 6.

Table 6 – Tensile test result for polypropylene and polypropylene reinforced with long unidirectional glass fiber.

	PP				PP + glass fiber			
	perpendicular ($\perp$)		parallel (||)		perpendicular ($\perp$)		parallel (||)	
	E [MPa]	σ_{max}[MPa]	E [MPa]	σ_{max}[MPa]	E [MPa]	σ_{max}[MPa]	E [MPa]	σ_{max}[MPa]
N	10		11		7		9	
x	567	26	646	30	2816	11	31967	813
s	48.6	0.2	49.4	1.0	207.5	45353,0	2471.2	76.5

Polypropylene was tested according to ISO 527-3. Stress strain curve can be seen in Figure 43.
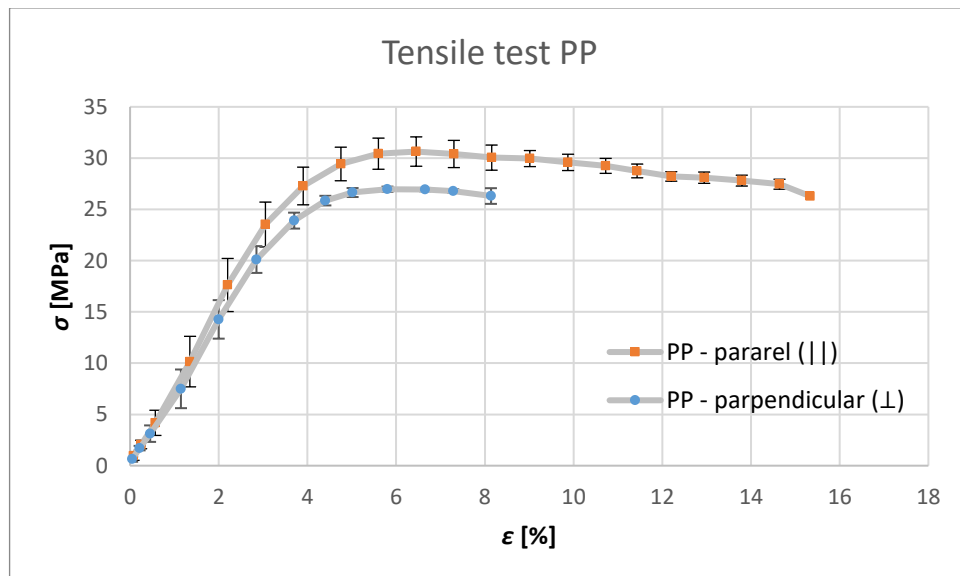
Figure 43 – Stress – strain curve for extruded polypropylene in tension with error bars. Anisotropy was seen, results perpendicular to extrusion direction ($\perp$) has worse mechanical properties, than for cells loaded parallel to extrusion direction (\|\|). Data are consistent.

Glass fiber reinforced polypropylene was tested according to ISO 527-4. Stress strain curve can be seen in Figures 44 and 45.
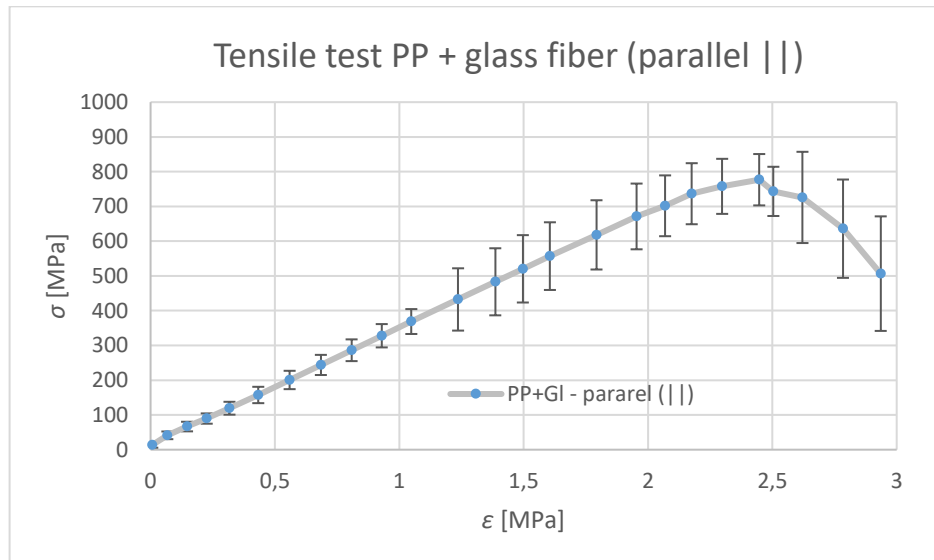

Figure 44 – Stress – strain curve for polypropylene reinforced with long glass fibers (proUD 0°) loaded in tension parallel to fibers.
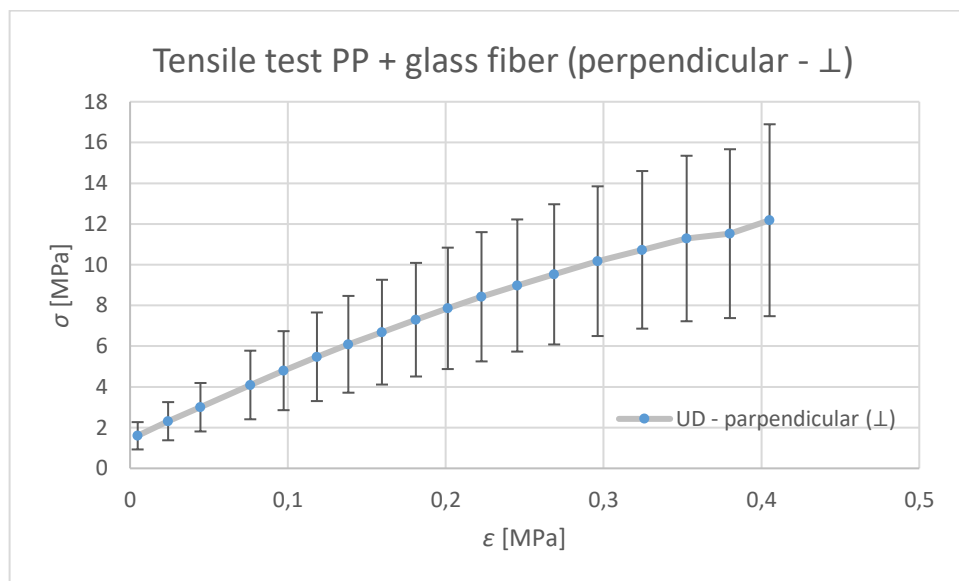

Figure 45 – Stress – strain curve for polypropylene reinforced with long glass fibers (proUD 0°) loaded in tension perpendicular to fibers.

Testing was difficult due to it being so thin and slipping out of the testing jaws. But data were consistent and significant anisotropy was observed as in all long fiber reinforced composites. Samples after testing were investigated under SEM, this can be seen in Figures 46 and 47.
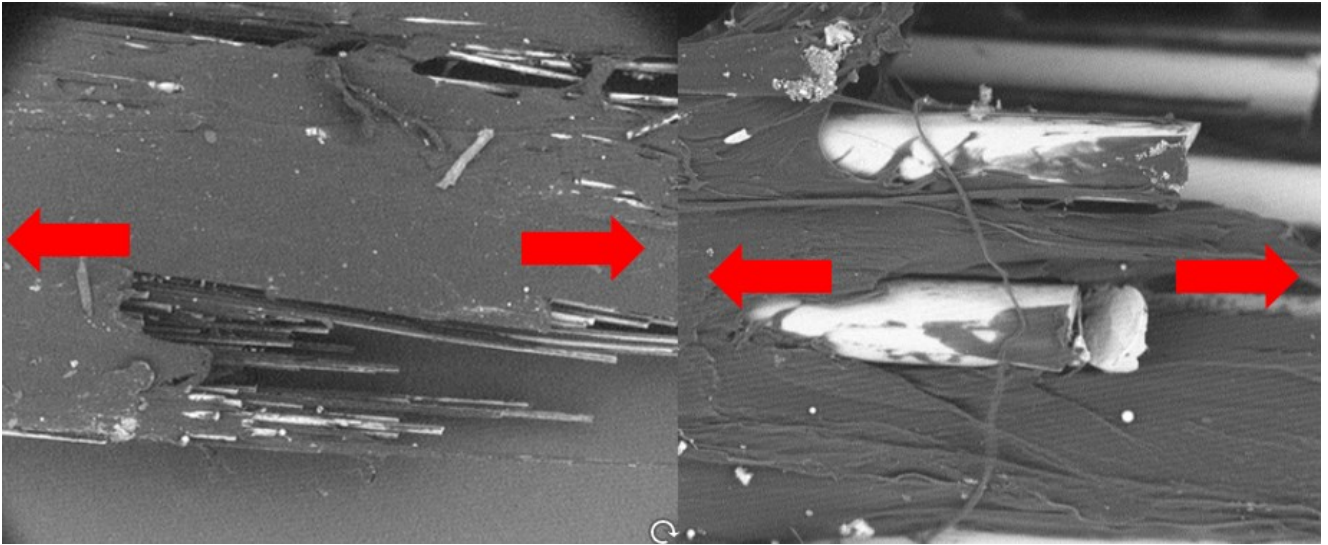
Figure 46 – Sample loaded parallel to fibers direction under SEM. 150 x times magnifications (left) and 2000 x times magnification (right). Red arrows – loading direction.
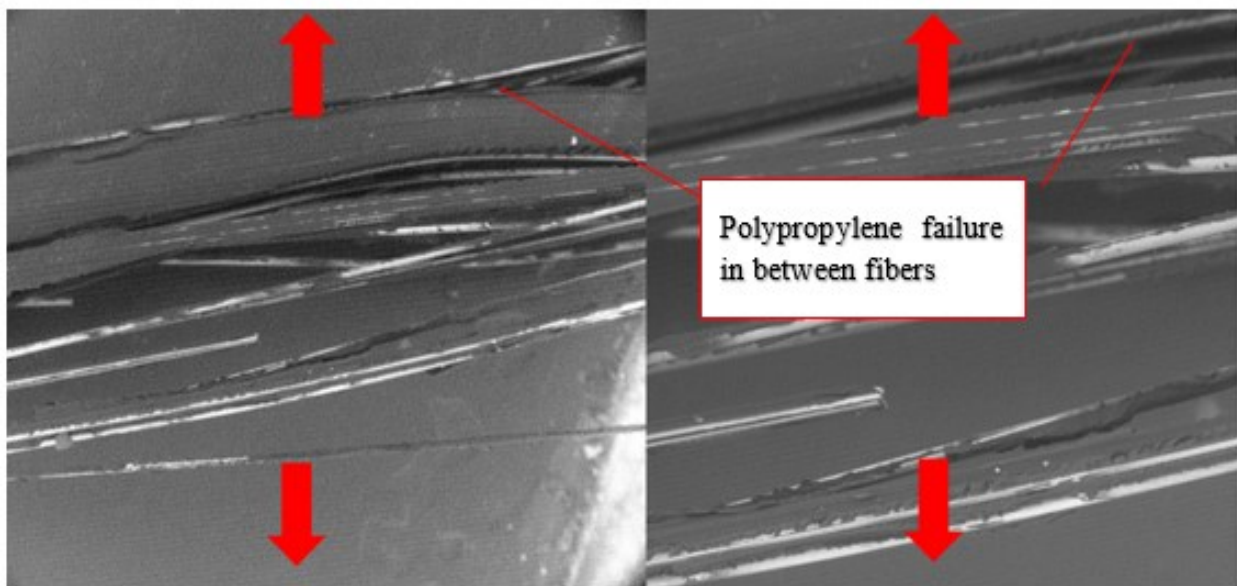

Figure 47 – Sample loaded perpendicular to fibers direction under SEM. 150 x times magnifications (left) and 500 x times magnification (right). Red arrows – loading direction.

In sample loaded parallel to fiber direction fracture of glass fiber was observed (Figure 44), in greater magnification interface debonding between polar glass and nonpolar polypropylene can be observed, this corelates well with literature findings [47]. It can be said that glass fibers are responsible for most of the strength in this direction.

In sample loaded perpendicular to fiber direction fracture of glass fiber was observed (Figure 45) glass fibers were not fractured, some were snapped, but that was caused by secondary bending of fibers, after crack initiation, not by tension loading. Primary failure mod was polypropylene failing in between fibers.

8.2 Compression test

Compression test was conducted according to ASTM C 364. In accordance with literature finding all samples failed due to loss of stability as can be seen in Figure 48.
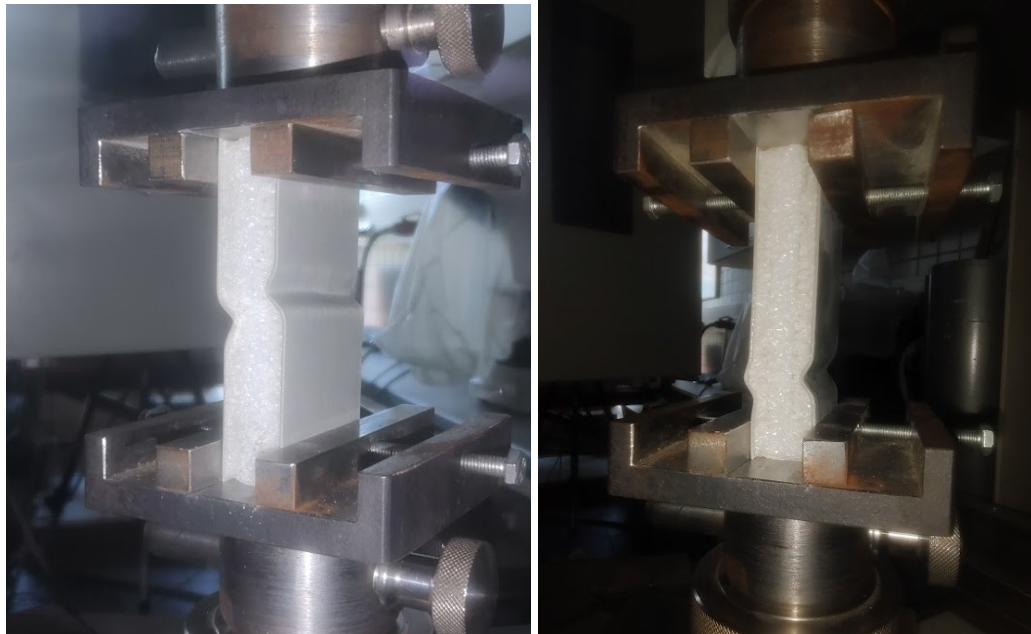

Figure 48 – Failure of sample with polypropylene skins due to loss of stability. Acceptable failure (left), unacceptable failure (right).

Despite measuring at least 12 samples of each type, several had to be invalidated due to unacceptable failure near the jaws, as required by the standard. Obtained values are presented in Table 7, the stress – strain graphs can be seen in Figures 49 and 50.

Table 7 – Edgewise compression test results.

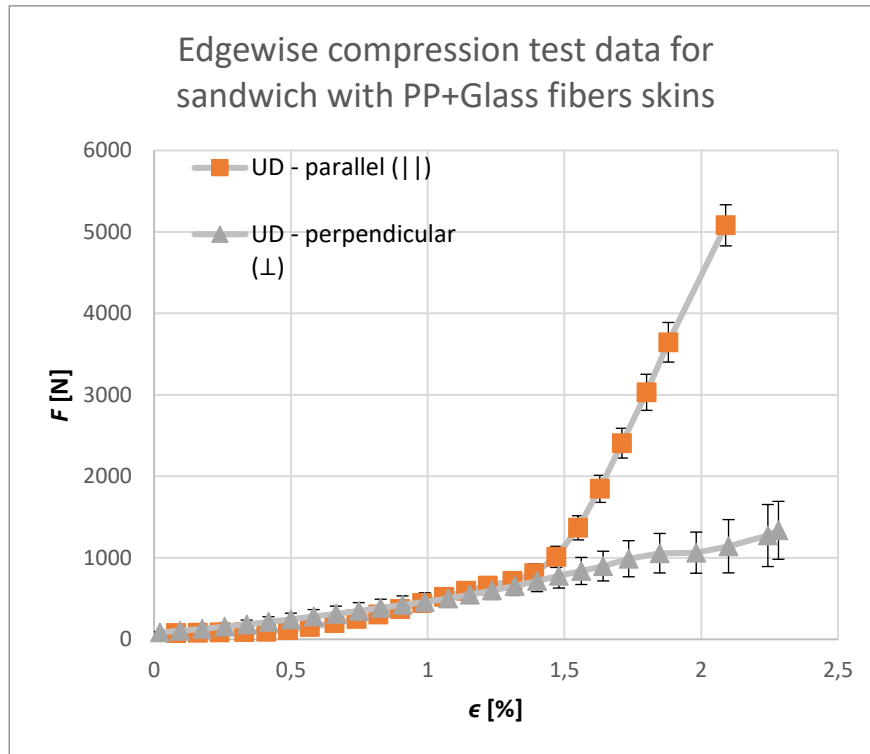|	PP				PP + glass fiber			
	perpendicular ($\perp$)		parallel ($\parallel$)		perpendicular ($\perp$)		parallel ($\parallel$)	
	E [MPa]	σ_{max}[MPa]	E [MPa]	σ_{max}[MPa]	E [MPa]	σ_{max}[MPa]	E [MPa]	σ_{max}[MPa]
N	7		10		5		6	
x	2333	46	2260	48	2133	25	12026	82
s	112.0	1.9	149.4	0.9	130.0	3.6	474.2	6.0

Figure 49 – Stress strain curve for edgewise compression test on sandwich with PP+Glass fibers skins.
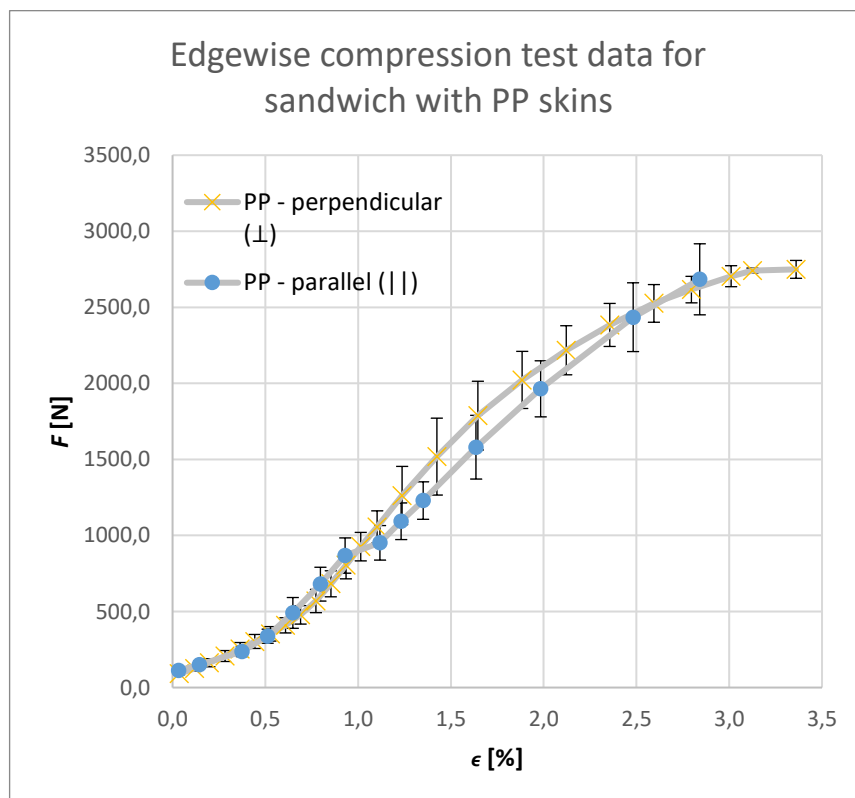

Figure 50 – Stress strain curve for edgewise compression test on sandwich with PP skins.

Polypropylene reinforced with glass fibers displayed significantly higher modulus and max stress when loaded in direction of fibers, compared to when loaded perpendicular to fibers. It is because in order to loss stability sample has to deform (inwards or outwards), but glass fibers resist this deformation. This was anticipated, interesting is that polypropylene with glass fibers showed lower modulus and maximum stress compared to extruded polypropylene (filled with talc). Glass fibers in this perpendicular configuration not only that they don't prevent deformation, but they even induce instability, leading to loss of stability.

For polypropylene in parallel to extrusion direction and perpendicular to extrusion direction data were not significant enough to prove anisotropy.

Maximum strength in compression was not relevantly measured in this test as all specimens failed due to loss of stability.

9 MECHANICAL OPTIMISATION

 Structure was optimized for flexural rigidity to given wight. Structure was optimized as sandwich structure with asymmetrical skins with specified width and unit length. All calculations were conducted in excel spreadsheet. Main variables for optimization were skins thickness (t_1, t_2) and material composition of skins. Effect of core and skins orientation on predicted value of stiffness was also investigated. Key mechanical properties used for optimization can be seen in Table 8.

Table 8 – Data used for calculations

PP + GL			PP		
E_1 (+) [MPa]	E_2 (-)[MPa]	ρ_1 [kgm^{-3}]	E_1 (+)[MPa]	E_2 (-)[MPa]	ρ_2 [kgm^{-3}]
32 000	12 000	1600	670	2 300	1250

Firstly, neutral axis position was determined using Equation 26, which was modified to determine position of neutral axis – e.

$$e = \frac{E_1 t_1 \left(\frac{t_1}{2} + t_3 + \frac{t_2}{2}\right) + E_3 t_3 \left(\frac{t_3}{2} + \frac{t_2}{2}\right)}{E_1 t_1 + E_3 t_3 + E_2 t_2} \tag{38}$$

where:

$E_{1,2,3}$ – layer elasticity modulus (numbering by stiffness – stiffest = 1)

$t_{1,2,3}$ – layer thickness

e – centroid location (distance from the middle axis of the lower skin to

the neutral axis)

Then flexural rigidity can be predicted.

Flexural rigidity is then:

$$K = b \cdot \left[\frac{E_1 t_1^3}{12} + \frac{E_2 t_2^3}{12} + \frac{E_3 t_3^3}{12} + E_1 t_1 (d - e)^2 + E_2 t_2 e^2 + E_3 t_3 \left(\frac{t_3 + t_2}{2} - e\right)^2\right] \tag{39}$$

where:

$E_{1,2,3}$ – layer elasticity modulus (numbering by stiffness – stiffest = 1)

$t_{1,2,3}$ – layer thickness

d – distance of centroids of the skins ($d = t_1/2 + t_2/2 + t_3$) [36]

e – centroid location

b – width of sandwich structure (can be dismissed for unit rigidity)

Weight of sandwich structure is easily calculated:

$$m = b \cdot [\rho_1 t_1 + \rho_2 t_2 + \rho_3 t_3] \tag{40}$$

where:

$\rho_{1,2,3}$ – layer density (numbering by stiffness – stiffest = 1)

$t_{1,2,3}$ – layer thickness

b – width of sandwich structure (can be dismissed for unit weight)

Specific flexural rigidity is than calculated by dividing flexural rigidity by weight.

$$\Omega = \frac{K}{m} \tag{41}$$

where:

K – flexural rigidity

m – weight

Example calculations for sandwich structure with asymmetrical skins $t_1 = 2$ mm and $t_2 = 3$ mm (AS = 1,5 – see Equation 46) and values from Table 7. For this optimization to work it is needed to specify overall sandwich thickness – $h = 20$ mm. Centroid location is then:

$$e = \frac{E_1 t_1 \left(\frac{t_1}{2}+t_3+\frac{t_2}{2}\right)+E_3 t_3 \left(\frac{t_3}{2}+\frac{t_2}{2}\right)}{E_1 t_1 + E_3 t_3 + E_2 t_2} = \frac{32\,000\,000 \cdot 0.002\left(\frac{0.002}{2}+0.015+\frac{0.003}{2}\right)+1\,000\,000 \cdot 0.015\left(\frac{0.015}{2}+\frac{0.003}{2}\right)}{32\,000\,000 \cdot 0.002 + 1\,000\,000 \cdot 0.015 + 12\,000\,000 \cdot 0.003} =$$

11.60 mm $\tag{42}$

where:

$E_{1,2,3}$ – layer elasticity modulus (numbering by stiffness – stiffest = 1)

$t_{1,2,3}$ – layer thickness

e – centroid location (distance from the middle axis of the lower skin to

the neutral axis)

For width $b = 20$ mm. Flexural rigidity is:

$$K = b \cdot \left[\frac{E_1 t_1^3}{12} + \frac{E_2 t_2^3}{12} + \frac{E_3 t_3^3}{12} + E_1 t_1 (d-e)^2 + E_2 t_2 e^2 + E_3 t_3 \left(\frac{t_3 + t_2}{2} - e \right)^2 \right] = 0.02 \cdot$$

$$\left[\frac{32\,000\,000 \cdot 0.002^3}{12} + \frac{12\,000\,000 \cdot 0.003^3}{12} + \frac{1\,000\,000 \cdot 0.015^3}{12} + 32\,000\,000 \cdot 0.002(0.0175 - \right.$$

$$\left. 0.0112)^2 + 12\,000\,000\,000 \cdot 0.0112^2 + 1\,000\,000 \cdot 0.015 \left(\frac{0.018}{2} - 0.0112 \right)^2 \right] =$$

$$143.5 \; N \cdot m^2 \tag{43}$$

where:

$E_{1,2,3}$ – layer elasticity modulus (numbering by stiffness – stiffest = 1)

$t_{1,2,3}$ – layer thickness

d – distance of centroids of the skins ($d = t_1/2 + t_2/2 + t_3$) [36]

e – centroid location

b – width of sandwich structure (can be dismissed for unit rigidity)

Weight is calculated:

$$m = b \cdot [\rho_1 t_1 + \rho_2 t_2 + \rho_3 t_3] = 0.02 \cdot [1600 \cdot 0.002 + 1600 \cdot 0.003 + 80 \cdot 0.015] =$$
$$0.159 \; \text{kg} \cdot \text{m}^{-1} \tag{44}$$

where:

$\rho_{1,2,3}$ – layer density (numbering by stiffness – stiffest = 1)

$t_{1,2,3}$ – layer thickness

b – width of sandwich structure (can be dismissed for unit weight)

Finally specific flexural rigidity is calculated.

$$\Omega = \frac{K}{m} = \frac{143.5}{0.159} = 732.37 \; N \cdot m^3 \cdot kg^{-1} \tag{45}$$

where:

K – flexural rigidity

m – weight

In Excel those calculations were conducted for 3 main variations and 4 sub variations.

Variations:

1. Sandwich structure with skins from polypropylene reinforce with long glass fiber (proUD0°)

2. Sandwich structure with skins from extruded polypropylene

3. Sandwich structure with skin in tension from polypropylene reinforce with long glass fiber (proUD0°) and skin in compression from extruded polypropylene

Sub variation lies in changing thickness of skin in compression relative to skin in tension and differs for all variations.

Resulting data can be seen in Figures 50,52 and 53

Asymmetry – *AS*:

$$AS = \frac{t_2}{t_1} \qquad (46)$$

where:

$t_{1,2}$ – layer thickness
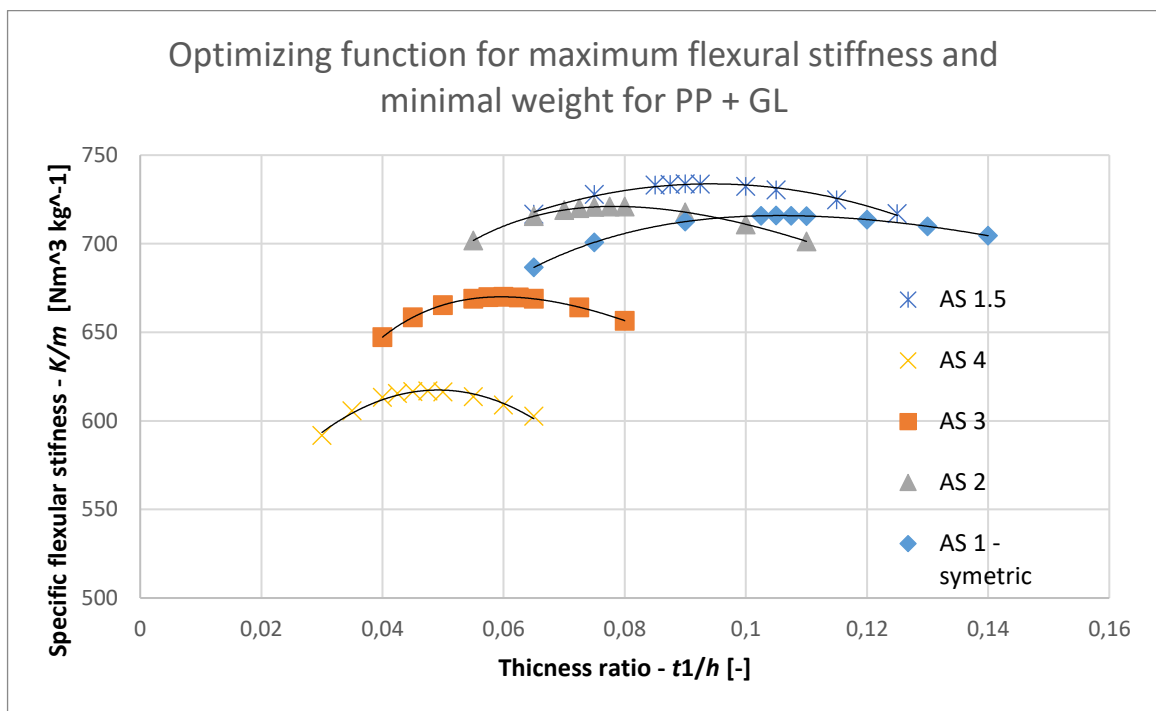
Figure 51 - Optimizing function for maximum flexural stiffness and minimal weight for PP + GL.
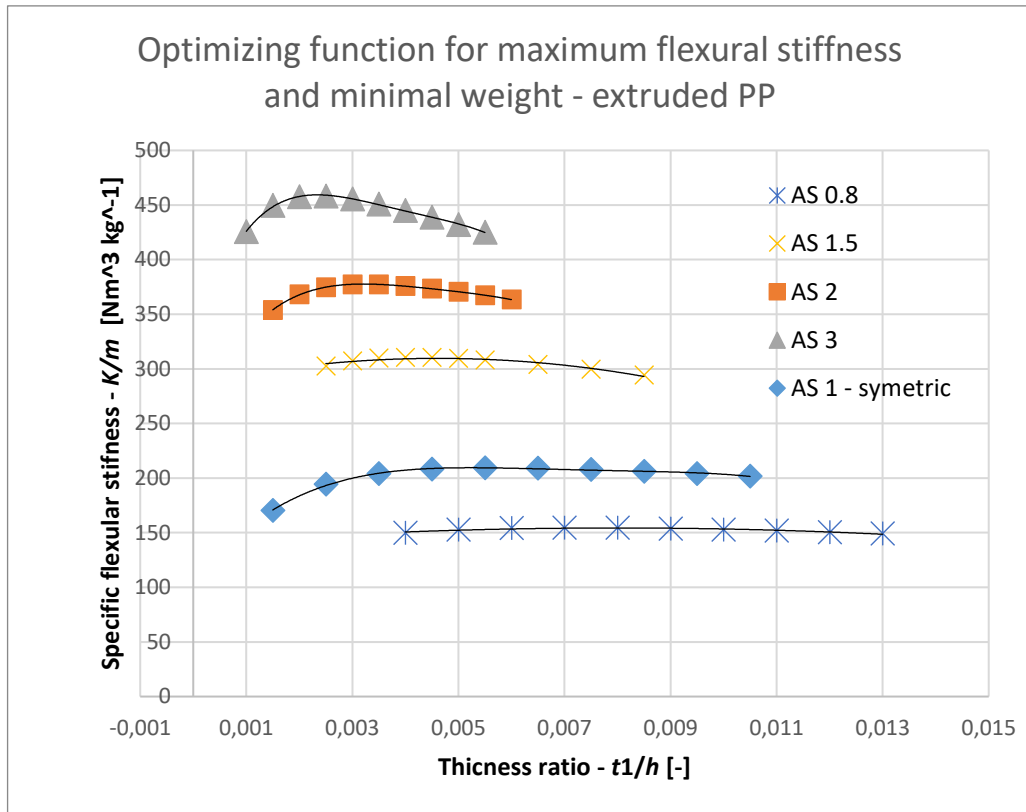
Figure 52 - Optimizing function for maximum flexural stiffness and minimal weight extruded PP.
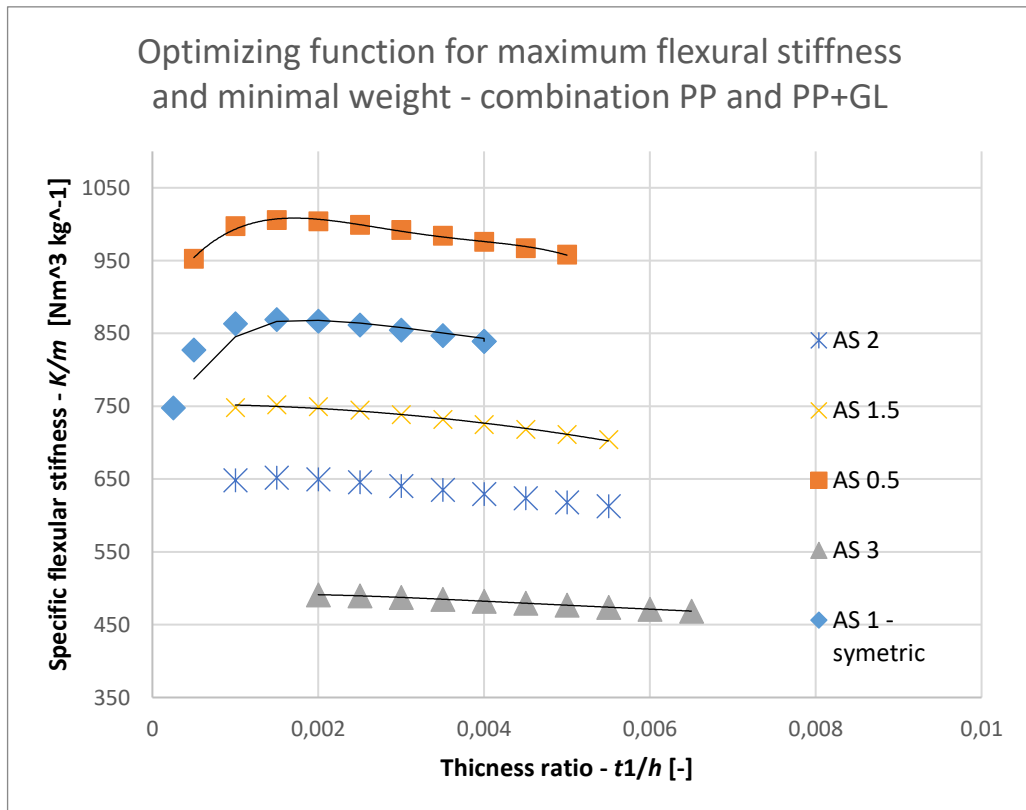
Figure 53 - Optimizing function for maximum flexural stiffness and minimal weight - combination PP and PP+GL.

All optimization curves have characteristic trend. Optimized structure is in local maximum, which can bee seen from graphs (Figures 49,50,51), or exact data of specific flexural rigidity. It can also be found using derivations. Local maximum is:

$$\frac{\partial}{\partial t_1}\left(\frac{K}{m}\right) = 0 \qquad (47)$$

where:

K – flexural rigidity

m – weight

For structure with both skins from polypropylene reinforced with long glass fibers (proUD0°) optimization found even local maximum to asymmetry of skins, local maximum was found by plotting values for each calculation into one graph (Figure 49). Local maximum for asymmetry was AS = 1.5 at $t_1/h = 0.09$. This is due to different elastic modulus of skins in compression and tension.

For skins from extruded polypropylene or combinations local maximum was not found, as value of specific flexural rigidity continues to grow exponentially. For skins with extruded polypropylene specific flexural rigidity grows with growing value of asymmetry. For combination of skin materials opposite can is true, value of flexural rigidity grows with decreasing value of asymmetry.

This optimization approach has it´s limitations. Biggest of which is that it doesn't take into account manufacturability and cost. Manufacturability can be integrated as limits of thicknesses for each variant. Cost can be plugged into optimization as cost for specified area or volume and replace density in Equation 40.

It is also possible to optimize for maximum strength, but as loading mode is not specified this optimization is not suitable. As loading mode (single force, uniform load, bending moment, temperature difference) and support configuration (single support, cantilever beam, etc.) would affect final result greatly and there for would each require specific optimization.
..

9.1 Bend testing

To evaluate obtained data from mechanical tests and mechanical optimization bend test was carried out. Test was conducted according to ASTM C 393, sample size described earlier.

As testing machine was not equipped with device, that could accurately measure deflection in middle of the test sample, it was not possible to determine what affect had shear stiffness of core and flexural rigidity on final deflection. Therefor it was needed to perform three point bend test and four point bend test. Thant using equations from ASTM C 393 both can be calculated and compared to predicted values. Recorded data with error bars for 1. Series are shown in Figure 54.
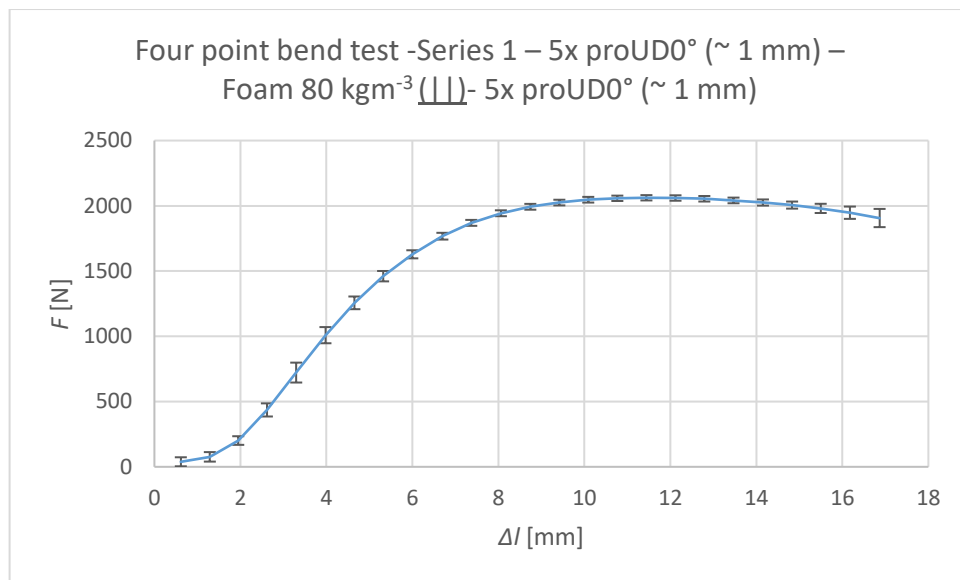
Figure 54 - Four point bend test data -Series 1.

From both bending test only force at given displacement are important. Maximum stress at maximum displacement are often used for calculations. But during testing skins were failing due to indentation, which may altered data. So data from linear part of curve may result in more precise calculation (for series 1 – $F_{max} \approx 2000$ N at $\Delta l_{max} \approx 10$ mm, but value $F \approx 1000$ N at $\Delta l_{max} \approx 4$ mm may result in more precise calculation, because Δl_{max} consist of beam deflection, but also from skin deflection due to indentation).

Data obtained from test can be seen in Tables 9 and 10 with predicted values of flexural rigidity – K and shear modulus of core – G in Table 11.

Flexural rigidity and shear modulus of core was calculated using equations from ASTM C393

Flexural rigidity:

$$K = \frac{F_1 L_1^3 \left[1 - \left(11 \cdot L_1^2 / 8L_1^2\right)\right]}{48\delta_1 \left[1 - \left(2F_1 L_1 \delta_2 / F_2 L_2 \delta_1\right)\right]} \tag{49}$$

where:

F_1 – Force from three-point bend test

F_2 – Force from four-point bend test

$L_{1,2}$ – Major distance between supports

δ_1 – Deflection in three-point bend test

δ_2 – Deflection in four-point bend test

$$G = \frac{F_1 L_1 c \left[8L_1^2 / 11L_2^2 - 1\right]}{\delta_1 b (h + t_3)^2 \left[\left(16F_1 L_1^3 \delta_2 / 11F_2 L_2^3 \delta_1\right) - 1\right]} \tag{50}$$

where:

F_1 – Force from three-point bend test

F_2 – Force from four-point bend test

$L_{1,2}$ – Major distance between supports

δ_1 – Deflection in three-point bend test

δ_2 – Deflection in four-point bend test

b – Sandwich thickness

h – Sandwich height

t_3 – Core height

Table 9 - Measured data in three point bend test.

Measured data in three point bend test				
	Series 3 - UD 6/4	Series 4 - UD 9/6	Series 5 -PP ($\perp$)	Series 6 -PP (II)
N	3	2	2	4
xF_{max} [N]	1024.2	1362.0	198.4	263
sF_{max} [N]	1.9	15.3	33.6	6.9
$x\delta_{max}$ [mm]	8	13	9	7
$s\delta_{max}$ [mm]	0.6	0.2	2.3	0.6

Table 10 - Measured data in four point bend test.

Measured data in four point bend test						
	Series 1- UD 5/5	Series 2 - UD 3/2	Series 3 - UD 6/4	Series 4 - UD 9/6	Series 5 - PP ($\perp$)	Series 6 - PP (II)
N	5	3	1	2	1	2
xF_{max} [N]	2064	1665	2107	2406	729	380
sF_{max} [N]	20.7	151.0		107.2		50.2
$x\delta_{max}$ [mm]	12	9	14	13	21	18
$s\delta_{max}$ [mm]	0.6	1.1		0.8		4.1

Table 11 - Data used to calculate flexural rigidity and core shear stiffness.

Data used to calculate flexural rigidity and core shear stiffness				
	Series 3 - UD 6/4	Series 4 - UD 9/6	Series 5 -PP ($\perp$)	Series 6 -PP (II)
F_3 [N]	558.0	673.0	110.0	163.0
δl_3 [mm]	2.0	2.5	3.3	3.2
F_4 [N]	1574.0	1970.0	380.0	316.0
δl_4 [mm]	4.5	5.4	15.0	10..3
h [mm]	20.45	20.6	20.3	20.4
t_3 [mm]	17.6	17.0	19.5	19.6
K - ASTM C393 [N/mm2]	$2.86 \cdot 10^7$	$4.59 \cdot 10^7$	$1.27 \cdot 10^6$	$1.37 \cdot 10^6$
K - predicted [N/mm2]	$1.29 \cdot 10^8$	$2.37 \cdot 10^8$	$6.19 \cdot 10^6$	$6.99 \cdot 10^6$
G - ASTM C393 [MPa]			1.2	1.3
G - ISO 1922 [MPa]			52	76

Although expected, the difference between the measured and predicted values is substantial. This trend is described well literature findings and corelates with past experiments[39][46].

All tested samples failed due to indentation of upper (thicker) skin. This can be avoided only by making skinss thicker, or core thinner (thinner core > lower rigidity > less force applied on skins). But this was not possible due to manufacturing limitations. For thicker skins (Series 3,4) significant shear deformation of core was observed. But due to core from polypropylene being relatively flexible it did not cracked, as would more rigid material. This can be seen in Figure 55.
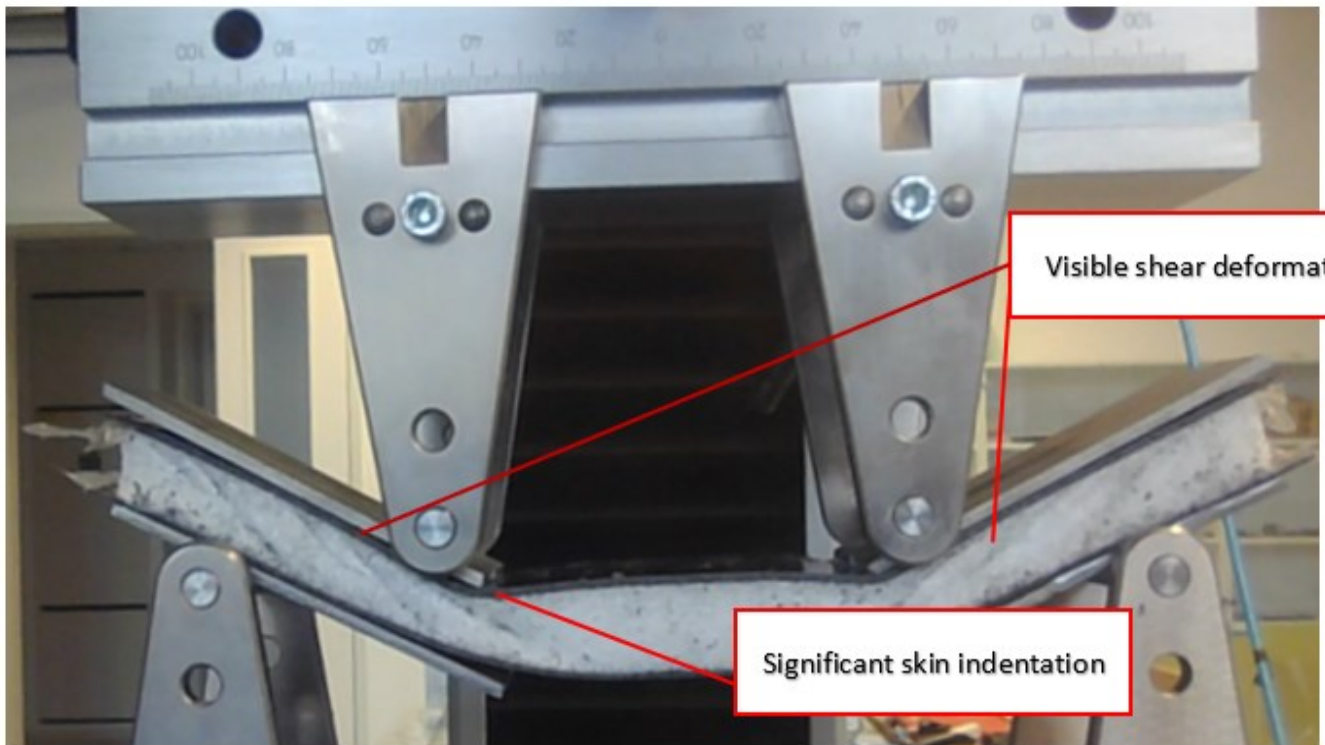
Figure 55 – Failed sample in four point bend test, with visible skin indentation and shear deformation region.

From Figure 55 is clearly visible, that shear truly occur only between support, as in stress distribution prediction in Figure 35. Difference between predicted and measured values for series 3 and 4 [**Series 3** – 4x proUD0° (~ 0.8 mm) – Foam 80 kgm-3 (∥) - 6x proUD0° (~ 1.2 mm; **Series 4** – 6x proUD0° (~ 1.2 mm) – Foam 80 kgm-3 (∥)- 9x proUD0° (~ 1.8 mm)] can be seen in Figure 56.
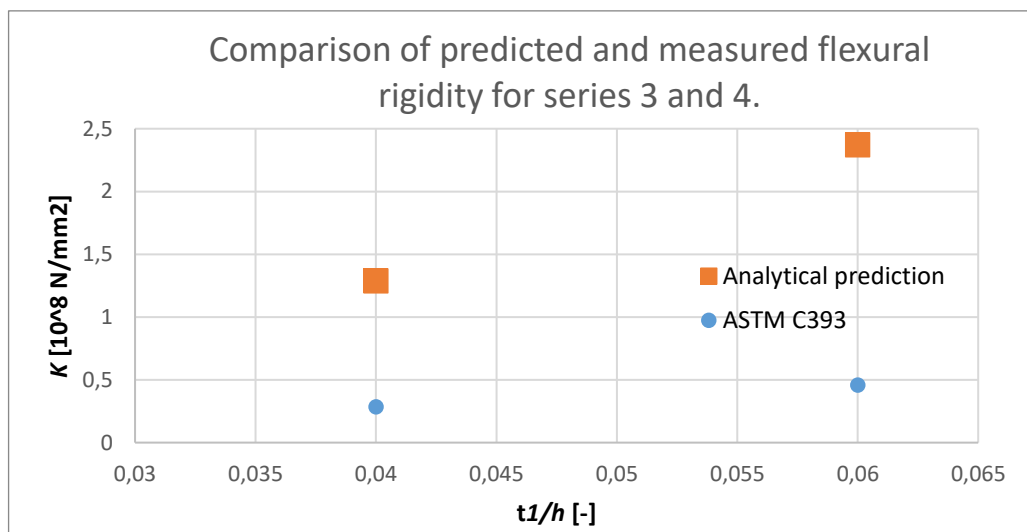

Figure 56 - Comparison of predicted and measured flexural rigidity for series 3 and 4.

CONCLUSION

This study explores the mechanical properties and optimization strategies of sandwich structures made solely from polypropylenes. Through meticulous experimentation and rigorous analysis, this study aimed to illuminate the remarkable potential of thermoplastic materials in revolutionizing the realm of sandwich construction. The research spanned a wide array of tests and examinations, covering the core and skin materials, as well as the overall behavior of the sandwich structures.

The core of this study revolved around the mechanical performance of polypropylene foam, a material of particular interest due to its altered cell orientation. Notable values for key parameters such as compressive strength, shear strength, and elastic modulus were measured. For instance, in compression tests parallel to the extrusion direction, polypropylene foam exhibited elastic moduli ranging from 9.4 MPa to 22.3 MPa, depending on density. Similarly, in compression tests perpendicular to the extrusion direction, the elastic moduli ranged from 0.4 MPa to 2.4 MPa. These results underscore the considerable mechanical potential of polypropylene foam as a core material for sandwich structures as well as reflect the effect of cell orientation and density on mechanical properties.

Furthermore, experiments with skin materials, including extruded polypropylene and polypropylene reinforced with long glass fibers, yielded valuable insights into their tensile and compressive properties.

While this study showcased the promising mechanical characteristics of polypropylene sandwich structures, it also uncovered some challenges and limitations. Discrepancies between measured (Ser. 4 – $K = 4.59 \cdot 10^7$ N/mm^2) and predicted values (Ser 4 - $K = 2.37 \cdot 10^8$ N/mm$^{2)}$, particularly in flexural rigidity and core shear stiffness, underscored the complexities involved in structural optimization. Moreover, the propensity for upper skin indentation and core shear deformation highlighted the need for further refinement in design and manufacturing processes and need for better testing methods.

Despite these challenges, this study represents a significant step forward in understanding and harnessing the potential of polypropylene sandwich structures. By providing a comprehensive analysis of their mechanical behavior and optimization strategies, it lays the groundwork for future advancements in this burgeoning field, with implications spanning industries from construction to automotive engineering.

BIBLIOGRAPHY

[1] KLEPNER, Daniel a SENDIJAREVIC, Vahid. *Polymeric Foams and Foam Technology*. 2nd ed. Hanser, 2004. ISBN 1-56990-336-0.

[2] HARDING, R.H. *Morphologies of cellular materials. Resinography of cellular plastics*. ASTM STP 414. 1967.

[3] , Expert Market Research. Global Expanded Polypropylene (EPP) Foam Market Size, Share: By Raw Material: Synthetic Polypropylene, Bio-based Polypropylene; By Form: Fabricated EPP, Moulded EPP, Others; By Application: Automotive, Dunnage, Furniture, Food Packaging, HVAC, Sports and Leisure, Others; Regional Analysis; Competitive Landscape; 2024-2032. Online. Roč. 2023. Dostupné z: https://www.expertmarketresearch.com/reports/expanded-polypropylene-epp-foam-market. [cit. 2023-11-01].

[4] A Review on Manufacturing, Properties and Application of Expanded Polypropylene. Online. *MIT International Journal of Mechanical Engineering*. 2014, roč. 2014, č. 4, s. 22-28. Dostupné z: https://www.mitpublications.org.in/yellow_images/1392611109_logo_Paper_04.pdfvv. [cit. 2023-11-01].

[5] EU. Directive 2000/53 - End-of life vehicles - Commission Statements. In: . 2003.

[6] THEENATHAYALAN, R.; THIRISHA, S.N. a SUGANYA, R. Impact of different concrete ingredients on the microstructure of lightweight concrete – A comprehensive review. Online. *Materials Today: Proceedings*. 2022, roč. 62, č. 6, s. 4392-4396. ISSN 22147853. Dostupné z: https://doi.org/10.1016/j.matpr.2022.04.886. [cit. 2023-11-09].

[7] CHUNG, Chen-Yuan; HWANG, Shyh-Shin; CHEN, Shia-Chung a LAI, Ming-Chien. Effects of Injection Molding Process Parameters on the Chemical Foaming Behavior of Polypropylene and Polystyrene. Online. *Polymers*. 2021, roč. 13, č. 14. ISSN 2073-4360. Dostupné z: https://doi.org/10.3390/polym13142331. [cit. 2023-11-13].

[8] MENDOZA-CEDENO, Steven; KWEON, Mu Sung; NEWBY, Sarah; SHIVOKHIN, Maksim; PEHLERT, George et al. Improved Cell Morphology and Surface Roughness in High-Temperature Foam Injection Molding Using a Long-Chain Branched Polypropylene. Online. *Polymers*. 2021, roč. 13, č. 15, s. -. ISSN 2073-4360. Dostupné z: https://doi.org/10.3390/polym13152404. [cit. 2023-11-13].

[9] BARLOW, A.; HILL, L.A. a MEEKS, L.A. Radiation processing of polyethylene. Online. *Radiation Physics and Chemistry (1977)*. 1979, roč. 14, č. 3-6, s. 783-796. ISSN 01465724. Dostupné z: https://doi.org/10.1016/0146-5724(79)90114-6. [cit. 2023-11-22].

[10] XIA, Bihua; DONG, Weifu; ZHANG, Xuhui; WANG, Yang; JIANG, Jie et al. Preparation of Controllable Cross-Linking Polyethylene Foaming Materials and Their Properties. Online. *Journal of Wuhan University of Technology-Mater. Sci. Ed*. 2022, roč. 37, č. 5, s. 1014-1019. ISSN 1000-2413. Dostupné z: https://doi.org/10.1007/s11595-022-2625-9. [cit. 2023-11-27].

[11] WU, Meng-Heng; WANG, Cheng-Chien a , Chuh-Yung. Preparation of high melt strength polypropylene by addition of an ionically modified polypropylene. Online. *Polymer*. 2020, roč. 202, č. -, s. -. ISSN 00323861. Dostupné z: https://doi.org/10.1016/j.polymer.2020.122743. [cit. 2023-11-27].

[12] *Process for foaming a sheet of ethylenic resin during downward movement of the sheet* (US). Sekisui Chemical Co Ltd. Přihl.: 1973-01-16. Uděl.: 1969-09-26. US3711584A.

[13] *Process for producing thermoplastic resin foam* (US). Toray Industries Inc. Přihl.: 1971-02-09. Uděl.: 1965-02-25. US3562367A.

[14] *Surface heating of a foamable polyolefin preform prior to foaming and crosslinking* (US). Furukawa Electric Co Ltd. Přihl.: 1968-11-25. Uděl.: 1972-03-21. US3651183A.

[15] *Production of thermoplastic resin foam* (JPS). Showa Denko Materials Co Ltd. Přihl.: 1978-03-03. Uděl.: 1979-09-12. JPS54117568A.

[16] *Foam Extrusion Principles and Practice, Second Edition*. 2nd ed. Taylor & Francis, 2014. ISBN 9780429184703.

[17] GIBSON, L a ASHBY, M. *Cellular solids: structure and properties*. 2nd ed. Cambridge solid state science series. Cambridge: Cambridge University presss, 1997 (1999 pbk ed). ISBN 05-214-9911-9.

[18] RUMIANEK, Przemysław; DOBOSZ, Tomasz; NOWAK, Radosław; DZIEWIT, Piotr a AROMIŃSKI, Andrzej. Static Mechanical Properties of Expanded Polypropylene Crushable Foam. Online. *Materials*. 2021, roč. 14, č. 2, s. 7-8. ISSN 1996-1944. Dostupné z: https://doi.org/10.3390/ma14020249. [cit. 2024-03-10].

[19] ŠUBA, Oldřich. *Dimenzování a navrhování výrobků z polymerů*. Vyd. 3. Zlín: Univerzita Tomáše Bati ve Zlíně, 2019. ISBN 978-80-7318-948-8.

[20] MOONEN, Jarrod; RYAN, Shannon; KORTMANN, Lukas; PUTZAR, Robin; FORRESTER, Crystal et al. Evaluating UHMWPE-stuffed aluminium foam sandwich panels for protecting spacecraft against micrometeoroid and orbital debris impact. Online. *International Journal of Impact Engineering*. 2023, roč. October 2023, č. vol. 180, s. 1-9. ISSN 0734743X. Dostupné z: https://doi.org/10.1016/j.ijimpeng.2023.104668. [cit. 2024-02-14].

[21] SAB-PROFIEL. *Roofing panels*. Online. SAB-profiel. 2024. Dostupné z: https://www.sabprofiel.com/products/roof/roofing-panels/. [cit. 2024-02-14].

[22] SUN, Xi; JIAN, Zhiqian; SU, Xixi; HUANG, Peng; GAO, Qiang et al. Aluminum Foam Sandwich: Pore Evolution Mechanism Investigation and Engineering Preparing Optimization. Online. *Materials*. 2023, roč. 16, č. 19, s. -. ISSN 1996-1944. Dostupné z: https://doi.org/10.3390/ma16196479. [cit. 2024-02-14].

[23] HAN, Sungjin; SUNG, Minchang; JANG, Jinhyeok; JEON, Seung-Yeol a YU, Woong-Ryeol. The effects of adhesion on the tensile strength of steel-polymer sandwich composites. Online. *Advanced Composite Materials*. 2021, roč. 30, č. 5, s. 443-461. ISSN 0924-3046. Dostupné z: https://doi.org/10.1080/09243046.2020.1835793. [cit. 2024-02-15].

[24] PETRAS, Achilles. *Design of Sandwich Structures*. Online, Thesis. Cambrige: University of Cambrige, 1999. Dostupné z: https://www.repository.cam.ac.uk/handle/1810/236995. [cit. 2024-02-14].

[25] HUBER, Tim; PANG, Shusheng a STAIGER, Mark P. All-cellulose composite laminates. Online. *Composites Part A: Applied Science and Manufacturing*. 2012, roč. 43, č. 10, s. 1738-1745. ISSN 1359835X. Dostupné z: https://doi.org/10.1016/j.compositesa.2012.04.017. [cit. 2024-02-17].

[26] ATHUL, Joseph; VINYAS, Mahesh; VISHWAS, Mahesh a DINESHKUMAR, Harursampath. Introduction to Sandwich Composite Panels and Their Fabrication Methods. Online. In: *Introduction to Sandwich Composite Panels and Their Fabrication Methods*. CRC Press, 2022, s. 1-25. ISBN 9781003143031. Dostupné z:

https://www.taylorfrancis.com/chapters/edit/10.1201/9781003143031-1/introduction-sandwich-composite-panels-fabrication-methods-athul-joseph-vinyas-mahesh-vishwas-mahesh-dineshkumar-harursampath. [cit. 2024-02-17].

[27] APARNA, M. Lakshmi; CHAITANYA, G.; SRINIVAS, K. a RAO, J. Appa. Fabrication of Continuous GFRP Composites using Vacuum Bag Moulding Process. Online. *International Journal of Advanced Science and Technology*. 2016, roč. 2016, č. vol. 87, s. 37-46. ISSN 20054238. Dostupné z: https://doi.org/10.14257/ijast.2016.87.05. [cit. 2024-02-17].

[28] DAVIM, J.Paulo a REIS, Pedro. Drilling carbon fiber reinforced plastics manufactured by autoclave—experimental and statistical study. Online. *Materials & Design*. 2003, roč. 24, č. 5, s. 315-324. ISSN 02613069. Dostupné z: https://doi.org/10.1016/S0261-3069(03)00062-1. [cit. 2024-02-17].

[29] VAN DE VELDE, Kathleen a KIEKENS, Paul. Thermoplastic pultrusion of natural fibre reinforced composites. Online. *Composite Structures*. 2001, roč. 54, č. 2-3, s. 355-360. ISSN 02638223. Dostupné z: https://doi.org/10.1016/S0263-8223(01)00110-6. [cit. 2024-02-17].

[30] ZHANG, Lingfeng; LIU, Weiqing; WANG, Lu a LING, Zhibin. Mechanical behavior and damage monitoring of pultruded wood-cored GFRP sandwich components. Online. *Composite Structures*. 2019, roč. 215, č. -, s. 502-520. ISSN 02638223. Dostupné z: https://doi.org/10.1016/j.compstruct.2019.02.084. [cit. 2024-02-17].

[31] REIS, João Pedro; DE MOURA, Marcelo a SAMBORSKI, Sylwester. Thermoplastic Composites and Their Promising Applications in Joining and Repair Composites Structures: A Review. Online. *Materials*. 2020, roč. 13, č. 24, s. 5-7. ISSN 1996-1944. Dostupné z: https://doi.org/10.3390/ma13245832. [cit. 2024-02-20].

[32] PASSARO, Alessandra; CORVAGLIA, Paolo; MANNI, Orazio; BARONE, Luigi a MAFFEZZOLI, Alfonso. Processing-properties relationship of sandwich panels with polypropylene-core and polypropylene-matrix composite skins. Online. *Polymer Composites*. 2004, roč. 25, č. 3, s. 307-318. ISSN 0272-8397. Dostupné z: https://doi.org/10.1002/pc.20025. [cit. 2024-02-20].

[33] CHEN, Youming a DAS, Raj. A review on manufacture of polymeric foam cores for sandwich structures of complex shape in automotive applications. Online. *Journal of Sandwich Structures & Materials*. 2022, roč. 24, č. 1, s. 789-819. ISSN 1099-6362. Dostupné z: https://doi.org/10.1177/10996362211030564. [cit. 2024-02-20].

[34] NOFAR, Mohammadreza; UTZ, Julia; GEIS, Nico; ALTSTÄDT, Volker a RUCKDÄSCHEL, Holger. Foam 3D Printing of Thermoplastics: A Symbiosis of Additive Manufacturing and Foaming Technology. Online. *Advanced Science*. 2022, roč. 9, č. 11, s. 7-14. ISSN 2198-3844. Dostupné z: https://doi.org/10.1002/advs.202105701. [cit. 2024-03-10].

[35] KABIR, S M Fijul; MATHUR, Kavita a SEYAM, Abdel-Fattah M. A critical review on 3D printed continuous fiber-reinforced composites: History, mechanism, materials and properties. Online. *Composite Structures*. 2020, roč. 232. ISSN 02638223. Dostupné z: https://doi.org/10.1016/j.compstruct.2019.111476. [cit. 2023-05-20].

[36] ZENKERT, D. *Handbook of sandwich construction*. Engineering Materials Advisory Services, 1998. ISBN 978-0947817961.

[37] ZOHOURKARI, Iman; ZOHOOR, Mehdi a ANNONI, Massimiliano. Investigation of the Effects of Machining Parameters on Material Removal Rate in Abrasive Waterjet Turning. Online. *Advances in Mechanical Engineering*. 2014, roč. 6. ISSN 1687-8140. Dostupné z: https://doi.org/10.1007/s40799-022-00585-2. [cit. 2023-10-05].

[38] ŠUBA, Oldřich; KUBIŠOVÁ, Milena; ŠUBA JR, Oldřich; MĚŘÍNSKÁ, Dagmar a PITNEROVÁ, Lenka. Study of bending resistance of sandwich structures. Online. *IOP Conference Series: Materials Science and Engineering*. 2020, roč. 726, č. 1, s. 1-6. ISSN 1757-8981. Dostupné z: https://doi.org/10.1088/1757-899X/726/1/012006. [cit. 2024-03-14].

[39] ŠUBA, Oldřich; ŠUBA JR., Oldřich; RUSNÁKOVÁ, Soňa; BONDREA, I.; SIMION, C. et al. Effects of Core Softness and Bimodularity of Fibreglass Layers on Flexural Stiffness of Polymer Sandwich Structures. Online. *MATEC Web of Conferences*. 2017, roč. 121, č. 121, s. 2-5. ISSN 2261-236X. Dostupné z: https://doi.org/10.1051/matecconf/201712103022. [cit. 2024-03-14].

[40] *The method of production of reoriented lightweight polyolefin sheets: Způsob výroby reorientovaných lehčených polyolefinových desek* (CZ). Ing. Ondřej KRÁTKÝ. Přihl.: 07.09.2022. Uděl.: 27.09.2023. PV 2022-379. Dostupné z: https://isdv.upv.gov.cz/webapp/!resdb.pta.frm. [cit. 2024-04-23].

[41] *Proflol proUD0°*. Online. Profol. 2024. Dostupné z: https://www.profol.de/en/ud-tape/. [cit. 2024-05-01].

[42] *Catalog: Machines, Instruments and Laboratory Equipments: Static Materials Testing Machine Zwick/Roell | 1456*. Online. In: FT UTB. 2024. Dostupné z: https://ft.utb.cz/wp-content/uploads/2019/03/1456.jpg. [cit. 2024-04-28].

[43] INTERNATIONAL ORGANIZATION FOR STANDARDIZATION. ISO 527 - 4:2023, *Plastics - Determination of tensile properties - Part 4: Test conditions for isotropic and orthotropic fibre-reinforced plastic composites*. 2023.

[44] TAO, Jie; LI, Feng; ZHAO, Qilin; ZHANG, Dongdong a ZHAO, Zhibo. In-plane compression properties of a novel foam core sandwich structure reinforced by stiffeners. Online. *Journal of Reinforced Plastics and Composites*. 2018, roč. 37, č. 2, s. 134-144. ISSN 0731-6844. Dostupné z: https://doi.org/10.1177/0731684417737631. [cit. 2024-04-28].

[45] CABRERA, N.O.; ALCOCK, B. a PEIJS, T. Design and manufacture of all-PP sandwich panels based on co-extruded polypropylene tapes. Online. *Composites Part B: Engineering*. 2008, roč. 39, č. 7-8, s. 1183-1195. ISSN 13598368. Dostupné z: https://doi.org/10.1016/j.compositesb.2008.03.010. [cit. 2024-05-04].

[46] RAHIMIDEHGOLAN, Foad a ALTENHOF, William. Compressive behavior and deformation mechanisms of rigid polymeric foams: A review. Online. *Composites Part B: Engineering*. 2023, roč. 253, č. -, s. 1-7. ISSN 13598368. Dostupné z: https://doi.org/10.1016/j.compositesb.2023.110513. [cit. 2024-04-04].

[47] ETCHEVERRY, Mariana a BARBOSA, Silvia E. Glass Fiber Reinforced Polypropylene Mechanical Properties Enhancement by Adhesion Improvement. Online. *Materials*. 2012, roč. 5, č. 12, s. 1084-1113. ISSN 1996-1944. Dostupné z: https://doi.org/10.3390/ma5061084. [cit. 2024-05-03].

LIST OF ABBREVIATIONS

ABS – Acrylonitrile Butadiene Styrene

AS – Asymmetry

ASTM – American Society for Testing and Materials

CAGR – Compound Annual Growth Rate

E^* - Foam Modulus of Elasticity

$E_{1,2,3}$ – Layer Elasticity Modulus (Numbering by Stiffness – Stiffest = 1)

E_i – Flexural Modulus of Element

E_s – Unfoamed Polymer Modulus of Elasticity

FFF – Fused Filament Fabrication

G^* - Foam Shear Modulus

G_3 – Shear Modulus of Core

HDPE – High Density Polyethylene

ISO – International Organization for Standardization

MPa – Megapascals

N – Newtons

PA – Polyamide

PE – Polyethylene

PEEK – Polyether Ether Ketone

PEI – Polyetherimide

PLA – Polylactic Acid

PP – Polypropylene

PP+GL – Polypropylene Reinforced with Glass Fibers

PUR – Polyurethane

PVC – Polyvinyl Chloride

SEM – Scanning Electron Microscope

T – Temperature

UV – Ultraviolet

USD – United States Dollar

W – Watt

X-rays – X-rays

XPP – Expanded Polypropylene

β-rays – Beta Rays

δ – Displacement

δ_M – Displacement by Bending Moment

δ_T – Displacement by Shear Forces

δ – Total Displacement

$\varepsilon(y)$ – Strain Based on the Position in y

$\sigma(y)$ – Stress Based on Position in y

ε – Strain δ/l

σpl – Stress When Plastic Deformation Occurs

σys – Yield Strength of Cell Wall Material

ρ – Density

$\rho*$ - Foam Density

ρ_s – Unfoamed Polymer Density

τ – Shear Stress

τ_3 – Shear Stress in Core

τ_a – Maximum Allowed Shear Stress

τ_c – Combined Shear Stress

b – Original Width

b_R – Reduced Width

d – Distance of Centroids of the Skins (d=t1+t2)

e – Centroid Location (Distance from the Middle Axis of the Lower Skin to the Neutral Axis)

I – Second Moment of Area

J – Second Moment of Area

K – Flexural Rigidity

K_0 – Bending Stiffness of the Skins about the Neutral Axis

K_1 – Bending Stiffness of the Skins about Their Individual Neutral Axes

K_2 – Bending Stiffness of the Core

m – Mass

n – Degree of Constraint at the End of the Elements (Based on Euler's Relations for the Buckling of Thin Members)

p – Gas Pressure in Cell After Deformation

p_0 – Gas Pressure in Cell Before Deformation

r – Radius of Curvature of the Neutral Plane

S – Cross-section Area

$\sigma(y)$ – Stress Based on Position in y

T – Normal Force

t – Time

t_e – Cell Edge Thickness

t_f – Cell Wall Thickness

w% - Weight Percentage

x – Median

Ω - Specific Flexural Rigidity

LIST OF FIGURES

LIST OF TABLES

APPENDICES

Appendix P I: Profol proUD0°

Appendix P II: 3M 8010 DP Adhesive

APPENDIX P I: PROFOL PROUD0°

Nachhaltige Leichtbau-Composites mit effizienter Großserienfertigung

INNOVATIVE TECHNOLOGIE – MADE IN GERMANY

„Die Herstellung recyclingfähiger Produkte, eine nachhaltige Produktion und effiziente Nutzung von Ressourcen sind unser Standard. Wir evaluieren kontinuierlich unseren Einsatz an Energie und Rohstoffen in den Produktionsprozessen und im gesamten Unternehmen – ein aktiver Beitrag zum Umweltschutz."

„Dieser Leitsatz ist das Fundament der Unternehmenskultur bei Profol", so der CEO und Eigentümer Dr. Philipp Schieferdecker. In allen Produktionsbereichen der Herstellung der Cast-Polypropylen-Folien und der der Leichtbau-Composites steht der Fokus auf nachhaltiger und effizienter Großserienfertigung.

Heutige Leichtbaukonzepte werden häufig nur über einen Austausch der Werkstoffe realisiert, obwohl eine zielgerichtete Entwicklung für effektive und konsequente Leichtbauweisen bei Verwendung neuer Werkstoffe zwingend notwendig ist.

Profol Greiz GmbH

Die Leichtbau-Composites Materialien von Profol finden Einsatz in allen zukunftsorientierten Projekten unterschiedlichster Märkte.

Automotive

Caravan

Truck

Building & Construction

E-mobility
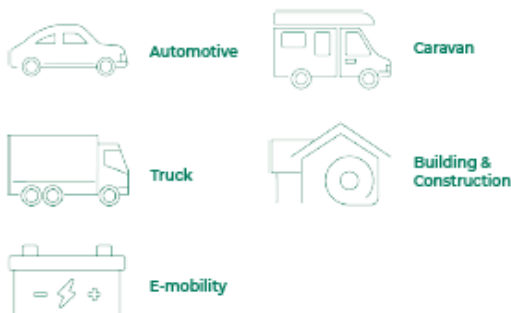
Die thermoplastischen faserverstärkten Kunststoffe (FVK/CFTRP) bilden dabei einen wichtigen Baustein im Leichtbau. Polypropylen als teilkristalliner Matrixwerkstoff eignet sich dafür auf Grund seiner amorphen und kristallin angeordneten Phasen.

Thermoplaste zeichnen sich durch hohe Beständigkeit gegen Chemikalien, eine geringere Kriechneigung sowie verbesserte mechanische Eigenschaften aus. Auch nehmen die mechanischen Eigenschaften bei Erreichen der Glasübergangstemperatur (TG) nicht abrupt ab, sondern bleiben bis kurz vor Erreichen der Schmelztemperatur erhalten.

Ein weiterer Vorteil ist die größere Prozessvielfalt. Eine Kombination aus Spritzgießen, Laminieren und Thermoformen, etwa das Pressen und Hinterspritzen von Organoblechen, ermöglicht komplexe Geometrien.

profol Performa

LÖSUNGEN VON PROFOL

Grundlage der Leichtbau-Composites von Profol bildet das uni-direktionale, endlosfaserverstärkte Tape, das sog. UD-Tape.
Profol hat an seinem Standort in Greiz eine effiziente Großserienfertigung zur Herstellung vom proUD-0° Tape errichtet.

proUD-0°

Der ressourcenschonende Einsatz sämtlicher Energien und die Wiederverwendung rücklaufender Produktions-energien ermöglichen eine deutliche Verbesserung der Effektivität und auch des CO_2-footprint. Profol hat die CO_2-Bilanz seiner Produkte durch das unabhängige Unternehmen „ClimatePartner" bewerten lassen.

	Glasfaser-PP Halbzeugplatte	Aluminium Halbzeugplatte	Stahlblech Halbzeugplatte
Gewicht [kg]	5,79	12,28	27,68
Länge [mm]	2000	2000	2000
Breite [mm]	1250	1250	1250
Dicke [mm]	2	2	2
Material	Glasfaser, PP, Granulat	Aluminium	Rohstoff
Produktionsprozess	Produktion aus der Produktion der Profol herstellt	Walzen (Aluminium) (Quelle: ecoinvent, version 3.8 (2021), sheet rolling, aluminium RER)	Metallbearbeitung, Durchschnitt für die Berücksichtigung von Metallprodukten (Quelle: ecoinvent, version 2.2 (2010), metal working RER)

Climate Partner, Profol Composites

Das Ergebnis zeigt den deutlichen Vorteil vom thermo-plastischem Profol Faserverbund gegenüber den bis dato üblichen Verstärkungsmaterialien wie Aluminium und Stahl

proUD-tape			
Menge	Emission pro Einheit	Anteil relativ	Anteil absolut
1.000.000,00 kg	2,52 kgCO₂e	100,00%	2.521.281,62 kgCO₂e

Bei der UD-Tape-Herstellung werden bis zu 120 dieser auf Spulen gelieferten Glas-Rovings auf eine Produktbreite von 1,25 m aufgespreizt. Im Cast-Verfahren erfolgt die Zusammenführung mit der PP-Matrix. Die daran anschließenden Verfahrensschritte der Anlage sichern die gleichmäßige Umschließung des Glases mit der PR-Matrix.

Das im Großserienprozess hergestellte UD-Tape hat eine Dicke von d = 0,2 mm und wird bis zu einer Lauflänge von 2.200 m aufgewickelt.
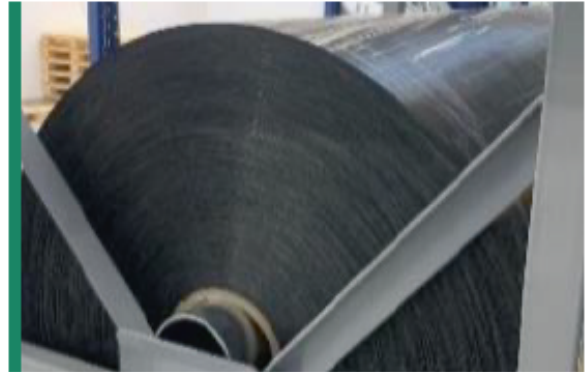
proUD-0°Rollenware

Die Ermittlung der mechanischen Kennwerte erfolgt in Anlehnung an die Standards der Automobilbranche.

Das proUD-0° Tape hat in seiner Standard-Ausführung einen Fasermassegehalt von 72 %. Fertigungen für Spezial-anwendungen sind möglich und erlauben z.B. bei einem 60 % Anteil die Aufbringung einer Struktur als Anti-Rutsch Effekt.

Höhere Anteile von bis zu 80 % sind fertigungstechnisch möglich. Profol setzt hierbei den Fokus stets auf vollkonsolidiertes Tape. Dies ist die Grundlage für weitere Verarbeitung und Sicherstellung der thermischen Verbindung.

Faser-Masse-Gehalt[1] bis zu m_{Glas} = 72 %
Flächengewicht[2] ρ_A = 320 g/m2

Im Zugversuch[3] ergibt sich hieraus:

Zugmodul Σ = 37.000 MPa
Zugfestigkeit σ_M = 1.000 MP

[1] m_{Glas} nach DIN EN ISO 1172
[2] ρ_A nach DIN EN ISO 10352
[3] nach DIN EN ISO 527-4

profol
Performs

VARIABILITÄT

UD-Tapes haben die Eigenschaft durch die gerichteten, ununterbrochenen Glasfasern, die anfallenden Krafteinwirkungen gezielt im Bauteil zu verteilen. Unterstützt wird diese Wirkung durch den Einsatz von Fasern in Querrichtung. Die Profol GmbH hat ein patentiertes Fertigungsverfahren installiert, das es erlaubt ein UD-Tape mit einer 90°-Ausrichtung qualitativ hochwertig und kostengünstig im Endlos-Verfahren als Rollenware herzustellen. Das proUD-90° Tape ist in einer Breite von 1,25 m erhältlich.

proUD-90°

proUD-90°Rollenware

Diese verschieden gerichteten UD-Tapes proUD-0° und proUD-90° werden für die Herstellung von Organoblechen verwendet, die in die beschriebene thermoplastische Kunststoffmatrix eingebettet sind.

Bei thermoplastischen Matrixsystemen sind durch die Trennung des Werkstoff- und Bauteil-Herstellungsprozesses deutlich kürzere Verarbeitungszeiten bei der Bauteilproduktion realisierbar, die großserientaugliche Zykluszeiten ermöglichen können. Ebenso ist eine thermische Mehrfachumformung der Organobleche möglich.

Bei Erwärmung des Organobleches erlaubt die thermoplastische Matrix eine plastische Verformung in die gewünschte Geometrie.

Durch Hinterspritzen werden zeitgleich lokale Verstärkungen und Funktionselemente eingebracht. Diesen Prozess kann eine konventionelle Spritzgießmaschine mit entsprechenden Anpassungen taktneutral durchführen. Für das Erzielen der benötigten Festigkeitsstrukturen wird im Vergleich zum konventionellen Spritzguss in der Regel ein geringerer Spritzdruck benötigt, ebenso kann die Spritzguss Temperatur verringert werden. In der Folge können Bauteilwandungen dünner ausgeführt werden.

Die Profol GmbH nennt dieses glasfaserverstärkte Thermoplast-Composite Progano®.

progano

Kontinuierliche Progano®-board Produktion

Die mechanischen Eigenschaften von Progano® wie Steifigkeit, Zugfestigkeit und Wärmeausdehnung sind gegenüber vergleichbaren metallischen Bauteilen besser. Im Gegensatz zu Metallblechen sind das Zug- und Druck-verhalten sowie andere mechanische und thermische Eigenschaften nicht isotrop.

Für die automobile Großserienfertigung eines Strukturbau-teils aus Progano® können Elemente eingebettet werden. Elemente wie eine Rippenstruktur und Schraubdome aus glasfaserverstärktem Polypropylen erhöhen die Steifigkeit und bieten faserschonende Schnittstellen für Anbauteile.

Im Vergleich zu äquivalenten Bauteilen aus Stahl können nicht nur bis zu 40 % des Gewichts eingespart werden, die neue Bauweise verringert auch die Komplexität der Fertigung und somit Werkzeugkosten.
Durch die Hybrid-Spritzgussfertigung fallen viele Einzel-teile oder auch Schweißbaugruppen weg.

Compression-Molding

Weiterer Vorteil: Eine Oberflächenbehandlung zum Schutz vor Korrosion ist nicht mehr notwendig.

Die Voraussetzungen einer Großserienfertigung dienten bei der Gestaltung und Festlegung der Fertigungsprozesse als Grundlage für Profol. Sämtliche Prozesse erfüllen diese Vorgabe und gewährleisten eine Großserienfertigung nach der ISO 9001:2015-Zertifizierung.

Zur Auslegung des kundenspezifischen Bauteils wird das faserverstärkte thermoplastische Organoblech bei Profol entsprechend zusammengestellt. Im kontinuierlichen Fertigungsverbund können bis zu 10-Lagen UD-Tape zu einem Progano®-Mutterblech konsolidiert werden. Die Ausrichtung der einzelnen Lagen wird in Abhängigkeit der späteren Anwendung definiert und umgesetzt.

Auf diese Weise werden die Progano®-Mutterbleche her-gestellt. Sie weisen eine Breite von 1, 20m und eine Länge von 3,00 m auf.
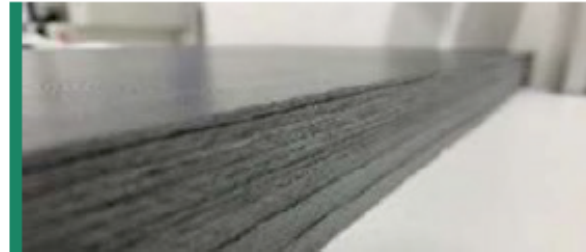
Progano® Musterbleche unterschiedlicher Lagenanzahl

MECHANISCHE KENNWERTE VON PROGANO®

Als Standard Composite Organoblech wurde ein 10-lagiger Aufbau definiert mit einer 4:1 Verteilung der proUD-0° zu proUD-90° Tapes. Der Verbund hat eine Dicke von d = 2,00 mm.

Es ist eine Vielzahl an Möglichkeiten des Lagenaufbaus gegeben, wobei ein symmetrischer Aufbau in Bezug auf die Planlage der späteren Anwendung stets vorteilhafter ist.
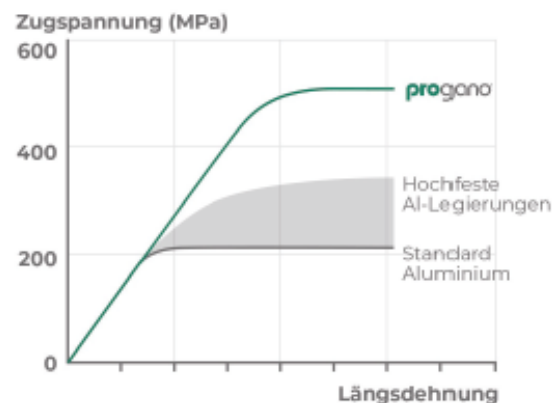
Das Progano®-10-82 erreicht mit seinem 10-lagigem Aufbau mit 8x proUD-0° und 2x proUD-90° Lagen in den durchgeführten Laboruntersuchungen ausgezeichnete mechanische Kennwerte.

3-Punkt-Biegeversuch nach DIN EN ISO 14125

E-Modul   bis zu Σ = 30.000 MPa
Bruchkraft d_{rB} = 510 MPa

VERSUCHSDURCHFÜHRUNGEN

Versuche aus der Automobilindustrie zeigen den zuverlässigen Einsatz von proUD-Tape und Progano®-board. Eine Form des Durchschlagtests weist ein deutlich besseres Resultat des Progano®-boards aus gegenüber einer Aluminiumplatte.

Aluminiumplatte 2 mm
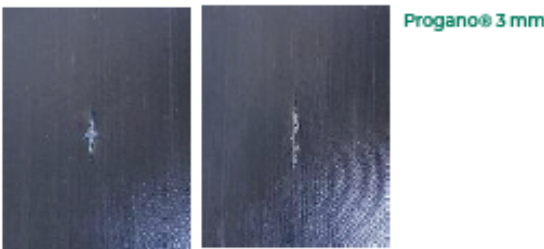
Vorderseite   Rückseite

Progano® 3 mm

Vorderseite   Rückseite

Der Prüfkörper durchschlägt die 2 mm starke Aluminiumplatte vollständig, wohingegen das 3 mm starke Progano®-board den Stoß abfängt, auch wenn auf der Rückseite der Prüfplatte Fasern ausgerissen sind.
Den Vorteil von UD-basierten Organoblechen verdeutlicht das unten aufgeführte Schaubild.
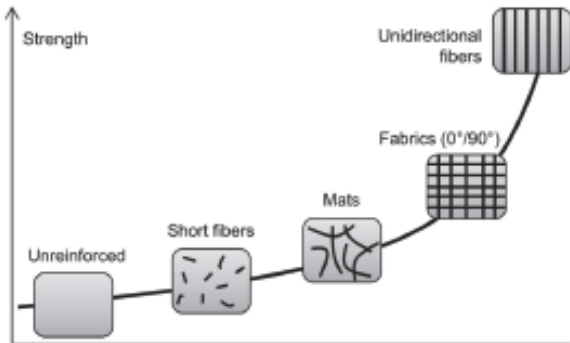
Beziehung zwischen Festigkeit und Faserstruktur

Quelle: MATERIALI COMPOSITI | Caratteristiche – Proprietà – Tecnologie di produzione | Università degli Studi di Cagliari

Durch die Transformation der Automobilindustrie hin zu Elektrofahrzeugen gewinnen Brandprüfungen speziell im Bereich der Batteriekästen mehr an Bedeutung.

Die neu aufgestellte Brandnorm nach UL 2596 beschreibt genau eine solche Situation. Profol hat sein Material diesem Test unterzogen und nach heutigem Stand gute Ergebnisse erzielt.

Die seit längerem bekannten Brennversuche nach DIN 75200 und FMVSS 302 wurden ebenfalls mit dem Progano®-board durchlaufen.

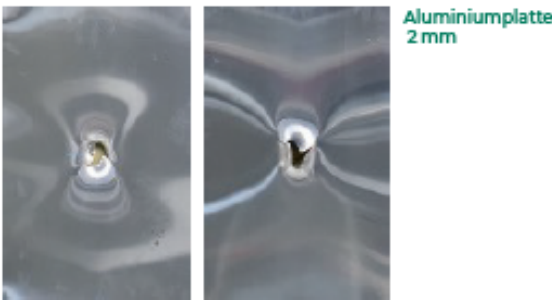| Probe	Progano 10-82					
	Einheit	1	2	3	4	5
Probekörper						
Herkunft		Platte	Platte	Platte	Platte	Platte
Länge	mm	355	355	355	355	355
Breite	mm	100	100	100	100	101
Größte Dicke	mm	1,97	1,93	1,94	1,97	1,97
Kleinste Dicke	mm	1,95	1,91	1,93	1,93	1,95
Prüfung						
Stützdraht		nein	nein	nein	nein	nein
Weg	mm	-	-	-	-	-
Zeit	s	-	-	-	-	-
Brenngeschw. (B)	mm/min	0	0	0	0	0

Prüfnorm: DIN 75200
Prüfeinrichtung: Brennkasten Fa."WAZAU", Berlin
Prüfflammhöhe: 38mm
Zündzeit: 15 s

specimen	Progano 10-82					
	Unit	1	2	3	4	5
specimen		Plate	Plate	Plate	Plate	Plate
length	mm	355	355	355	355	355
width	mm	100	100	100	100	100
largest thickness	mm	1,97	1,93	1,94	1,97	1,97
smallest thickness	mm	1,95	1,91	1,93	1,93	1,95
Test						
holder with wires		no	no	no	no	no
distance	mm	-	-	-	-	-
time	s	-	-	-	-	-
Burn rate (BR)	mm/min	0	0	0	0	0

TEST STANDARD: FMVSS 302   MAX. BURN RATE: 102 mm/min   FULLFILLED

Prüfnorm: FMVSS 302
Prüfeinrichtung: Brennkasten Fa."WAZAU", Berlin
Prüfflammhöhe: 38mm
Zündzeit: 15 s

APPENDIX P II: 3M 8010 DP ADHESIVE

3M
Scotch-Weld™ Structural Plastic Adhesives
DP8010 Blue ● DP8010NS Blue

Technical Data Sheet   **October 2018**

Product Description

3M™ Scotch-Weld™ Structural Plastic Adhesive DP8010 Blue and DP8010NS Blue are two-part, acrylic-based adhesives (10:1 ratio by volume) that can bond many low surface energy plastics, including many grades of Polypropylene, Polyethylene and TPO's without special surface preparation.

These adhesives can replace screws, rivets, plastic welding, and two-step processes which include chemical etchants, priming or surface treatments in many applications.

Features

- Ability to structurally bond polyolefins without special surface preparation
- Regular and Non-Sag Formulations
- Excellent water and humidity resistance
- One step process; no pre-treatment of polyolefin substrates necessary
- Convenient hand-held applicator

- Ability to bond dissimilar Substrates
- Room temperature cure
- Very good chemical resistance
- Solvent-free adhesive system
- Available in bulk

Typical Uncured Properties

Note: The following technical information and data should be considered representative or typical only and should not be used for specification purposes. Unless otherwise indicated, all properties measured at 72°F (22°C).

Property		3M™ Scotch-Weld™ Structural Plastic Adhesive DP8010 Blue	3M™ Scotch-Weld™ Structural Plastic Adhesive DP8010NS Blue
Color	Base (B)	Blue-Green	
	Accelerator (A)	Clear and nearly colorless	
Viscosity¹	Base (B)	27,000 cP	64,000 cP
	Accelerator (A)	17,000 – 40,000 cP	17,000 – 40,000 cP
Density	Base (B)	8.5 lb/gal	
	Accelerator (A)	8.3 – 8.7 lb/gal	
Mix ratio	By volume	10:1	
	By weight	10:1	
Work life²		Approx. 8 minutes	
Open time³		10 minutes	
Skin Time⁴		Approximately 3 minutes (See Below)	
Time to handling strength⁵		60 minutes	

1. Viscosity measured using Brookfield RTV, spindle #7, 20 RPM @ 80°F (27°C)
2. Maximum time that adhesive can remain in a static mixing nozzle and still be expelled without undue force on the applicator.
3. Maximum time allowed after applying adhesive to one substrate before bond must be closed and fixed in place.
4. An open bead line will show some skinning in approximately 3 minutes. It is possible to bond parts with good strength if the parts are made within 10 minutes. Therefore, the adhesive has a 10 minute open time for making bonds.
5. Minimum time required to achieve 50 psi of overlap shear strength, measured on HDPE

Note: The data in this sheet were generated using the 3M™ EPX Applicator System equipped with an EPX static mixer, according to manufacturer's directions. Thorough hand-mixing will afford comparable results.

3M™ Scotch-Weld™ Structural Plastic Adhesive
DP8010 Blue • DP8010NS Blue

Note: The following technical information and data should be considered representative or typical only and should not be used for specification purposes. Unless otherwise indicated, all properties measured at 72°F (22°C)

Typical Mixed Properties

Property	3M™ Scotch-Weld™ Structural Plastic Adhesive DP8010 Blue	3M™ Scotch-Weld™ Structural Plastic Adhesive DP8010 Blue
Color	Blue-Green	
Full cure time	24 hours	
Dispense Viscosity (73°F)	25,000 cP	64,000 cP

Typical Cured Physical Properties

Property		3M™ Scotch-Weld™ Structural Plastic Adhesive DP8010 Blue
Physical		
Shore D Hardness		55-60
Storage Modulus (DMA)		970 MPa
Tensile Strength (ASTM D638)		1300 PSI
Tensile Modulus (ASTM D638)		77,000 PSI
Strain at Break (ASTM D638)		90%
Thermal		
Tg (Glass Transition Temperature)	(DMA)	61°C
Coefficient of	Below Tg	116
Thermal Expansion	Above	245
(in/in/°C)	Tg	
Electrical		
Dielectric Strength (ASTM D 149)		603 V/mil
Volume Resistivity ((ASTM D 257)		4.10E+11 (Ω-cm)
Surface Resistivity (ASTM D257)		8.00E+10 (Ω)
Dielectric Constant (ASTM D150)		4.36 at 1 KHz
Dissipation Factor (ASTM D150)		0.068 at 1 KHz

3M™ Scotch-Weld™ Structural Plastic Adhesive
DP8010 Blue • DP8010NS Blue

Typical Cured Physcial Properties *(continued)*

Note: The following technical information and data should be considered representative or typical only and should not be used for specification

Overlap Shear (psi)[7], ASTM D1002

Substrate	3M™ Scotch-Weld™ Structural Plastic Adhesive DP8010 Blue	3M™ Scotch-Weld™ Structural Plastic Adhesive DP8010NS Blue
Aluminum (MEK/abrade/MEK)	1960 CF	1780 CF
Cold-rolled steel (MEK/abrade/MEK)	1800 CF	1870 CF
Stainless Steel (MEK/abrade/MEK)	1820 CF	1990 CF
Copper (MEK/abrade/MEK)	1870 CF	1500 CF
Galvanized steel (MEK/abrade/MEK)	1330 CF	840 mixed
PP (IPA wipe)	1150 SF	1150 SF
LDPE (IPA wipe)	360 SF	360 SF
HDPE (IPA wipe)	1040 SF	1100 SF
UHMW-PE (IPA wipe)	770 CF	750 SF
Gelcoat (fiberglass--smooth side)	900 SF	1100 SF
Acrylic	1100 SF	1190 SF
PVC	1730 SF	1740 SF
PC	760 AF	740 AF
ABS	1250 SF	1240 SF
Polystyrene (HIPS)	580 SF	570 SF
FRP (Epoxy)	2830 CF	2860 CF
Acetal	90 AF	70 AF
SMC (Fiberglass--rough side)	760 SF	800 SF
Glass	530 SF	670 SF
PTFE (IPA/abrade/IPA)	320 AF	360 AF

Overlap Shear (psi); Etched Aluminum, at Temperature[7], ASTM D1002

Temperature	3M™ Scotch-Weld™ Structural Plastic Adhesive DP8010 Blue	3M™ Scotch-Weld™ Structural Plastic Adhesive DP8010NS Blue
-20°F (-29°C)	2000 mixed	2000 mixed
73°F (23°C)	1800 CF	1700 CF
120°F (49°C)	1000 mixed	700 mixed
150°F (66°C)	450 AF	340 AF
180°F (82°C)	300 AF	100 AF

6. Overlap shear values measured using ASTM D1002; adhesives allowed to cure for 7 days at room temperature; ¾" overlap; 0.010" bond line thickness; samples pulled at 0.1 in/min for metals and 2 in/min for plastics; all surfaces prepared with light abrasion and solvent clean; substrates used were 1/16" thick aluminum and 1/8" thick plastics; failure modes: AF: adhesive failure CF: cohesive failure SF: substrate failure mixed: AF/CF

3M™ Scotch-Weld™ Structural Plastic Adhesive
DP8010 Blue ● DP8010NS Blue

Typical Cured Physcial Properties *(continued)*

Note: The following technical information and data should be considered representative or typical only and should not be used for specification

Environmental Resistance[8] Expressed as Percent Retention of Control Strength (Measured on 1/8" thick HDPE via Overlap Shear, ASTM D1002)

Condition	Substrate	3M™ Scotch-Weld™ Structural Plastic Adhesive DP8010 Blue	3M™ Scotch-Weld™ Structural Plastic Adhesive DP8010NS Blue
Control	HDPE	100% SF	100 % SF
160°F water soak		80% CF	80% CF
150°F/80% RH		95% CF	97% CF
NaOH 10% by wt		100% SF/CF	100% SF
HCl 16% by volume		100% SF	100% SF/CF
IPA soak		95% CF	91% CF
Diesel Fuel soak		97% SF/CF	93% SF
50% Antifreeze soak		100% SF/CF	100% SF
Gasoline soak		70% CF	70% CF
Acetone soak		20% AF	25% AF

8. Values indicate overlap shear test performance retained after 14 days of continuous exposure relative to a control sample left at room temperature; samples conditioned for 7 days at room temperature and 50% relative humidity prior to tests.

Floating Roller Peel (lb/inch width)[9] ASTM D3167

Substrate	3M™ Scotch-Weld™ Structural Plastic Adhesive DP8010 Blue and 3M™ Scotch-Weld™ Structural Plastic Adhesive DP8010NS Blue
HDPE	Substrate Failure

[9] Floating roller peel values measured using ASTM D3167; allowed to cure for 24 hours at room temperature; 1" wide samples; 0.017" bond line thickness; samples pulled at 20 in/min. Flexible HDPE was 1mm thick and rigid HDPE was 4.8mm thick.
AF: adhesive failure   CF: cohesive failureSF: substrate failure

Directions For Use

1. To obtain the highest strength structural bonds, paint, oxide films, oils, dust, mold release agents, and all other surface contaminants must be completely removed. The amount of surface preparation depends on the required bond strength and environmental aging resistance desired by user. For suggested surface preparations on common substrates, see the section on surface preparation.

2. Mixing
   For Duo-Pak Cartridges
   Store cartridges with cap end up to allow any air bubbles to rise towards the tip. To use, simply insert the cartridge into the EPX applicator and start the plunger into the cylinders using light pressure on the trigger. Then remove the cap and expel a small amount of adhesive to ensure material flows freely from both sides of cartridge. For automatic mixing, attach an EPX mixing nozzle to the cartridge and begin dispensing the adhesive. For hand mixing, expel the desired amount of adhesive and mix thoroughly. Mix approximately 15 seconds after obtaining a uniform color.

3M™ Scotch-Weld™ Structural Plastic Adhesive
DP8010 Blue • DP8010NS Blue

For Bulk Containers

**Directions
For Use
*(continued)***

Mix thoroughly by weight or volume in the proportion specified on the product label or in the typical uncured properties section. Mix approximately 15 seconds after obtaining a uniform color.

3. Apply adhesive and join surfaces within the open time listed for the specific product. Larger quantities and/or higher temperatures will reduce this working time.
4. Allow adhesive to cure at 60°F (16°C) or above until completely firm. Applying heat up to 150°F (66°C) will increase cure speed.
5. Keep parts from moving during cure. Apply contact pressure or fixture in place if necessary. Optimum bond line thickness ranges from 0.005 to 0.020 inch; shear strength will be maximized with thinner bond lines, while peel strength reaches a maximum with thicker bond lines.
6. Excess uncured adhesive can be cleaned up with ketone type solvents.*

*Note: When using solvents, extinguish all ignition sources, including pilot lights, and follow the manufacturer's precautions and directions for use.

**Surface
Preparation**

3M™ Scotch-Weld™ Structural Plastic Adhesives are designed to be used on metal, wood, and most plastic surfaces. The following cleaning methods are suggested for common surfaces:

Steel:
1. Wipe free of dust and dirt with pure solvent such as acetone or isopropyl alcohol.*
2. Sandblast or abrade using clean fine grit abrasives.
3. Wipe again with clean solvent to remove loose particles.*

Aluminum:
1. Wipe free of dust and dirt with pure solvent such as acetone or isopropyl alcohol.*
2. Sandblast or abrade using clean fine grit abrasives.
3. Wipe again with clean solvent to remove loose particles.*
4. When using a primer, apply adhesive within 4 hours of primer application.

Plastics/Rubbers:
1. Wipe with isopropyl alcohol.*
2. Abrade using fine grit abrasives.
3. Wipe with isopropyl alcohol.*

Glass:
1. Solvent wipe surface using acetone or MEK.*
2. Apply a thin coating of a silane adhesion promoter to the glass surfaces to be bonded and allow to dry completely before bonding.

*Note: When using solvents, extinguish all ignition sources, including pilot lights, and follow the manufacturer's precautions and directions for use.

3M™ Scotch-Weld™ Structural Plastic Adhesive
DP8010 Blue ● DP8010NS Blue

Storage	Store product at 40°F (4°C). Do not freeze. Allow product to reach room temperature prior to use.
Shelf Life	3M™ Scotch-Weld™ Structural Plastic Adhesives when stored in unopened original containers kept at recommended storage conditions have a shelf life of 3 months for 55 gal. drums, 9 months for 5 gal. pails and 18 months in duo-pak
Precautionary Information	Refer to Product Label and Material Safety Data Sheet for health and safety information before using this product. For additional health and safety information, call 1-800-364-3577 or 651-737-6501.
For Additional Information	To request additional product information or to arrange for sales assistance, call toll free 1-800-362-3550 or visit www.3M.com/structuraladhesives.
Technical Information	The technical information, guidance, and other statements contained in this document or otherwise provided by 3M are based upon records, tests, or experience that 3M believes to be reliable, but the accuracy, completeness, and representative nature of such information is not guaranteed. Such information is intended for people with knowledge and technical skills sufficient to assess and apply their own informed judgment to the information. No license under any 3M or third party intellectual property rights is granted or implied with this information.
Product Selection and Use	Many factors beyond 3M's control and uniquely within user's knowledge and control can affect the use and performance of a 3M product in a particular application. As a result, customer is solely responsible for evaluating the product and determining whether it is appropriate and suitable for customer's application, including conducting a workplace hazard assessment and reviewing all applicable regulations and standards (e.g., OSHA, ANSI, etc.). Failure to properly evaluate, select, and use a 3M product and appropriate safety products, or to meet all applicable safety regulations, may result in injury, sickness, death, and/or harm to property.
Warranty, Limited Remedy, and Disclaimer	Unless a different warranty is specifically stated on the applicable 3M product packaging or product literature (in which case such warranty governs), 3M warrants that each 3M product meets the applicable 3M product specification at the time 3M ships the product. 3M MAKES NO OTHER WARRANTIES OR CONDITIONS, EXPRESS OR IMPLIED, INCLUDING, BUT NOT LIMITED TO, ANY IMPLIED WARRANTY OR CONDITION OF MERCHANTABILITY, FITNESS FOR A PARTICULAR PURPOSE, OR ARISING OUT OF A COURSE OF DEALING, CUSTOM, OR USAGE OF TRADE. If a 3M product does not conform to this warranty, then the sole and exclusive remedy is, at 3M's option, replacement of the 3M product or refund of the purchase price.
Limitation of Liability	Except for the limited remedy stated above, and except to the extent prohibited by law, 3M will not be liable for any loss or damage arising from or related to the 3M product, whether direct, indirect, special, incidental, or consequential (including, but not limited to, lost profits or business opportunity), regardless of the legal or equitable theory asserted, including, but not limited to, warranty, contract, negligence, or strict liability.

$$\boxed{\text{ISO 9001}}$$

3M